PLUG-IN ELECTRIC VEHICLE CHARGING CONTROL FOR WIND POWER INTEGRATION ENHANCEMENT

LUO XIAO

Ph.D

The Hong Kong Polytechnic University

2016

The Hong Kong Polytechnic University

Department of Electrical Engineering

PLUG-IN ELECTRIC VEHICLE CHARGING CONTROL FOR WIND POWER INTEGRATION ENHANCEMENT

LUO XIAO

A thesis submitted in partial fulfillment of the requirements

for the Degree of Doctor of Philosophy

May 2016

CERTIFICATE OF ORIGINALITY

I hereby declare that this thesis is my own work and that, to the best of my knowledge and belief, it reproduces no material previously published or written, nor material that has been accepted for the award of any other degree or diploma, except where due acknowledgement has been made in the text.

_____(Signed)

_____LUO Xiao_____(Name of student)

Abstract

Global environmental crises, such as the global climate change and awful air pollution in major cities over the world, are causing profound changes to both the power system and the transportation sector. On one hand, power systems worldwide are evolving towards a greener version by integrating increasing amount of renewable energy sources, especially wind power (WP). On the other hand, as an effective way to reduce greenhouse gas emission, plug-in electric vehicles (PEVs) are currently incentivized in many countries and more and more types of PEV are being rolled out by various automakers. With the adoption of PEV surging, a rapid increase of PEV charging load can be expected in the coming years.

The uncertainty and variability of WP generation will weaken the controllability on the supply side of the power system and require more fast-reacting reserve, while bulk uncontrolled PEV charging may severely stress the network at all voltage levels, threatening the system reliability, lowering its efficiency, and jeopardizing the system economy. Controlled PEV charging, however, could be a valuable source for large-scale demand response (DR). The DR is identified as a very effective tool to facilitate smooth WP integration, and clean electricity from WP to propel PEVs can significantly decarbonize the transportation sector. Thus, a lot of synergies can be explored between the PEV charging load and the WP generation.

As an effort to safely accommodate the PEV charging load at the initial stage of PEV adoption before the upgrade of the network infrastructure, this thesis firstly proposes a real-time scheduling scheme for PEV charging in low-voltage residential distribution network. This scheme schedules PEV charging to either minimize system losses or prevent over-low voltage, depending on the PEV

penetration level. Since most often voltage drop would become a binding constraint when a low-voltage distribution feeder is subject to high PEV penetration level, a scheduling method is first developed to enlarge the voltage safety margin. Then, a novel factor is derived to allow the scheduling scheme to be flexibly adjusted from being voltage-safety-oriented to loss-minimization-oriented, or vice versa. Simulation results verify that the proposed scheduling scheme is fast and effective with circuit losses close to optimal at low PEV penetration level and voltage drops maintained within the tolerable limit at high PEV penetration level.

To facilitate the PEV demand response, a decentralized charging control scheme is devised in this thesis. In the proposed control scheme, individual PEV would autonomously adjust its power in response to two system-level directional signals. Since the power adjustment would also take into account the PEV's urgency level of charging (ULC), the charging/discharging power among PEVs will be distributed automatically according to their heterogeneous charging requirements. The mechanism that can trigger divergent PEV power adjustment is analyzed to obtain the stability condition for the proposed control scheme. For the control inaccuracy caused by interrupted individual PEV power adjustments, a remedy is proposed and proved. As an application, the power of a PEV fleet is controlled by the proposed decentralized charging control scheme to compensate undesired fluctuations in a wind farm's power output. Simulation results verify that the controlled PEV power can respond to undesired WP fluctuations timely and accurately, and the power distribution among PEVs is consistent with the heterogeneous PEV charging requirements.

Increasing amount of WP in the power system will force conventional generators to go through more frequent cycling operations which have damaging effects on generator components. In this context, a 3-level hierarchical scheme is proposed to utilize the PEV power to hedge against the unit ramp cycling (URC) operations. A general URC operation model is proposed for the first time. Net

load variation range (NLVR) is used to capture the WP forecast uncertainty. The top-level scheduling model reshapes the NLVR by coordinating PEV charging load to minimize the URC operations that can be caused by the possible net load realizations in the NLVR. Based on updated WP forecasts, the middle-level dispatch model exempts the over-scheduled anti-URC regulation onus on PEVs to promote PEV charging. Nevertheless, the actual dispatch of net load is confined within the reshaped NLVR from the top-level scheduling to avoid overly restoring the PEV power. At the bottom-level is the proposed decentralized charging control scheme to implement the PEV power dispatch instruction. Simulation results show that with the proposed hierarchical scheme, the PEV-aided URC operation mitigation is effective and most of the desired charging energy is preserved to satisfy the charging requirements for the majority of PEVs. The effectiveness of the proposed scheme is shown to be robust to WP forecast errors.

The associated cost to accommodate the WP uncertainty and variability (WPUnV) in a power system is referred as the wind power uncertainty cost (WPUC) which would increase rapidly with WP penetration level. This thesis investigates to what extent the controlled PEV power would help reduce this WPUC. A comprehensive WPUC model is proposed in which generator cycling costs are included. Also, the proposed decentralized charging control scheme is used to obtain a realistic response of the PEV load to the system dispatch instruction. With the WPUnV decomposed into two components, namely hourly WP forecast errors and sub-hourly WP fluctuations, the WPUC raised by each of the components will be evaluated. Simulation results show that generator cycling costs are non-negligible parts of the WPUC and controlled PEV power has a favorable effect on reducing the overall WPUC. The controlled PEV power, however, may not be as helpful as expected to mitigate the WPUC induced by the WP forecast errors on hourly scale. Yet, the WPUC raised by sub-hourly WP fluctuations can be largely reduced with the controlled PEV power.

Acknowledgement

First and foremost, I would like to express my sincere gratitude to my chief supervisor, Dr. Kevin K. W. Chan, for his continuous support and encouragement throughout my PhD study and research. His knowledge, experience and intelligence always impress me and enlighten me. He helped me solve all kinds of academic problems so patiently. His optimistic attitude to life encourages me to keep going every time I fail. He also gives me freedom to choose my interested topics and provides me insightful suggestions all along. To me, Dr. Chan is not only my supervisor but also my trusted and respected friend. It is my honor and fortune to study under his guidance.

I also would like to give special thanks to my good friends Dr. Bin Zhou and Dr. Shiwei Xia, for the stimulating discussions we had, for all the help they given me, and for the day and night we worked together. I learnt a lot of important things from them, not only the research skills and experiences but also the can-do attitude and hardworking spirit. I will always remember the past four years with them. My sincere thanks also go to my paper reviewers and thesis examiners for their constructive comments to this research.

Moreover, I would like to thank my dear parents Xiaoqian Luo and Hua Zheng for their selfless and unconditional love, support, and encouragement ever since I was born. I also owe many thanks to my girlfriend Ying Liu for her thoughtfulness to let me concentrate on my study and consolation to dissolve my frustration.

Without all these people backing me up, I would never have been able to complete my PhD study.

Last but not least, I would like to acknowledge the support of my research studentship awarded by The Hong Kong Polytechnic University.

Table of Contents

Lists of Figures, Tables and Abbreviations

List of Figures

List of Tables

List of Abbreviations

BC	Battery capacity
BEV	Battery electric vehicle
CDF	Cumulative distribution function
DOD	Depth of discharge
DG	Diesel generator
DR	Demand response
DS	Directional signal
EDT	Expected departure time of PEV
ESS	Energy storage system
FGI	Forecast grouping interval
GHG	Greenhouse gas
G2V	Grid-to-vehicle power delivery
ICE	Internal combustion engine
NLVR	Net load variation range
PEV	Plug-in electric vehicle
PH	Probability histogram
PHEV	Plug-in hybrid electric vehicle
PVLF	Power/voltage levelling factor
RHS	Right-hand side
RMS	Root mean square
SOC	State of charge
SS	Sign signal
UC	Unit commitment
ULC	Urgency level of charging of PEV
URC	Unit ramp cycling
VDII	Voltage deviation impact index

V2G	Vehicle-to-grid power delivery
WP	Wind power
WPUC	Wind power uncertainty cost
WPUnV	Wind power uncertainty and variability

Chapter I

Introduction

1.1 Background and Literature Review

1.1.1 Prosperity of PEV: Challenges and Opportunities

Plug-in electric vehicles (PEVs), including plug-in hybrid electric vehicles (PHEVs) and battery electric vehicles (BEVs), are seen as the next generation of automobile. The driving force behind the development of PEV is the worse-than-ever global environmental problems. According to a report published by the International Energy Agency (IEA) in 2011 [1], if the current fossil fuel based energy generation and consumption continues, energy-related greenhouse gas (GHG) emissions will double by 2050, which will dramatically aggravate the global warming problem, imposing destructive impact on the ecosystem of our planet. The increased oil demand also accelerates the depletion of oil resources, which is raising concerns in many countries on their national energy security. Conventional internal combustion engine (ICE) vehicle is a major contributor to the GHG emission. For example, in the US 2006, 28% of the total GHG emission is from the transportation sector [2]. The PEV is one of the key technologies needed to address the global environmental crisis. Synergizing with renewable energy resources, PEVs can be powered by clean electricity, which will decarbonize the transportation sector effectively.

Currently, PEV is being promoted in several countries [3-5] and auto manufacturers are rolling out more and more PEV models [6]. Global PEV sale was more than doubled between 2011 and 2012, and the number of on-the-road PEVs worldwide increased 76% from around 405,000 in 2013 to about 712,000

in 2014 [7, 8]. For the future, IEA has predicted that with the coordinated effort from governments, the auto industry and other related stakeholders, the sale of PEVs could reach 5 million per year by 2020, and in the long-term, it was possible for the PEV to achieve 50% market share by 2050 [1]. The study in [6] also forecasts a noticeable increase in the adoption of PEV in the US.

Though PEVs do not have direct GHG emission when running on electricity, they do have well-to-wheel emissions as the electricity charging the PEV can be generated from burning fossil fuels. Nevertheless, the environmental benefit from PEVs is still prominent compared with ICE vehicles. The well-to-wheel analysis of PEVs [9] showed that based on the generation mix of the US in 2010, PHEV and BEV can achieve a 38 lb and 45 lb GHG emission reduction per year, respectively, compared with conventional gasoline vehicles. Another investigation also showed that for the US, even in regions with most dominant coal fired power plants, PEVs are still able to reduce about a quarter of the GHG emission over ICE vehicles [10]. The Electric Power Research Institution has examined the 2050 scenario and estimated that PEVs can contribute to 163-612 million metric tons of GHG emission reduction per year by 2050, depending on the PEV market share and the evolvement of the mix of generating technologies [11].

Challenges Caused by PEV Charging and Solutions

As PEV adoption becomes increasingly widespread, uncontrolled charging load will start causing problems to power systems. Many studies have examined the impact of PEV charging on power systems. In [12, 13], it was found that charging activities of private PEVs tend to concentrate in the afternoon which coincide with the daily peak load period. The coincidence will increase the already-high peak load. Thus, more peak load generators would have to be started, pushing up the fuel cost of generation. Besides, the power loss of the network will increase rapidly as the PEV penetration level rises, causing extra

cost to utilities. From security perspective, multiple PEVs being charged within the same area might cause line overloading and excessively low voltages in the distribution network [14, 15] which is a sign of power quality deterioration. In addition, the heavy PEV charging load could cause sustained excessive loading in distribution transformers, leading to increased transformer fuse blowing and customer outages [16].

To handle the aforementioned challenges associated with PEV charging, researchers around the world have reached a common consensus that PEV charging load should be controllable; otherwise, network infrastructure would need to be upgraded. Many solutions have been proposed in the literature and some of them are introduced here. Two methods were proposed in [14] to alleviate the heavy loading caused by dump PEV charging. One method is to provide PEV owners economic incentive through dual tariff and the other is to enable direct charging control. Yet, the first method can cause PEV charging activities to concentrate in low-cost period which creates new peak load, and the second method requires a powerful intelligent control center to schedule each PEV. The energy price and the availability of renewable energy are often used as signals to direct PEV charging to be away from peak hours. A fuzzy logic power-flow controller is introduced in [17], which determines the charging rate for each PEV based on the charging priority so as to maximize the utilization of renewable energy and minimize the impact of PEV charging on the system load profile. Similarly, the study [18] assessed different charging strategies in terms of their grid impact, utilization of local generation, and PEV driving ranges. The authors in [19] proposed a novel navigation system for PEV rapid charging. Since the system takes into account the traffic condition as well as the status of power system, the charging load can be properly distributed in the network so as to avoid overloading a particular region. The authors in [20] proposed a stochastic scheduling and dispatch model to coordinate PEV load and conventional generation with wind generation. Flattened net load profile is

achieved with reduced system operating cost. Nevertheless, the stochastic optimization model is computationally expensive to solve. In [16], the problem of distribution transformer overloading caused by heavy PEV charging load was investigated. The authors did not seek to control PEV charging. Instead, they used a binomial probability model to calculate the probability of a distribution transformer being over-loaded due to PEV charging, such that the susceptible transformers can be identified and replaced. Besides the aforementioned studies, many other researches for mitigating the detrimental impact of uncontrolled PEV charging on power systems can be found in the literature [21-24].

Opportunities Associated with PEV Charging

When behaving as responsive load, PEVs have great potential to participate in power system regulations. Private vehicle users usually park their cars for most of the time in a day and they tend to adhere to some routine schedules. For example, a study [25] showed that most private cars in the US are parked more than 95% of time in a day and generally follow the very similar daily schedule. This indicates that PEVs can remain grid-connected for a long period of time and thus can be used as small energy-storage devices to provide ancillary services for the power system.

Controllable PEV power is a source of fast-reacting reserve. Conventionally, the power system faces a tradeoff between maintaining more reserve for higher reliability and pursuing lower operating cost. PEVs as a reserve provider can not only ensure sufficient reserve in the system but also free generators from reserve duties to improve the system economy [26]. The research in [27] regarded PEVs as a storage and reserve provider and proposed a model to determine the optimal bidding for the PEV aggregator in the energy and reserve markets. The results indicate that the aggregator can obtain benefits from properly managing PEV power and the utility can enjoy the inexpensive reserve from PEVs. The analysis in [28] showed that the reserve capacity offered by PEVs can be greatly reduced

due to the heterogeneous driving patterns of individual PEVs. This indicates that it may be better off for PEVs to provide reserve together with other conventional reserve providers.

Controllable PEV charging load adds extra flexibility to the power system, which can effectively facilitate the integration of renewable energy sources. In [29], a stochastic optimization model including PEV charging load and renewable energy sources is proposed, with the objective of maximizing the use of renewable energy sources while satisfying the individual PEV's charging rate limit and deadline. The authors in [30] explored the synergy between PEV load and wind power (WP). They proposed a hierarchical control scheme where PEVs provide fast-reacting reserve to WP and compensate for system frequency deviation. Thus, the system cost of accommodating WP can be decreased. In [31], a collaborative dispatch strategy was proposed for the PEV charging load to respond to the varying output of renewable energy sources, where the uncertainties in renewable power generation and PEV load are taken into account.

PEV charging control can also help improve system reliability and well-being. Studies in [32, 33] evaluated the impact of PEV charging on system reliability when PEVs are refueled by battery swapping. The results showed that the system reliability can be effectively enhanced. In [34], vehicle-to-home and vehicle-to-grid (V2G) power delivery were investigated when the distribution system is operated in islanding mode or in grid connected mode. It is found that in all scenarios the system reliability can be enhanced. In [35], the authors proposed that PEVs can be used as interruptible load or temporary power source via V2G in case of outage to improve the well-being of the generating system.

PEV is seen as an important player in the power market of future smart grids. In [36], an automated demand response (DR) mechanism for a PEV fleet is designed to meet a predetermined load scheduling obligation to the market while ensure the PEV charging requirements to be satisfied. In [37], the controlled PEV power is proposed to participate in flexible ramp market either as independent

provider of ramp capacity or via cooperation with generators. The authors in [38] proposed an optimal bidding strategy for a PEV aggregator to minimize total charging cost and also satisfy charging requirements.

To summarize, the PEV is the key to decarbonize the transportation sector. PEV adoption has increased rapidly in the past few years and is predicted to increase further in the coming years. When a large number of PEVs are connected to the power system, uncontrolled PEV charging load can have adverse impacts on the system's economy and security. Thus, PEV charging activities need to be coordinated. When acting as responsive load, PEVs can provide storage and fast-reacting reserve to facilitate the system regulation.

1.1.2 Wind Power Integration Enhancement with Demand Response

Power systems worldwide have been evolving towards a greener version by integrating more and more renewable energy sources, especially WP. The last few decades have seen substantial increase in WP capacity in many countries. For example, in Germany, the renewable electricity production has increased from 3.1% in 1990 to 17.0% in 2010 and is projected to further increase to at least 30% by 2020 [39]. When the WP penetration level is relatively low, the impact of WP on the balance between demand and generation in the power system is limited, and thus, it can be simply modeled as a negative load. When the WP penetration level is high, the WP uncertainty and variability (WPUnV) will have a major impact on system operations and thus need to be taken into account in the power system scheduling, dispatch and control.

Difficulties in Large-scale Wind Power Integration

Because the sites with rich wind energy resource depend on natural conditions, the transmission of WP may route through heavily loaded lines. Moreover, since wind farms are often located far away from load centers, long-distance transmission would be required. Therefore, large-scale WP integration

would often cause transmission congestion in the network [40]. With the system load growing rapidly, the congestion problem may become more profound.

In systems where the generator profile is dominated by inflexible thermal units, there can be insufficient upward and downward regulation reserves to accommodate large-scale WP. For example, in the northwestern provinces of China, 15%-25% WP is curtailed every year because a large number of inflexible combined heat and power units in those provinces fail to provide sufficient regulation reserves. It is estimated that the WP curtailment incurred a ¥1.6 billion economic loss in 2012 [41]. Fast-reacting units such as natural gas turbines or hydro generators can provide sufficient reserve capacity for WP [42, 43]. Yet, fast-reacting thermal units are not only expensive to use but also create new air pollution, which offsets the environmentally benefit attained from WP. The hydroelectric plant is fast to response and inexpensive to operate, and generates clean electricity. Nevertheless, it will be harmful to the river's ecosystem and its availability is geologically constrained.

WPUnV also creates difficulty for the WP delivery in following the schedule cleared in the power market, which is subject to imbalance penalty [44]. Thus, wind farms need to be used in conjunction with other dispatchable power sources to reduce intermittency. As the WP penetration level goes up, more and greater net load ramps will be resulted. Since inertia contribution from wind turbines is insignificant [45], keeping balance between system load and generation would be increasingly difficult, which leads to frequency deviation problem. In distribution networks, the WP variations trigger more frequent tap change in substation transformers, leading to accelerated wear and tear of the tap changers [46].

Synergy between Wind Power and PEV

The combination of WP and PEV is synergistic. On one hand, when acting as controllable load, PEVs can provide energy buffers to counterbalance undesired WP variations so as to facilitate smooth WP integration. On the other hand, the

reduction of GHG emission expected from using PEVs can be fully realized only if PEVs are powered by clean electricity. Therefore, great synergy exists between WP and PEV.

A lot of studies have looked into the WP's synergy with responsive demand, especially the PEV. Studies in [47, 48] showed that with the knowledge of customers' willingness to adjust their consumption as energy price change, the power system dispatch could better address the supply and demand balancing problem. In [49], the effect of demand shifting and peak shaving on WP integration cost is examined, where the demand is either directly controlled or assumed to be price-sensitive. The study in [50] assessed the impacts of demand response on the short-term reliability of the power system with significant WP. The results indicated that for the price-sensitive load, the demand participation uncertainty and the price elasticity uncertainty are two important factors affecting the effectiveness of the demand response. In the aforementioned four papers, the responsive demand is modeled only conceptually without considering specific load type and characteristics. In [51], the authors demonstrated that with PEVs participating in spot market and regulation market, the variations in system net load can be effectively reduced and PEV owners could save money. Similar results were found by the authors in [44], where a model was proposed to jointly minimize the PEV owners' cost and the wind farm owner's penalty cost for the actual WP deviating from the scheduled profile. In [52], the authors proposed a virtual power plant consisting of a wind farm and a fleet of PEVs, and showed how to schedule the power output of the virtual plant and the energy storage in PEVs to maximize the virtual plant's profit. Yet, in [44, 51, 52], PEV charging control method was not mentioned. In [30], a hierarchical control scheme was proposed to realize the synergy between WP and PEV. Sufficient reserve from PEVs is scheduled first. Then, the PEV power is dispatched to compromise any unforeseen WP deviations to ensure the optimized power system operations can

be realized. Nevertheless, this control scheme is at the cost of PEV charging energy losses, and the losses depend on the accuracy of WP forecast.

1.2 Incentives of Thesis

One of the main places where PEV will be charged is at home. Many recent studies have shown that random unscheduled PEV charging at home may significantly stress the low-voltage residential distribution system [53-56]. The associated problems include increased peak load and losses, excessive voltage drop and branch overloading. These studies also pointed out that, by properly scheduling and controlling PEV charging, the existing network infrastructure should be able to accommodate much higher PEV penetration level. The first intention of this thesis is to design a scheduling scheme for PEV charging in low-voltage residential distribution feeder. The objective of the scheduling scheme is to either minimize system losses or avoid over-low voltage during the charging period, depending on whether the PEV penetration level is sufficiently high to make the voltage drop become the binding constraint. The proposed scheduling scheme is an effort to realize smooth and safe accommodation of the PEV charging load at the initial stage of PEV adoption before the upgrade of the network infrastructure. To cope with frequent dynamic PEV arrivals and departures, the scheduling scheme needs to be fast enough for real-time application.

PEVs have a great potential to serve as large-scale fast-reacting reserve, which is very important to future smart grids with high penetration of WP. Nevertheless, a large number of dispersedly located PEVs need to be controlled for the aggregate PEV power to participate in system regulation. The second intention of this thesis is thus to devise a decentralized PEV charging control scheme. One prospective usage of the controlled PEV power is to compensate undesired WP fluctuations. This is important because rapidly growing wind

power capacity in power systems is weakening the controllability on the supply side, making it more difficult to keep the balance between generation and demand, which indicates possible degradation of the system load frequency control. Several researchers have proposed to control PEV charging for system frequency regulation. In [57, 58], aggregate V2G model and charging strategies were proposed and applied to frequency regulation. Only lumped control on aggregate PEV power was considered, however, and control on individual PEV power was neglected. In [59], a PEV-integrated frequency control method was proposed where a central control entity determines each PEV's charging/ discharging power based on the ranking of battery state-of-charge (SOC) so as to meet individual PEVs' charging requirements. Centralized control, however, may not be applicable to a large PEV fleet. In [60, 61], each PEV measures system frequency locally and adjusts its power according to a predetermined droop characteristic against frequency deviation. Though this scheme is distributed and scalable, installing frequency measurement devices for plenty of PEVs can be very costly. Moreover, the accuracy of the measured frequency signal can be readily affected by noises and errors [62], and the effectiveness of this PEV-aided frequency regulation would be degraded as a result. With the proposed decentralized charging control scheme, the aggregate PEV power is expected to be able to respond to undesired WP fluctuations so as to help maintain the generation-demand balance and enhance the frequency regulation. Besides, the proposed scheme should also be able to ensure each PEV's charging requirement can be fulfilled so as not to jeopardize the PEV user's convenience.

Higher penetration of wind energy would result in more and greater net load variations. Besides, the number of thermal units online will decrease as the system demand is increasingly supplied by WP. As a result, the thermal units will have to go through more frequent and significant cycling operations. Cycling operations would accelerate wear and tear to generating equipment and eventually shorten the generator's service life. The authors in [63] proposed to

include dynamic cycling costs in unit commitment (UC) to reduce the generator cycling operation. Nevertheless, the test results show that the reducing effect is limited and the majority of cycling operations are still inevitable. Energy storage systems (ESSs) have been proposed to mitigate the impact of unstable WP on system operations [64-70]. Large-scale ESS deployment for significant WP, however, is still very expensive [71, 72]. The third intention of this thesis is to utilize the PEV power to hedge against the unit ramp cycling (URC) operations in a system with considerable WP. Despite many ESS control methods have been developed in the literature, they may not be directly applicable to controlling PEV power. This is mainly because unlike the ESS that can be used solely for system regulation purpose, the PEV charging control needs to not only provide the desired system regulation but also fulfill the PEV charging requirements satisfactorily. Since the varying WP is a major contributor to the URC operations, the uncertainty in WP forecast should be properly handled to avoid over/under use of the PEV demand response. The overuse often leads to unnecessary loss of charging energy, while the underuse weakens the effectiveness of the PEV-aided URC mitigation. Therefore, the objective of the proposed hierarchical PEV power control scheme is to reduce the URC operations effectively with an acceptable sacrifice of PEV charging energy.

Besides the technical aspects, large-scale WP integration also has a noticeable impact on power system economy. One important cost is the wind power uncertainty cost (WPUC), which is incurred to the power system when it accommodates the WPUnV. The primary source of WPUC is the unscheduled use of the expensive fast-reacting generators. Besides, the cost associated with the generators' cycling operations is another non-negligible part of the WPUC, especially when the system integrates significant WP. DR has been widely proposed to cope with WPUnV such that extensive use of fast-reacting plants can be avoided. The authors in [49] evaluated the cost saving opportunities introduced by demand shifting in a system with abundant WP and found that up

to 30% cost saving can be achieved. In [73] and [74], indirect load control through real-time pricing was shown to be able to effectively decrease the WP integration cost. Similarly, the authors in [75] included price-elastic load in short-term generator scheduling, showing that WPUnV can be managed by DR more economically. Direct load control over electric water heaters was proposed in [76] to facilitate WP integration. Nevertheless, none of these studies has taken the generator cycling cost into consideration. Consequently, the cost of WP integration can be underestimated. Besides, the responsive demand is modeled simply in these studies without considering the characteristics of specific load type, and ideal load control is assumed with a lack of specific and implementable load control method. As a result, it is difficult to assess the exact response of the controllable load. Instead this thesis focuses on a specific type of load, i.e. the PEV, and investigates the effect of controlled PEV charging load on the WPUC.

1.3 Primary Contributions

First, a real-time scheduling scheme for PEV charging in low-voltage residential distribution systems is proposed. This scheduling scheme can be used either to minimize system losses or to avoid over-low voltage, depending on whether the voltage drop is a binding constraint or not. Biased PEV charging in accordance with the owners' charging requirements is realized in the proposed scheduling scheme. Moreover, due to its fast execution speed, the proposed scheduling scheme is scalable to increased number of PEVs and suitable for coordinating frequent PEV arrivals and departures in real time.

The charging control in the real-time scheduling scheme is centralized and hard to be applied to a large number of dispersedly located PEVs. To make the PEV power controllable for system regulation purpose, a decentralized PEV charging control scheme is proposed. The scheme is then applied to control PEV power to counterbalance undesired WP fluctuations so as to enhance the load

frequency control. Individual PEV under the proposed decentralized charging control adjusts its power autonomously based on two system-level directional signals and also its own urgency level of charging. The actual PEV power can track the target value requested for system regulation purpose timely and accurately. Also, differential allocation of compensating duties among PEVs can be realized to help satisfy the heterogeneous charging requirements. Simulation results show that with the proposed decentralized charging control, the undesired WP fluctuations can be largely compensated by the PEV power. As a result, frequency deviations induced by unstable WP are effectively alleviated.

With the objective of utilizing PEV power to hedge against the wind-induced URC operations, a 3-level hierarchical scheme is proposed to schedule, dispatch, and control the PEV power. The URC operation is explicitly defined and modeled. The uncertainty of WP forecast is considered by using WP uncertainty intervals. The PEV charging load is firstly scheduled in a conservative manner to ensure the effectiveness of the URC operation mitigation. Then, a mechanism of exempting over-scheduled anti-URC regulation onus on PEVs is deployed to reduce PEV charging energy losses. Compared with other benchmark schemes, simulation results show that the proposed scheme is more effective at mitigating URC operations while most of the desired PEV charging energy can be preserved to satisfy the charging requirements for the majority of PEVs. Moreover, the proposed scheme is shown to be more robust to severe WP fluctuations in unstable fast-moving weather condition, which indicates its greater capability to withstand WP forecast errors. An ex post facto cost analysis proves the economic viability of the proposed scheme.

Finally, a comprehensive WPUC model is proposed in which generator cycling costs are integrated. To accurately evaluate how the controlled PEV charging would affect the WPUC, perfect DR is not assumed. Instead, the decentralized PEV charging control scheme developed in Chapter III is adopted to model the exact behavior of the responsive PEV load. With the WPUnV

decomposed into two components, namely hourly WP forecast errors and sub-hourly WP fluctuations, the uncertainty costs raised by each of the components are evaluated. Simulations results showed that the controlled PEV charging load only has minor effect on reducing the WPUC induced by hourly WP forecast errors, while its value in mitigating the WPUC associated with sub-hourly WP fluctuations is much more significant.

1.4 Thesis Layout

The rest of this thesis consists of five chapters. Chapter II shows the development of the real-time scheduling scheme for PEV charging in low-voltage residential distribution systems. Chapter III proposes the decentralized PEV charging control scheme and demonstrates its application to counterbalance unexpected WP fluctuations. Chapter IV presents the hierarchical scheme for utilizing PEV power to hedge against the URC operations. Chapter V investigates the effects of controlled PEV charging load on reducing the WPUC. Finally, the conclusions of the thesis are drawn in Chapter VII with suggestions on the future work.

1.5 List of Publications

Journal paper

1. X. Luo, K. W. Chan, "Real-time scheduling of electric vehicles charging in low-voltage residential distribution systems to minimize power losses and improve voltage profile," *IET Generation, Transmission & Distribution*, vol. 8, no. 3, pp. 516-529, Mar. 2014.
2. X. Luo, S. W. Xia, and K. W. Chan, "A decentralized charging control strategy for plug-in electric vehicles to mitigate wind farm intermittency and

enhance frequency regulation," *Journal of Power Sources*, vol. 248, pp. 604-614, Feb. 2014.

3. S. W. Xia, X. Luo, and K. W. Chan, "Probabilistic transient stability constrained optimal power flow for power systems with multiple correlated uncertain wind generations," *IEEE Transactions on Sustainable Energy*, in press.
4. X. Luo, S. W. Xia, and K. W. Chan, "A hierarchical scheme for utilizing plug-in electric vehicle power against wind-induced unit ramp cycling operations," submitted to *IEEE Transactions on Power Systems*, TPWRS-00487-2016.
5. X. Luo, K. W. Chan, and M. W. Qin, "Effects of controlled PEV charging on wind power uncertainty cost," submitted to *IET Generation, Transmission & Distribution*, GTD-2016-0431.
6. S. W. Xia, X. Luo, K. W. Chan, M. Zhou, and G. Y. Li, "Optimal sizing of energy storage system for power grid planning with intermittent wind generations," in preparation for submission to *The International Journal of Energy*.
7. M. W. Qin, K. W. Chan, C. Y. Chung, X. Luo, and Ting Wu, "Optimal planning and operation of energy storage systems in radial networks for wind power integration with reserve support," *IET Generation, Transmission & Distribution*, in press.

Conference paper

8. X. Luo, S. W. Xia, and K. W. Chan, "A simple decentralized charging control scheme of plug-in electric vehicles for alleviating wind farm intermittency," *The 6th International Conference on Applied Energy*, May 30-June 2, 2014, Taipei, Taiwan.

9. S. W. Xia, X. Luo, and K. W. Chan, "A framework for self-healing smart grid with incorporation of multi-agents," *The 6th International Conference on Applied Energy*, May 30-June 2, 2014, Taipei, Taiwan.

Chapter II

Real-Time Scheduling of PEV Charging in Low-Voltage Residential Distribution Systems to Minimize Power Losses and Improve Voltage Profile

2.1 Introduction

One of the main places where PEVs will be charged is at home. Random unscheduled PEV charging at home may significantly stress the low-voltage residential distribution system, causing problems such as increased peak load and losses, excessive voltage drop and branch overloading [53-56]. However, with proper coordination of the PEV charging activities, the existing network infrastructure should be able to accommodate larger PEV charging load. In this chapter, a real-time scheduling scheme would be proposed for PEV charging in low-voltage residential distribution feeder. This scheme schedules PEV charging to either minimize system losses or prevent over-low voltage, depending on whether the PEV penetration level is high enough to make the voltage drop become the binding constraint. It has been shown in [77, 78] that when the PEV load is controlled to flatten the system voltage profiles, the voltage safety margin can be significantly enlarged compared with the random simultaneous PEV charging. It has also been proved in [79] that a PEV charging profile which minimizes system load variance can approximately minimize circuit losses. The scheduling scheme in [79], however, treated PEV charging at different nodes of the feeder equally when levelling system load profile, without considering the impact of PEV charging location on the network voltage drop. In fact, the distribution of PEV charging locations does affect the voltage at each node of the

network. For example, PEV charging located near the extremities of a radial feeder is more likely to incur excessive voltage drop than located near the sending end of the feeder. Since most often voltage drop would become the binding constraint when a low-voltage distribution feeder is subject to high-penetration PEV load [80], in the proposed scheduling scheme, an scheduling method which considers the impact of charging location on the network voltage drop is first developed to level the system voltage profiles, and then a novel factor is derived to allow adaptive switching of the PEV charging plan from being voltage-safety-oriented (to level voltage profiles) to loss-minimization-oriented (to level system load profile), or vice versa. Because of the simplicity of the proposed scheduling scheme, it is fast enough for real-time application to deal with frequent dynamic PEV arrivals and departures.

2.2 The Proposed Scheduling Scheme

2.2.1 Voltage Deviation Impact Index

In this study, the topology of the IEEE 37-node test feeder is adopted to represent a residential radial distribution feeder, which is shown in Fig. A.1. The network voltage level is downscaled from 4.8 kV to 220 V. For such a low-voltage radial feeder, an approximately linear relation between the node voltage and the node load has been reported in [80, 81]. This relation is due to high R/X ratio at the distribution level [82]. The voltage sensitivity at one node on a phase to the load change at any node on the same or another phase can be predetermined by performing a series of three-phase unbalanced load flow analyses. In this study, the power flow analyses are solved by using the forward-backward sweep method proposed in [83]. At each node on a phase, the expected PEV charging load in conjunction with the base load is added incrementally and the voltage variations at all nodes on the same phase are recorded to produce the following voltage sensitivity matrix:

$$\begin{bmatrix} \mu_{11} & \mu_{12} & \cdots & \mu_{1n} \\ \mu_{21} & \mu_{22} & \cdots & \mu_{2n} \\ \vdots & \vdots & \ddots & \vdots \\ \mu_{n1} & \mu_{n2} & \cdots & \mu_{nn} \end{bmatrix} \tag{2.1}$$

where $\mu_{ij} = (V_{\text{ref}} - V_j) / P_i$; n is the number of nodes; and μ_{ij} represents the voltage sensitivity at node j to the power at node i on the same phase, i.e., the voltage drop at node j caused by unit power consumed at node i on the same phase. In this work, the sending end voltage at node 1 is chosen as the reference voltage V_{ref} with fixed nominal magnitude of 1 pu. Though these sensitivities would vary with system loads, their variations are insignificant and they can be adopted approximately as constants to conveniently evaluate the impacts of PEV charging at one node of a phase on the voltage drop at any node on that phase. Besides, it is worth noting that due to unbalanced phase loading on a distribution network, the load change on one phase would affect not only the voltage on that phase but also the voltage on the other phases, resulting in different voltage values at one node for each phase. However, since the mutual impedances between phases are usually small when compared with the self-impedances of each phase [80, 81], the voltage-to-load sensitivities between nodes across phases are relatively insignificant in comparison with the sensitivities between nodes on the same phase as verified in Section 2.4.1. Therefore, for simplicity, the PEV charging scheduling will be considered only on individual phase in this study.

A voltage deviation impact index (VDII) μ_i can then be defined as the sum of all voltage sensitivities to the load change at node i:

$$\mu_i = \sum_{j=1}^{n} \mu_{ij} \tag{2.2}$$

This index measures to what extent the load at a given node would affect the voltage at all nodes on the same phase of the feeder, and could be used to schedule PEV charging for levelling node voltage profiles. The variation of VDII with daily system load will be illustrated in Section 2.4.1.

2.2.2 Method of Voltage Profile Levelling

The voltage profile at a node can be levelled by levelling the voltage deviation from the network's nominal voltage at that node. For the low-voltage radial feeder considered in this study, the voltage at one node on a phase mainly depends on the voltage at its predecessor on the same phase and the voltage drop on the line section between them. The voltage deviation at each of the individual nodes will therefore share a similar profile to the total voltage deviation of the phase. The total voltage deviation of a phase is defined as the sum of voltage deviations at all nodes on that phase. In the proposed scheduling scheme, the total voltage deviation due to base load is first calculated as:

$$\Delta V_{\text{Devi (base)},t} = \sum_{i=1}^{n} P_{\text{base},i,t} \cdot \mu_i \tag{2.3}$$

where $P_{\text{base},i,t}$ is the forecasted base load at node i at time t. As an example, Fig. 2.1 shows a typical plot of the sum of voltage deviations at all nodes on a phase due to base load from 18:00 h to 06:00 h the next day.

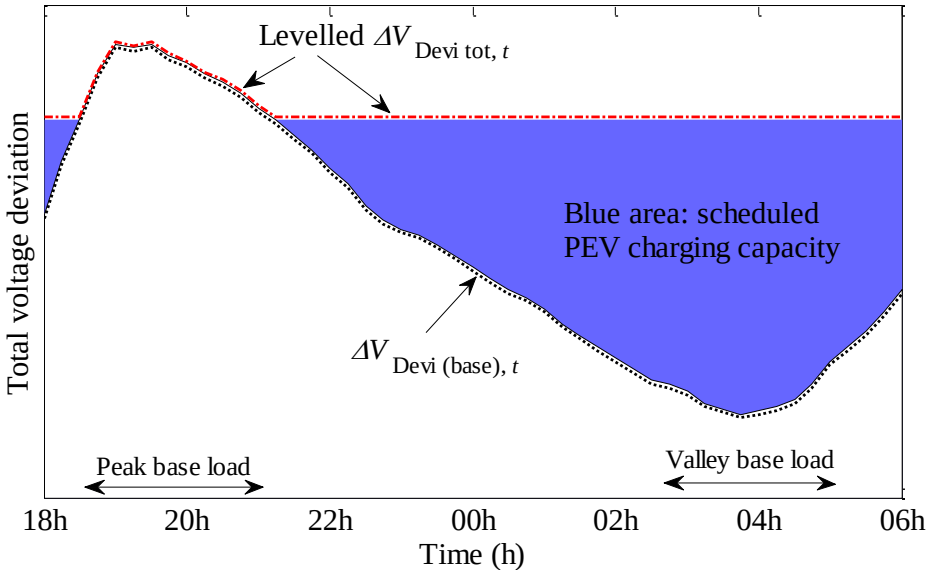

Fig. 2.1 Illustration of $\Delta V_{\text{Devi (base)},t}$ and levelled $\Delta V_{\text{Devi tot},t}$

Next, after the PEV load is added, the sum of voltage deviations at all nodes becomes:

$$\Delta V_{\text{Devi tot},t} = \Delta V_{\text{Devi (base)},t} + \Delta V_{\text{Devi (PEV)},t} = \sum_{i=1}^{n} P_{\text{base},i,t} \cdot \mu_i + \sum_{i=1}^{n} P_{\text{PEV},i,t} \cdot \mu_i \qquad (2.4)$$

where $P_{\text{PEV},i,t}$ is the PEV load at node i at time t. Consider a group of PEVs which are plugged in at time t_0 and plan to depart at time T. Integrating both sides of (2.4) gives

$$\int_{t=t_0}^{T} \Delta V_{\text{Devi tot},t}\ dt = \int_{t=t_0}^{T} \Delta V_{\text{Devi (base)},t}\ dt + \int_{t=t_0}^{T} \Delta V_{\text{Devi (PEV)},t}\ dt. \qquad (2.5)$$

The first integral term on the right-hand side (RHS) of (2.5) represents the area bounded by the curve of $\Delta V_{\text{Devi (base)},t}$ and the t-axis. The second integral term can be calculated as

$$\begin{aligned} &\int_{t=t_0}^{T} \Delta V_{\text{Devi (PEV)},t}\ dt = \int_{t=t_0}^{T} \left[\sum_{i=1}^{n} \left(P_{\text{PEV},i,t} \cdot \mu_i \right) \right] dt \\ &= \sum_{i=1}^{n} \left(\mu_i \cdot \int_{t=t_0}^{T} P_{\text{PEV},i,t}\ dt \right) = \sum_{i=1}^{n} \left(E_{\text{PEV},i} \cdot \mu_i \right) \end{aligned} \qquad (2.6)$$

where $E_{\text{PEV},i}$ is the required amount of charging energy to bring the PEV at node i to its desired battery SOC upon its expected departure time.

After the two integral terms on the RHS of (2.5) are calculated, a voltage deviation level L can be determined iteratively to obtain the levelled sum of voltage deviations at all nodes (i.e. the levelled $\Delta V_{\text{Devi tot},t}$ which is denoted by $\Delta V_{\text{Leveled Devi tot},t}$) such that the area between the $\Delta V_{\text{Leveled Devi tot},t}$ curve and the $\Delta V_{\text{Devi (base)},t}$ curve is equal to the integral of $\Delta V_{\text{Devi (PEV)},t}$, as shown in blue in Fig. 2.1. The iterative algorithm for calculating L is shown as follows.

Define **M** as the set of nodes with PEV connected, and

$P_{\text{PEV}}^{\max}$ as the maximum allowable PEV charging power.

Calculate the initial value of L:

$$L^{(1)} = \left(\int_{t=t_0}^{T} \Delta V_{\text{Devi (base)},t}\ dt + \int_{t=t_0}^{T} \Delta V_{\text{Devi (PEV)},t}\ dt \right) / \left(T - t_0 \right).$$

For $t_0 \le t \le T$,

If $L^{(1)} \le \Delta V_{\text{Devi (base)},t}$,

$\Delta V_{\text{Leveled Devi tot},t} = \Delta V_{\text{Devi (base)},t}$;

else

$$\Delta V_{\text{Leveled Devi tot},t} = \min\left(L^{(1)}, \Delta V_{\text{Devi (base)},t} + \sum_{j\in \text{M}} (P_{\text{PEV}}^{\max} \cdot \mu_j) \right)$$

end

Define $\varepsilon = \int_{t=t_0}^{T} \left(\Delta V_{\text{Leveled Devi tot},t} - \Delta V_{\text{Devi (base)},t} \right) dt - \int_{t=t_0}^{T} \Delta V_{\text{Devi (PEV)},t}\ dt$ and set i = 1.

While $|\varepsilon| > \varepsilon_{\text{stop}}$ **do**

$L^{(i+1)} = L^{(i)} - \varepsilon / (T - t_0)$;

Set $\Delta V_{\text{Leveled Devi tot},t} = \begin{cases} \min\left(L^{(i+1)}, \Delta V_{\text{Devi (base)},t} + \sum_{j\in \text{M}} (P_{\text{PEV}}^{\max} \cdot \mu_j) \right), & L^{(i+1)} > \Delta V_{\text{Devi (base)},t} \\ \Delta V_{\text{Devi (base)},t}, & L^{(i+1)} \le \Delta V_{\text{Devi (base)},t} \end{cases}$;

Update $\varepsilon = \int_{t=t_0}^{T} \left(\Delta V_{\text{Leveled Devi tot},t} - \Delta V_{\text{Devi (base)},t} \right) dt - \int_{t=t_0}^{T} \Delta V_{\text{Devi (PEV)},t}\ dt$;

$i = i + 1$.

end

Next, the charging rate for each PEV at each time step can be derived. The blue area in Fig. 2.1 indicates the scheduled PEV charging capacity in terms of total voltage deviation. At time t, the scheduled charging capacity in terms of energy can be obtained as follows:

$$dE_{\text{PEV}} = \left(\Delta V_{\text{Leveled Devi tot},t} - \Delta V_{\text{Devi (base)},t} \right) \cdot dt \Big/ \sum_{i=1}^{n} \left(E_{\text{PEV},i} \cdot \mu_i \right) \cdot \sum_{i=1}^{n} E_{\text{PEV},i} \qquad (2.7)$$

The PEV at node m would share this dE_{PEV} pro rata to its required amount of energy over the total required amount of energy of all PEVs, that is,

$$dE_{\text{PEV},m} = dE_{\text{PEV}} \cdot \left(E_{\text{PEV},m} \Big/ \sum_{i=1}^{n} E_{\text{PEV},i} \right) \qquad (2.8)$$

Substitute (2.7) into (2.8) to obtain the scheduled charging power for the PEV at node m at time t:

$$P_{\text{PEV},m,t} = \frac{dE_{\text{PEV},m}}{dt} = \frac{\left(\Delta V_{\text{Leveled Devi tot},t} - \Delta V_{\text{Devi (base)},t}\right)}{\sum_{i=1}^{n}\left(E_{\text{PEV},i} \cdot \mu_i\right)} \cdot E_{\text{PEV},m} \tag{2.9}$$

As can be seen from (2.9), to execute a scheduled charging plan on a group of PEVs which have the same or very close expected departure time, the controller only needs to form and send one charging power dispatch signal to all group members. This signal is the algebraic fraction in (2.9). Upon receiving this signal, each PEV can attain its charging power based on its required amount of energy. Thus, the communication burden on the controller can be mitigated. When there is more than one PEV group, the following is the dispatch signal for PEV group *k* at time *t*:

$$P_{\text{PEV},m,t} = \underbrace{\frac{\left(\Delta V_{\text{Leveled Devi tot},t} - \Delta V_{\text{Devi (base)},t}\right) \cdot \sum_{i=1}^{n} E_{\text{PEV},i}}{\sum_{i=1}^{n}\left(E_{\text{PEV},i} \cdot \mu_i\right) \cdot \sum_{j \in G_k} E_{\text{PEV},j}} \cdot p_k}_{\text{the charging power dispatching signal for PEV group } k \text{ at } t} \cdot E_{\text{PEV},m} \tag{2.10}$$

where G_k represents the PEV group *k*; p_k is a proportion dictating PEV group *k*'s share of the total scheduled charging capacity at time *t*. The determination of p_k will be covered in Section 2.2.4.

The number of PEV groups can be reduced further by grouping the PEVs having close expected departure times. For example, PEVs with expected departure time falling in the time interval *[T:T+0.5)* can be grouped together and regarded to have a common expected departure time *T*. The grouping can effectively ease the computation and communication burden of the controller without compromising the satisfaction of PEV charging requirements.

2.2.3 Power/Voltage Levelling Factor

The voltage profile levelling method can considerably enlarge the safety margin with respect to voltage drop limit, which is critical when PEV penetration level is high enough to make voltage drop become a binding constraint. On the other hand, when PEV penetration level is relatively low, minimizing circuit

losses would become the higher priority in PEV charging load scheduling. As proved in [79], losses minimization in a low-voltage radial feeder can be closely approached by system load levelling. In this section, the power/voltage levelling factor (PVLF) will be derived to enable convenient shift between loss-minimization-oriented scheduling and voltage-safety-oriented scheduling, depending on the PEV penetration level.

It should be noted that the levelled profile of the total voltage deviation of all nodes ($\Delta V_{\text{Leveled Devi tot},t}$) does not necessarily lead to levelled load profile. The reason is as follows.

Suppose from time instant t_k to t_{k+1} there are m PEVs being charged at nodes 1–m and the change in base load at node i is $\Delta P_{\text{base},i}$. In order to realize the $\Delta V_{\text{Leveled Devi tot},t}$ from t_k to t_{k+1}, the PEV load should change accordingly to satisfy

$$\sum_{i=1}^{n} -\left(\Delta P_{\text{base},i} \cdot \mu_i\right) = \sum_{j=1}^{m} \left(\Delta P_{\text{PEV},j} \cdot \mu_j\right) \tag{2.11}$$

where $\Delta P_{\text{PEV},j}$ is the change in the PEV load at node j. Since m is not necessarily equal to n and the change in PEV load does not necessarily match with the change in base load at any given node, most often the following inequality will hold:

$$\sum_{i=1}^{n} -\Delta P_{\text{base},i} \neq \sum_{j=1}^{m} \Delta P_{\text{PEV},j} \tag{2.12}$$

Therefore, $\Delta V_{\text{Leveled Devi tot},t}$ may not lead to the levelled system load profile.

Devising the PVLF

Suppose PVLF is used to modify the process of voltage-safety-oriented scheduling for system load profile levelling, from t_k to t_{k+1}:

$$PVLF \cdot \sum_{i=1}^{n} -\left(\Delta P_{\text{base},i} \cdot \mu_i\right) = \sum_{j=1}^{m} \left(\Delta P'_{\text{PEV},j} \cdot \mu_j\right) \tag{2.13}$$

such that

$$\sum_{i=1}^{n} -\Delta P_{\text{base},i} = \sum_{j=1}^{m} \Delta P'_{\text{PEV},j} \tag{2.14}$$

where $\Delta P'_{\mathrm{PEV},j}$ denotes the change in PEV load at node *j*.

As indicated in (2.13) and (2.14), the value of PVLF depends on the base load changes and needs to be calculated at every time step. Though measuring the base load changes in real-time could be supported in future smart girds equipped with advanced metering infrastructure and home area network, this is not assumed here so as to make the PVLF usable for even the existing systems. Further, the PVLF will be approximated as a constant such that it can be predetermined for convenient use in the scheduling.

As indicated by (2.3), the forecasted load profile at each node is needed to calculate the sum of voltage deviations at all nodes caused by base load ($\Delta V_{\mathrm{Devi\,(base)},t}$). However, given the uncertainties in the time of use and the loading of the devices/appliances in each household, it would be difficult and impractical to forecast individual household load profile. Instead, only the aggregate system load profile could be forecasted with acceptable accuracy, and in the scheduling process, each household is regarded to have a common load profile which is the forecasted aggregate system load profile averaged down to each household. Under this assumption, at each time step the base load changes at all nodes can be regarded as approximately equal:

$$\Delta P_{\mathrm{base},1} \approx \Delta P_{\mathrm{base},2} \approx \cdots \approx \Delta P_{\mathrm{base},n} = \Delta P_{\mathrm{base}} \tag{2.15}$$

Therefore, (2.14) becomes:

$$\Delta P_{\mathrm{base}} = -\frac{1}{n}\sum_{j=1}^{m} \Delta P'_{\mathrm{PEV},j} \tag{2.16}$$

Substitute (2.15) and (2.16) into (2.13) and solve the PVLF:

$$PVLF = n\sum_{j=1}^{m}\left(\Delta P'_{\mathrm{PEV},j}\cdot\mu_j\right) \Bigg/ \left(\sum_{j=1}^{m}\Delta P'_{\mathrm{PEV},j}\cdot\sum_{i=1}^{n}\mu_i\right) \tag{2.17}$$

According to (2.10)

$$\Delta P'_{\mathrm{PEV},j} = P_{\mathrm{PEV},j,t_{k+1}} - P_{\mathrm{PEV},j,t_k} \propto E_{\mathrm{PEV},j} \tag{2.18}$$

Substituting (2.18) into (2.17) gives:

$$PVLF = \frac{n\sum_{j=1}^{m}\left(E_{\mathrm{PEV},j}\cdot\mu_j\right)}{\sum_{j=1}^{m}E_{\mathrm{PEV},j}\cdot\sum_{i=1}^{n}\mu_i} \tag{2.19}$$

As can be seen from (2.19), the derived PVLF only depends on the required amount of energy of each PEV and the VDIIs of the nodes. Therefore, it can be predetermined as a constant when used in the scheduling. It is worth pointing out that different and non-smooth load profiles of the households in reality could make the PVLF calculated by (19) inaccurate in some time steps during the charging period. Nevertheless, without needing to measure the household load changes in real-time, the predetermined constant PVLF is simple to calculate and convenient to use for the scheduling. Simulations in Section 2.4.5 showed that the predetermined PVLF can indeed be used to approximately level the system load profile over the entire charging period even when realistic non-smooth base load profiles are considered.

Applying the PVLF in the Scheduling

Here, the PVLF is used to modify (2.5) and (2.10) in the previous scheduling. First, when $\Delta V_{\text{Leveled Devi tot},t}$ is attempted, the area bounded by the curve of $\Delta V_{\text{Leveled Devi tot},t}$ and t-axis is calculated as

$$\begin{aligned}\int_{t=t_0}^{T}\Delta V_{\text{Leveled Devi tot},t}\ dt = &\int_{t=t_0}^{T}\Delta V_{\text{Devi (base)},t}\ dt \\ &+\frac{1}{PVLF}\int_{t=t_0}^{T}\Delta V_{\text{Devi (PEV)},t}\ dt\end{aligned} \tag{2.20}$$

Then, the charging power for PEV at node m at time t expressed in (2.10) is modified as

$$P'_{\mathrm{PEV},m,t} = PVLF\cdot P_{\mathrm{PEV},m,t} \tag{2.21}$$

The way of applying the PVLF in the scheduling would keep the scheduled charging capacity, as indicated by the blue area in Fig. 2.1, unchanged irrespective of the PVLF's value such that all PEVs can be charged to their

desired SOC. What has been changed is the instantaneous charging rate of each PEV so as to level the system load profile.

Effects of Applying the PVLF in the Scheduling Process

When the PVLF is used in the scheduling, typical changes in $\Delta V_{\text{Leveled Devi tot},t}$ and the system load profile are shown in Fig. 2.2. Without using the PVLF (i.e. PVLF set to 1), the total voltage deviation is levelled at a compromise on the load levelling. Conversely, when the PVLF calculated by (2.19) is applied to the scheduling, the load levelling can be realized while some variations appear in the profile of total voltage deviation.

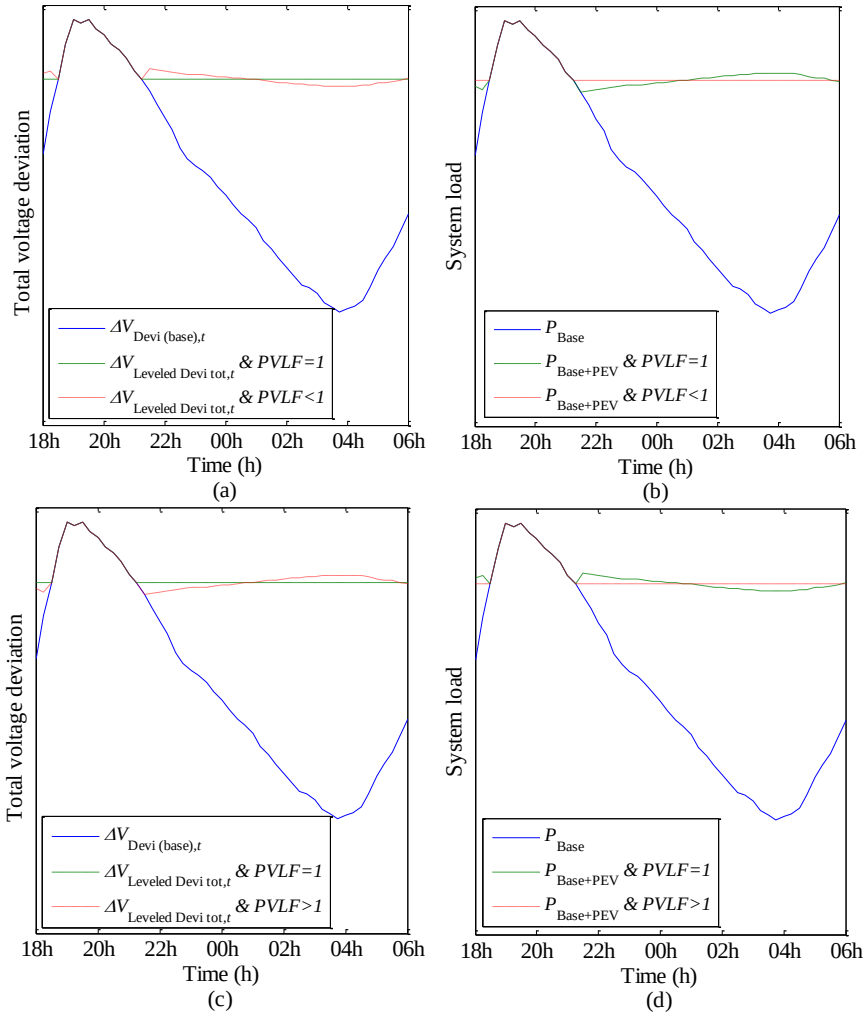

Fig. 2.2 Typical changes in $\Delta V_{\text{Leveled Devi tot},t}$ and the system load profile caused by applying the PVLF. Subfigure (a) and (b): $PVLF < 1$; (c) and (d): $PVLF > 1$

During the scheduling, if the lower voltage constraint is violated at a certain node, the PVLF shall be adjusted to shift the scheduling to be more voltage-safety-oriented until voltages at all nodes are maintained within tolerable limit.

2.2.4 Real-Time Scheduling

Real-time scheduling deals with random arrivals and departures of PEV. Whenever a PEV is plugged-in or out at a certain node, the scheduling shall be performed to update the charging plan.

To respect PEV owner's autonomy, a PEV owner can specify his/her expected departure time and desired final SOC. If the desired final SOC cannot be satisfied before the expected departure time even if the PEV is charged at its maximum allowable power, then this PEV is classified as 'unschedulable'; otherwise, it is 'schedulable'. Unschedulable PEVs take the maximum allowable charging rate and are treated as part of the base load in the scheduling.

The schedulable PEVs are further divided into groups. PEVs belonging to a certain group have the same or very close expected departure time. The next step of scheduling is to calculate $\Delta V_{\text{Leveled Devi tot},t}$ with the latest expected departure time which is regarded as the end of the scheduling horizon. The scheduled charging capacity is then distributed to the PEV groups in a discriminate manner. For example, as illustrated in Fig. 2.3, there are three groups of PEVs. The group with the earliest expected departure time is given sufficient scheduled charging capacity in time interval 1 (18h−02h). Subsequently, the group with the second earliest expected departure time is assigned sufficient scheduled charging capacity from the remains in time interval 1 and 2 (18h−04h). Finally, the group with the latest expected departure time utilizes the remaining scheduled charging capacity in time interval 1, 2 and 3 (18h−06h). As a result, in each time interval a proportion which dictates respective PEV group's share of the scheduled charging capacity can be determined.

In Fig. 2.3, after the amount of energy scheduled for charging is determined in each time interval, the corresponding PVLFs can be calculated in each time interval. Then the charging rate of each schedulable PEV can be determined by (2.21). One run of the scheduling is completed.

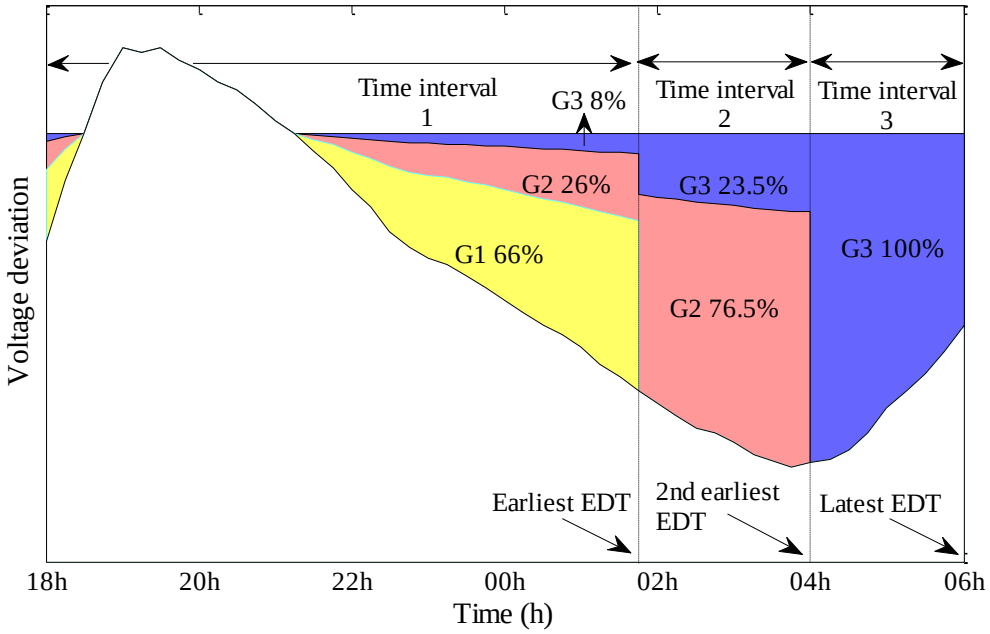

Fig. 2.3 An example of PEV groups' share of scheduled charging capacity biased by different expected departure time (EDT). G1, G2 and G3: PEV group 1, 2 and 3 with the earliest, second earliest and latest EDT, respectively.

Finally, the scheduling scheme would conduct three-phase unbalanced load flow analyses to check the voltage drop at each node. If the voltage limit is violated at some nodes, the PVLF will be reduced and the PEV charging will be rescheduled.

Fig. 2.4 shows the flow chart of the proposed real-time PEV charging scheduling scheme. It shall be noted that this scheduling scheme is based on the forecasted aggregate system load as forecasting individual household load profile is tedious and impractical. In the scheduling process when $\Delta V_{\text{Devi (base)},t}$ is calculated, each node is regarded to have a common load profile which is the forecasted aggregate load profile averaged down to each household. The

effectiveness of this proposed scheduling scheme subjected to household load uncertainties will be illustrated in Section 2.4.5.

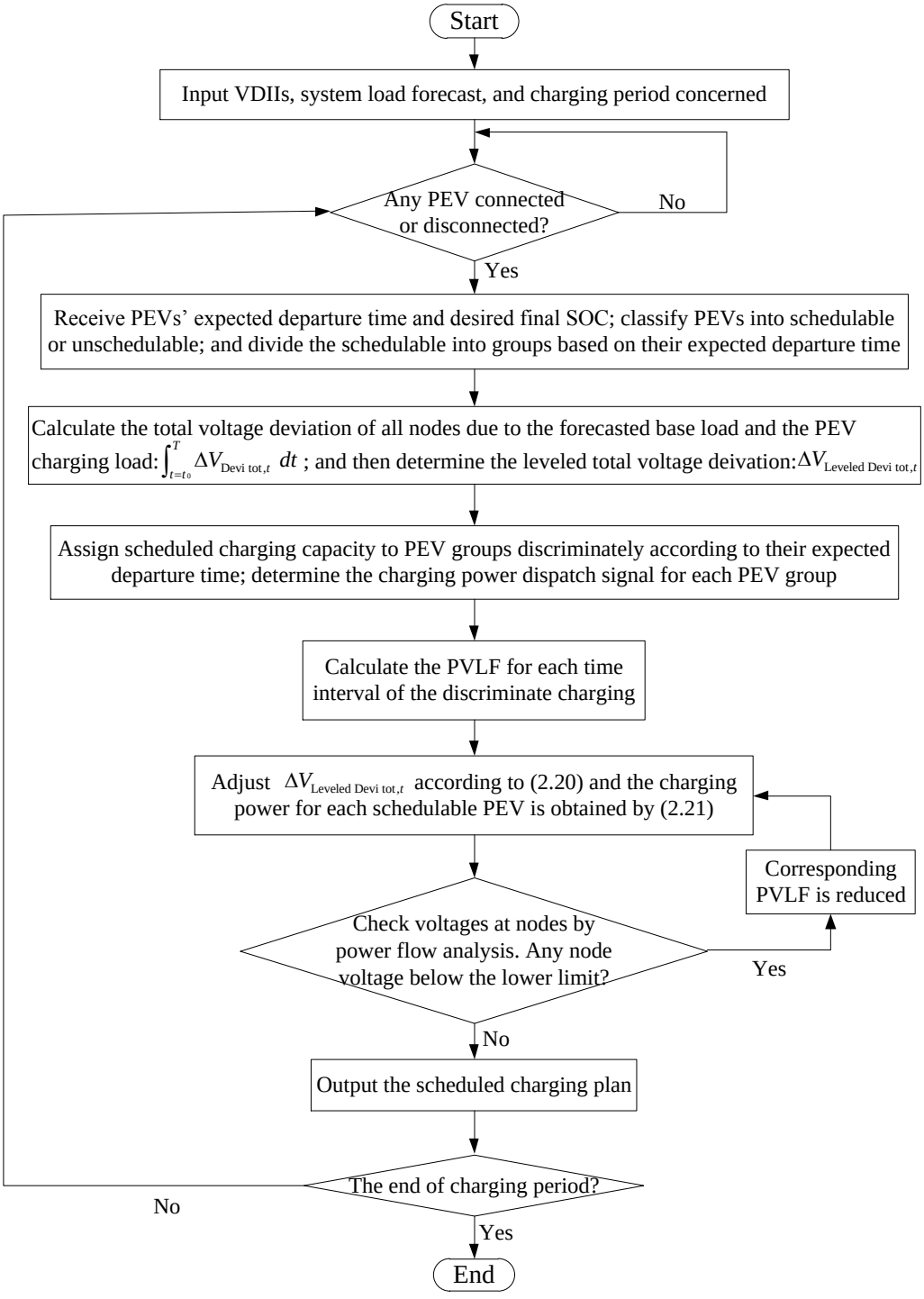

Fig. 2.4 The flow chart of the proposed real-time PEV charging scheduling scheme

2.3 Modeling of the Test System

2.3.1 Test Network

The topology of the IEEE 37-node test feeder [84], shown in Fig. A.1, is used to represent the low-voltage residential distribution feeder in the simulation. It operates at a nominal voltage of 220V with a voltage drop tolerance of 10%. The line impedances, including self-impedance Z_{self} of each phase and mutual impedance Z_{mutual} between phases, are adapted such that at peak base load the lowest node voltage is about 0.906 pu. The impedance data is recorded in Table A.1. Voltage at the root node (node 1) is fixed at 1 pu, serving as reference to voltage deviations at the other nodes. Except for the root node, each node of Phase A, B and C is equipped with a base load profile.

2.3.2 Base Load, Charging Load and Charging Period

In the case studies, both ideal and practical base load profiles would be used. As shown in Fig. 2.5, ideal base load profiles are smooth and would be used for clear illustration of the proposed scheduling scheme. From the basic ideal base load profile, plotted as the solid curve in Fig. 2.5, two additional profiles are generated by shifting the time ±1h. Each node on Phase A, B and C is randomly assigned with one of the three profiles when the ideal base load is used for simulation. Practical base load profiles are generated using the residential load model proposed in [85], which takes into account the use of common domestic devices/appliances such as cooking appliances, air conditioner, washer/dryer and electric water heater. Fig. 2.6 shows some of the generated practical household load profiles and the aggregate system load profile of Phase A used in the case studies. These practical base load profiles are used to investigate the performance of the proposed scheduling scheme subjected to household load uncertainties. In the simulation, each node on Phase A, B and C is randomly assigned with one of the practical profiles. The base load is modelled as a combination of 70%

constant power load and 30% constant impedance load. The power factor is set at 0.95 inductive.

By considering a standard single-phase 220V/13A outlet, the maximum PEV charging power $P_{\mathrm{PEV}}^{\max}$ is set as 2.86 kW. The PEV battery capacity is 14 kWh and the charger efficiency is assumed to be 90%. The charging period investigated starts from 5 pm until 8 am the next day and consists of 5-min timeslots. Besides, the real-time scheduling is also applied to cover a whole day period in Section 2.4.4.

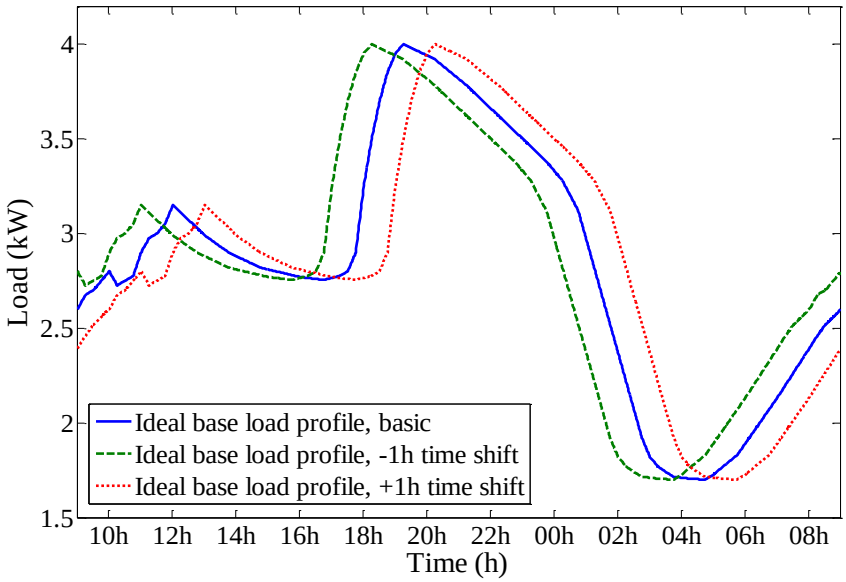

Fig. 2.5 Ideal daily base load profiles

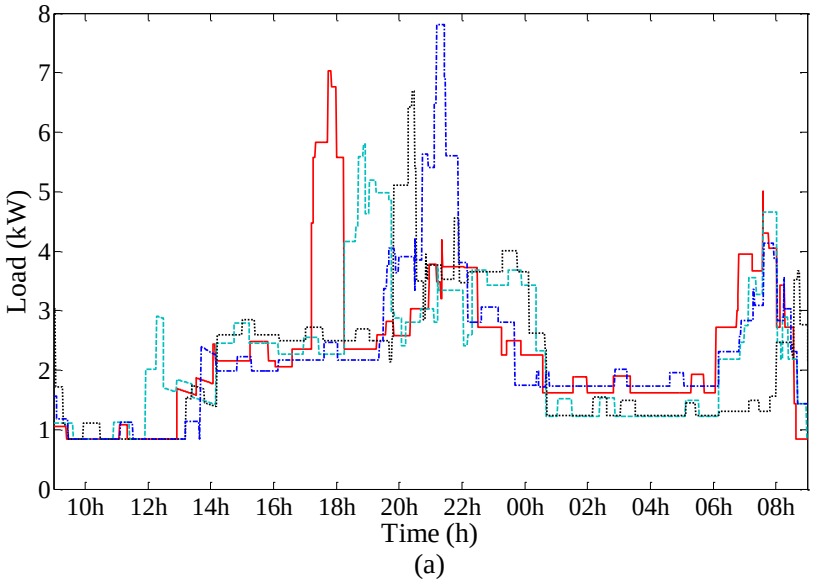

(a)

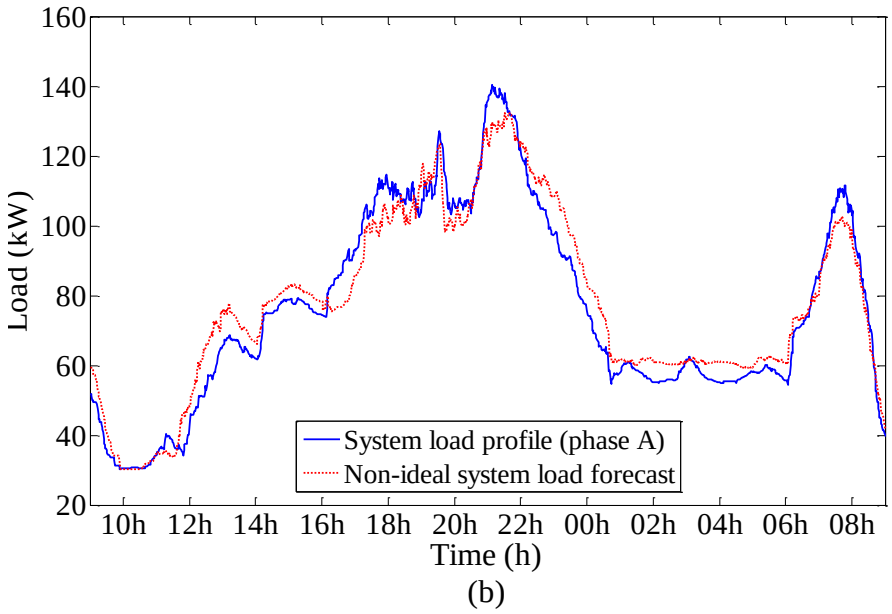

Fig. 2.6 Practical daily base load profiles: (a) some of the base load profiles for individual household; (b) the aggregate system load profile of Phase A and the non-ideal system load forecast

2.4 Results

2.4.1 Investigation on Voltage-to-Load Sensitivities and VDIIs

This section investigates the on-phase and across-phase voltage-to-load sensitivities, and shows how the values of VDII vary with the system load.

The practical base load profiles are used here. For each snapshot of the load profiles, stepwise increments are applied to the base load at each node of Phase A. Three-phase unbalanced load flow analyses are conducted to calculate the on-phase and across-phase voltage-to-load sensitivities. Once the sensitivity matrix in (2.1) is formed, VDIIs can be calculated by (2.2).

Fig. 2.7 plots the voltage variations at several selected nodes on different phases when the load at node 35 on Phase A is increased. The results presented in Fig. 2.7(a) show the adequacy of the assumed linear relation between the node voltages and the loads on the same phase. Fig. 2.7(a) also shows that voltages at

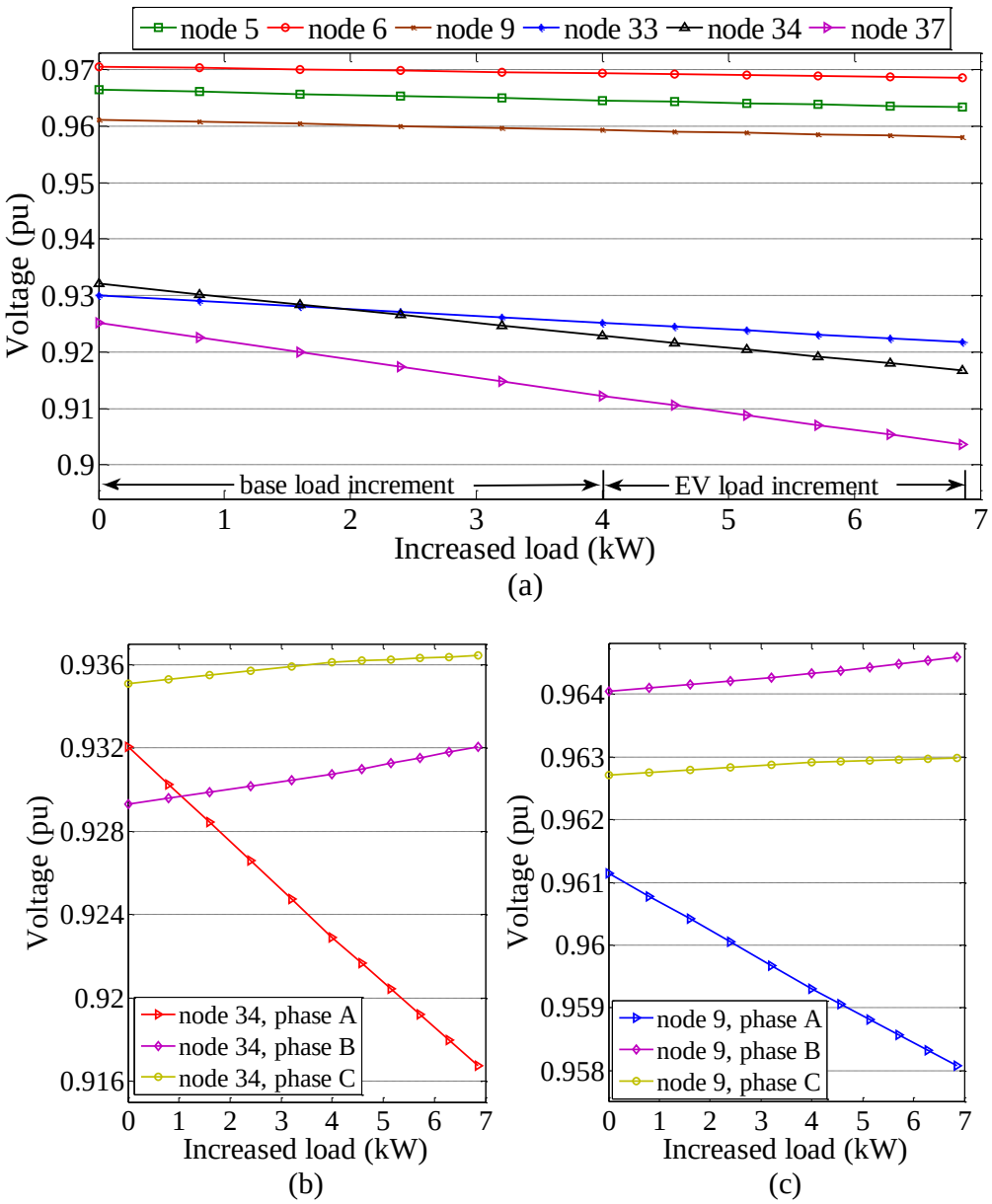

Fig. 2.7 On-phase and across-phase voltage sensitivities at 6 nodes to load increases at node 35 on Phase A: Subfigure (a) voltage variations on Phase A; (b) voltage variations at node 34 on each of the three phases; (c) voltage variations at node 9 on each of the three phases

the nodes near the extremities of the feeder (i.e., node 33, 34 and 37 in Fig. 2.7(a)) are more sensitive to the load change compared with those closer to the sending end of the feeder (i.e., node 5, 6 and 9 in Fig. 2.7(a)). The on-phase and across-phase voltage-to-load sensitivities at node 34 and 9 are presented in Fig. 2.7(b) and 2.7(c), respectively. It can be seen that the load increase at node 35 on Phase

A causes the voltages at node 34 and 9 to drop on the same phase and to slightly increase on the other two phases. This kind of voltage changes can be commonly observed in unbalanced distribution networks [86]. Fig. 2.7(b) and 2.7(c) also show that the on-phase voltage-to-load sensitivities are much more significant than the across-phase sensitivities. Therefore, for simplicity, only the on-phase voltage sensitivities are considered in the proposed scheduling.

Fig. 2.8 shows the VDIIs at selected nodes on Phase A varying with system load. The VDIIs become larger under heavy load conditions in the evening and in the morning. The maximum standard deviation of the VDII is 0.1533 at node 37. Since those variations are small, VDIIs can be approximated as constants in the scheduling.

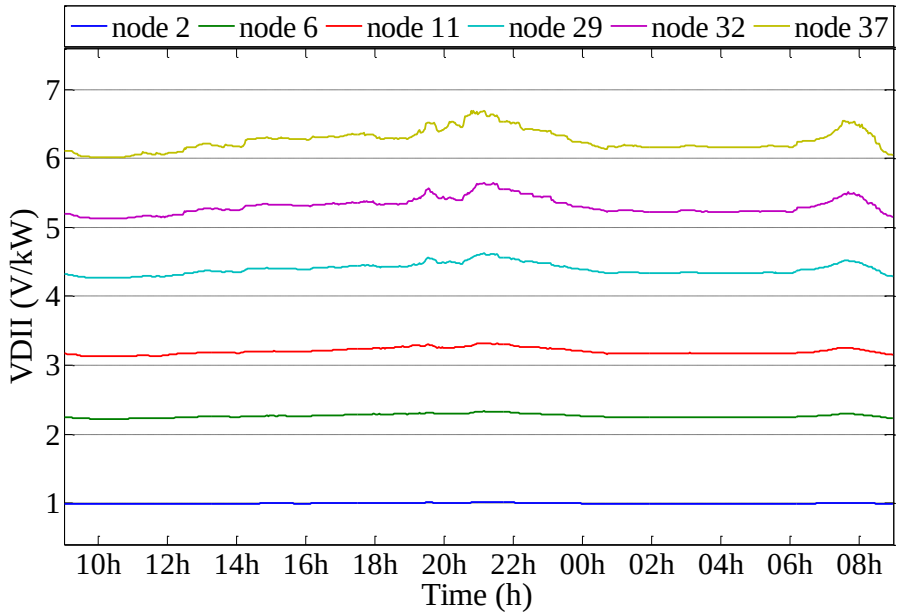

Fig. 2.8 VDII values at selected nodes on Phase A varying with the practical system load

2.4.2 Verification on the Effectiveness of the Proposed Scheduling Scheme

The proposed PEV charging scheduling scheme is benchmarked against the minimizing load variance scheme reported in [79] in terms of system load profile modification, circuit losses minimization, and run time.

Scenario A: Four PEV penetration levels, 20%, 30%, 50%, and 60%, are tested with the ideal base load profiles. The PEV loads are uniformly distributed on Phase A of the system. PEV batteries have initial SOC uniformly distributed between 10% and 20% and desired final SOC set as 95%. For comparison purpose, all PEVs are plugged-in at 5 pm and depart at 8 am the next day.

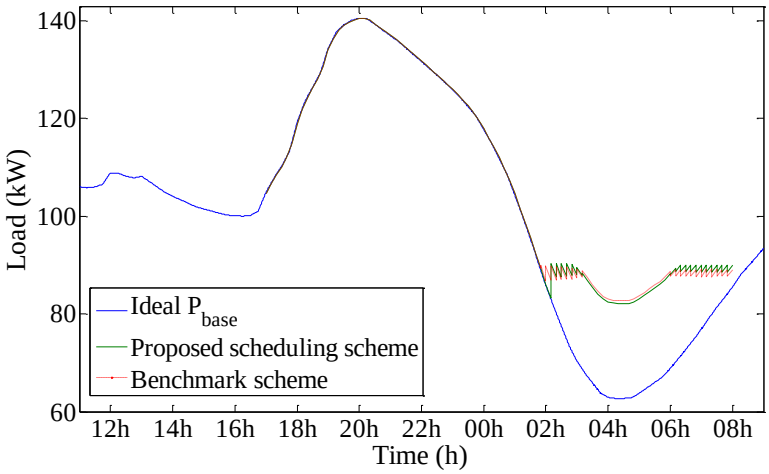

(a)

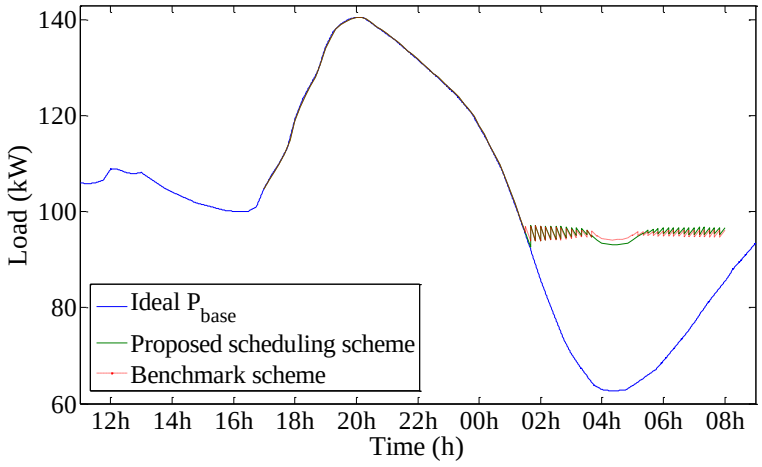

(b)

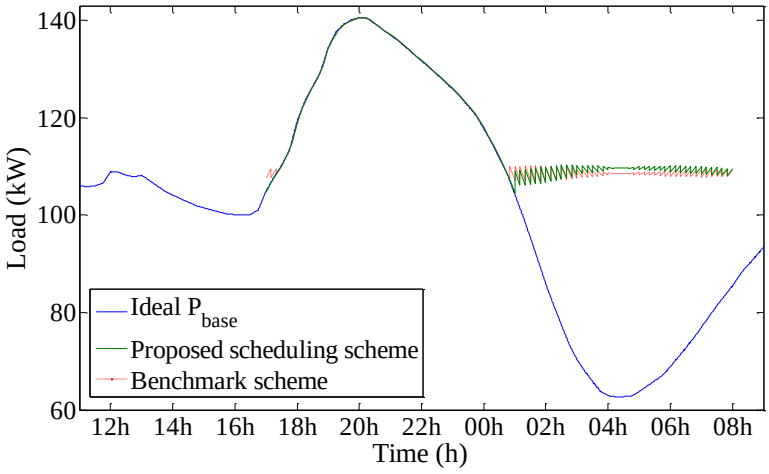

(c)

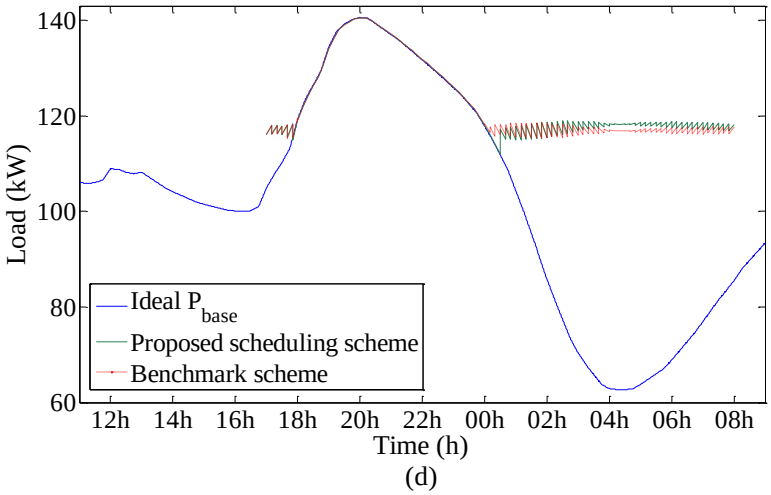

Fig. 2.9 System load profiles resulted from the proposed scheduling scheme and the benchmark scheme at (a) 20%, (b) 30%, (c) 50%, and (d) 60% PEV penetration level

From Fig. 2.9, it is clear that the system load profiles produced by the proposed scheduling scheme are fairly close to those produced by the minimum load variance scheme at all four PEV penetration levels. At low PEV penetration levels (20% and 30%), a concave section can be observed on the scheduled system load profile during the base load valley. This is caused by the maximum allowable charging power (2.86 kW) becoming the binding constraint in the scheduling. Thus, the system load profile can only be partially levelled in these cases. It can be seen that the charging rate limit does affect the schedulability of the PEVs, which in turn could affect the effectiveness of the proposed scheduling scheme. At high PEV penetration levels (50% and 60%), the charging power limit is no longer binding and the completely levelled system load profile is achieved. Both the proposed scheduling scheme and the benchmark scheme avoid increasing the peak load.

Fig. 2.10 shows voltage profiles at node 29, 24 and 31 of Phase A generated by the proposed scheduling scheme. Node 29, 24 and 31 are assigned with the basic, +1h time-shifted, and -1h time-shifted ideal base load profile, respectively. Because PVLF was used to level system load profile, some ramps can be

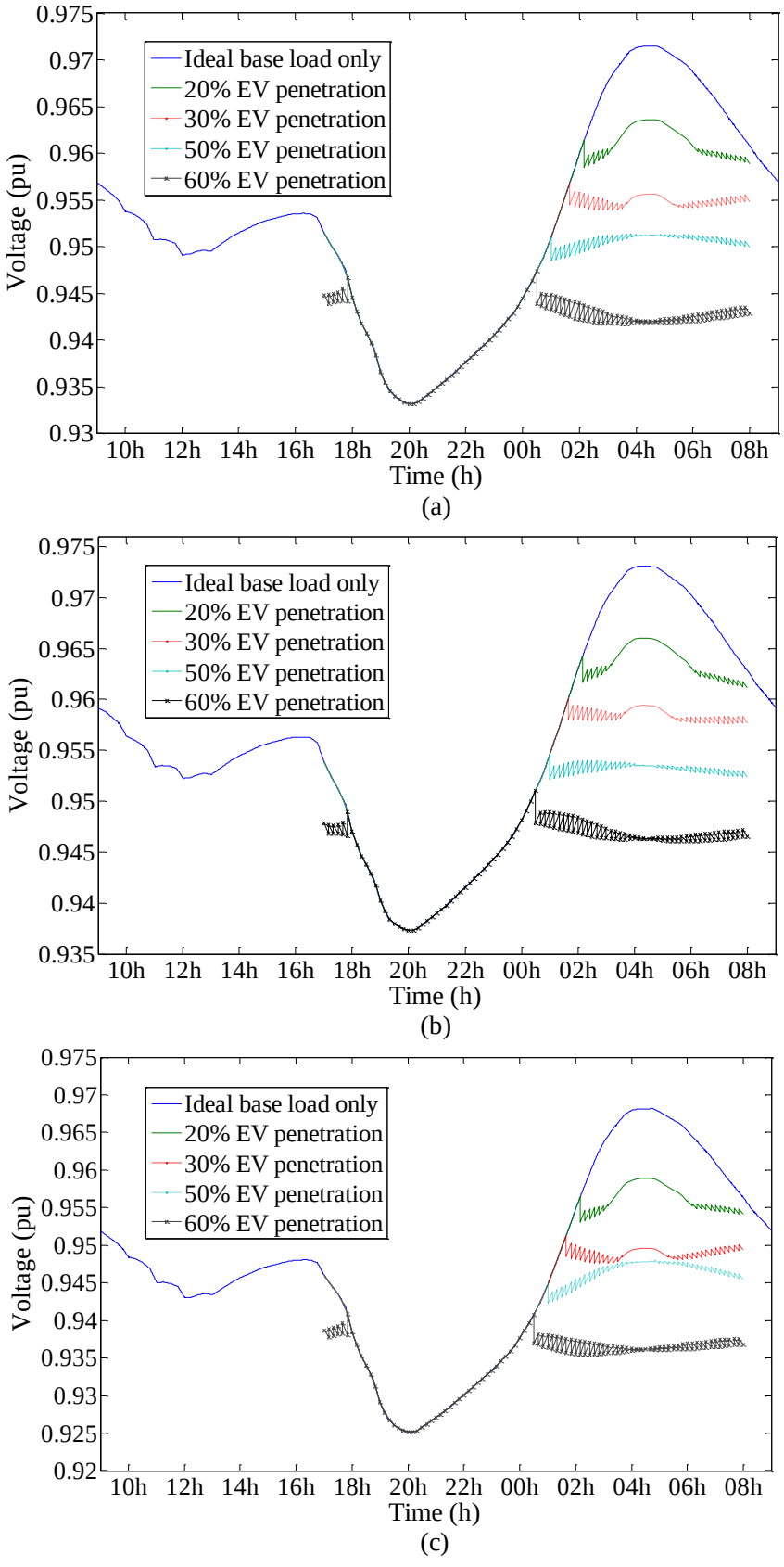

Fig. 2.10 Voltage profiles at 3 representative nodes on Phase A produced by the proposed scheduling scheme: (a) node 29; (b) node 24; (c) node 31

observed in these voltage profiles. It can be seen that though these three nodes have different load profiles, their voltage profiles are very similar. Moreover, the scheduled PEV charging which levels the total voltage deviations of all nodes is also able to approximately level the voltage profiles at individual node. This will be further investigated in Section 2.4.5 by considering the practical base load profiles.

The circuit loss on Phase A attributed to PEV charging load is shown in Table 2.1. The results show that the losses incurred by the PEV charging scheduled by the proposed scheme are only slightly worse than the losses caused by the charging planned by the benchmark scheme with differences within 1.79%. As the benchmark scheme has been proven to give nearly optimal circuit losses [79], the results confirm the capability of the proposed scheduling scheme to approach the minimum circuit losses when it is loss-minimization-oriented. At 60% PEV penetration level, the circuit loss caused by the scheduled charging amounts to 27.853 kWh on Phase A while that on Phase B and C is only -3.237 and 0.273 kWh, respectively. Therefore, the PEV charging load on one phase (Phase A) has far more significant impact on that phase than on the other phases.

Table 2.1 Circuit loss on Phase A attributed to PEV charging load

PEV penetration level	Circuit loss: the proposed scheme (kWh)	Circuit loss: the benchmark scheme (kWh)	Difference (%)
20%	5.855	5.812	-0.74
30%	10.322	10.218	-1.02
50%	19.841	19.533	-1.58
60%	27.853	27.364	-1.79

The computation time is imperative for real-time PEV charging scheduling. To compare the speed of the proposed scheduling scheme with the benchmark scheme, both methods are implemented in Matlab and run on a PC with Intel Core i3-540 processor. The results are presented in Table 2.2. The computation time of the proposed scheduling scheme is orders of magnitude faster than that of

the benchmark scheme. The computation time of the benchmark scheme also increases rapidly with the PEV penetration level whereas that of the proposed scheme is hardly affected. This is because the proposed scheduling scheme does not involve any computationally intensive optimization algorithms. The fast execution speed of the proposed scheme indicates its scalability for increasing number of PEVs.

Table 2.2 Computation time for PEV charging scheduling

PEV penetration level	The proposed scheme (s)	The benchmark scheme (s)
20%	0.329	2.620
30%	0.382	10.093
50%	0.480	21.192
60%	0.534	53.565

2.4.3 Illustration of More Voltage-Safety-Oriented Scheduling

PEV charging at nodes near the extremities of a radial feeder is more likely to suffer from excessive voltage drop than those close to the sending end. In such case, PVLF is usually greater than 1. When the loss-minimization-oriented charging plan is checked for voltage safety, if any node is found to have voltage below the lower limit, PVLF should be reduced and then the scheduling is rerun. This process repeats until the violation of voltage limit is eliminated.

Scenario B: The ideal base load profiles are employed here. An extreme situation is considered, where 18 PEVs (50% penetration) are to be charged on Phase A at the nodes with the first 18 largest VDIIs. All the PEVs are plugged-in at 5 pm and expected to depart at 8 am the next day.

The voltage profiles at node 37 of Phase A, which is the worst node in terms of voltage drop, are plotted in Fig. 2.11. With the first PVLF equal to 1.1953 for the load levelling, the voltage profiles resulted by the proposed scheme and the benchmark scheme are very similar. Lower voltage constraint is violated. As a stepwise decrement of 0.1 is applied to PVLF, the voltage limit violation is

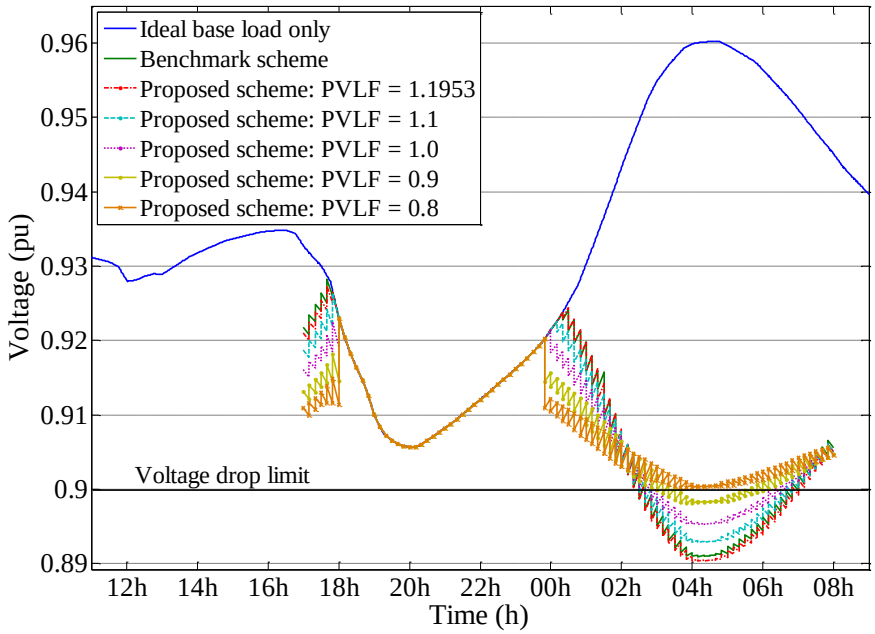

Fig. 2.11 Voltage drop mitigation at node 37 on Phase A by adjusting PVLF

gradually mitigated. When PVLF is reduced to 0.8, the lowest voltage at node 37 rises above 0.9 pu. The lower voltage limit is satisfied. Two conclusions can be drawn from Fig. 2.11. First, the benchmark scheme which does not consider the impact of charging location on voltage drop is likely to incur over low voltage when PEV load concentrates near the extremities of the feeder. Second, by using the PVLF, the proposed scheme can be flexibly adjusted to schedule a more voltage-safety-oriented charging profile that satisfies the voltage constraint.

2.4.4 Illustration of Real-Time PEV Charging Scheduling

Scenario C: The ideal base load profiles are adopted in this study. A typical household vehicle mobility pattern characterized by bulk morning departures and evening arrivals is considered. Suppose there are 24 PEVs (67% penetration) and all of them have departed in the morning before 9 a.m. Between 11:00 and 12:00 at noon, 6 PEVs return home and plan to leave again in the early afternoon between 14:00 and 15:30. These 6 PEVs have initial SOC between 35% and 45%, and their desired SOC are set to 90%. 20 PEVs return home between 5 p.m. and

7 p.m. To simulate random arrival, the remaining 4 PEVs arrive at 2 a.m. after the overnight charging has started. Each PEV is assigned with an expected departure time of 7, 8, or 9 a.m. the next day. However, 6 PEVs actually depart at 6:00 and 6:30 in the morning to simulate unplanned departure. Their initial SOC are between 20% and 30%, and their desired final SOC are set to 95%.

Fig. 2.12(a) shows the system load profile. As can be seen, the proposed PEV scheduling scheme only manages to level the system load profile partially from 11:00 to 15:30. This is because some of the PEVs returning home at noon turn out to be unschedulable due to their limited amount of plug-in time before their planned departures in a few hours. During the overnight charging period, it can be seen that whenever there is a change in PEV connection (i.e. PEV arrival or departure), the charging plan will be updated to account for this change and the system load is increased or decreased accordingly. When the number of connected PEV remains constant, the system load profile is levelled for loss minimization.

Fig. 2.12(b) displays the charging power profiles of 4 representative PEVs with equal initial SOCs. PEV_2, PEV_3 and PEV_4 arrive between 5 p.m. and 7 p.m., and plan to depart at 7, 8, and 9 a.m. the next day, respectively. PEV_1 arrives at 2 a.m. and plans to depart at 7 a.m. As shown in Fig. 2.12(b), PEV_1, which has the latest arrival time and the earliest expected departure time, receives the highest charging rate from 2 a.m. to 7 a.m. whereas PEV_4 which has the latest expected departure time is charged at the lowest rate. After 7 a.m., both PEV_1 and PEV_2 finish charging and the remaining PEVs obtain higher rates. The 4 representative PEVs are scheduled to be charged discriminately in order to satisfy the desired 95% SOC upon their respective expected departure time. Fig. 2.12(c) plots the corresponding SOC variations. All of the 4 PEVs manage to meet the desired final SOC by following the scheduled charging plan.

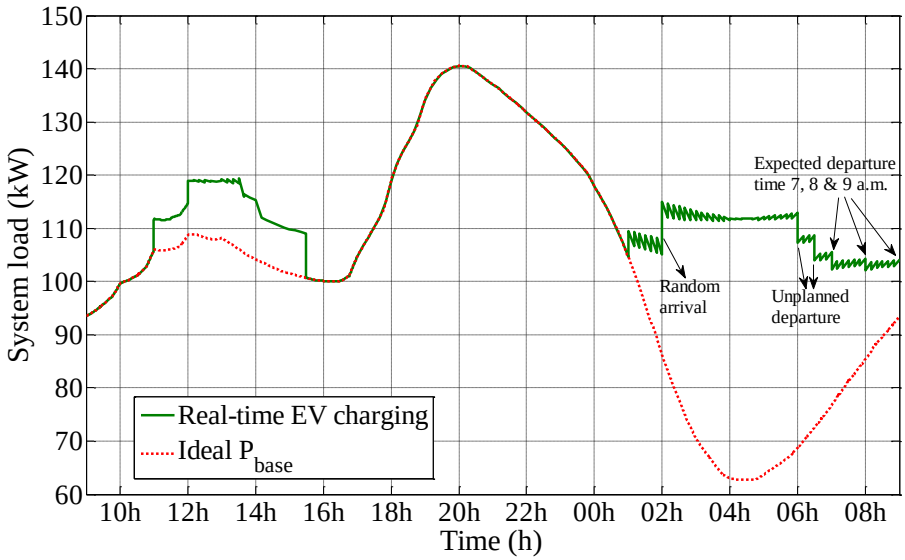

(a) System load profile on Phase A produced by the proposed scheduling

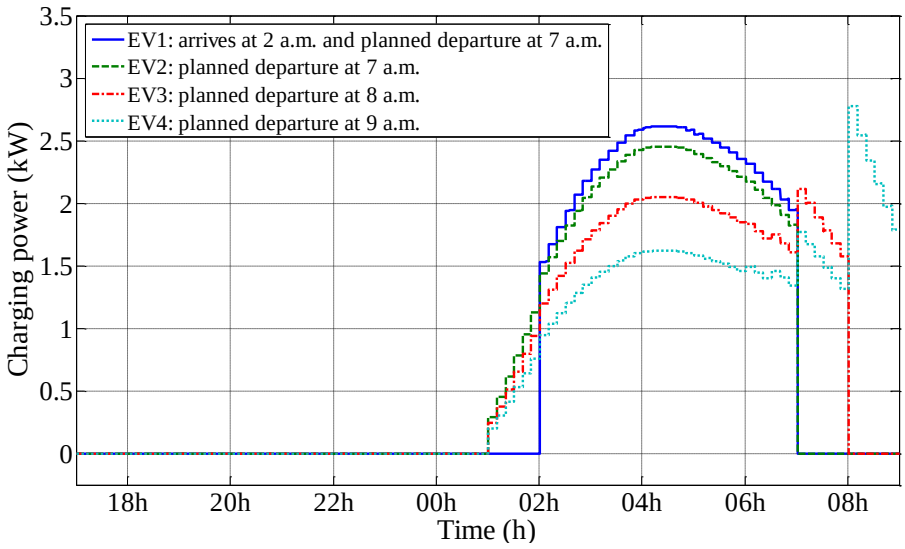

(b) Charging profiles of the 4 representative PEVs

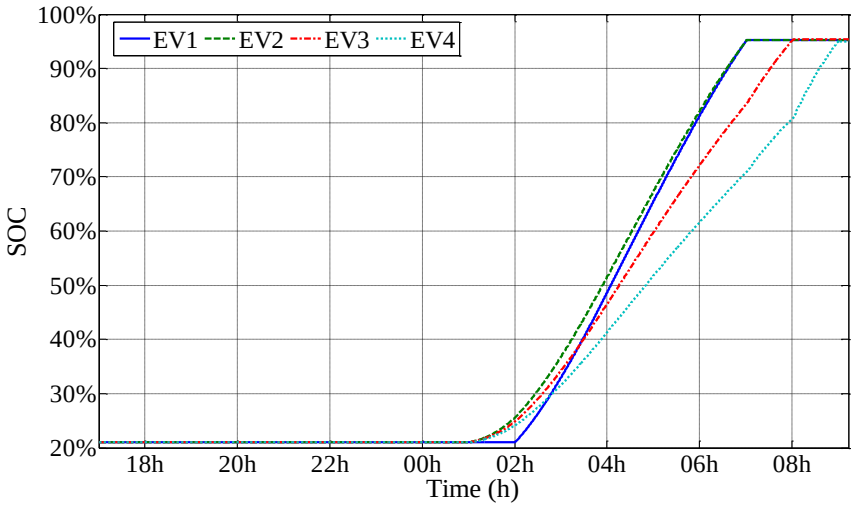

(c) SOC variations of the 4 representative PEVs

Fig. 2.12 Real-time PEV charging scheduling in Scenario C

2.4.5 Performance Evaluation with Practical Base Load Profiles

In this section, the proposed PEV scheduling scheme is tested in a more realistic situation where the load profiles at individual node are different and contain abrupt variances. The results from the proposed scheduling scheme are compared with those obtained by assuming ideal forecast on individual household load and using a heuristic optimization solver.

Scenario D: The practical base load profiles described in Section 2.3.2 are employed here. Each node on each phase is assigned with one of the practical load profiles while only the forecast of the aggregate system load is inputted to the scheduler. The performance of the proposed scheme is investigated in two cases: one with the ideal forecast on aggregate system load represented by the blue solid curve in Fig. 2.6(b); and the other with the non-ideal forecast as shown in red dotted curve in Fig. 2.6(b). 18 PEVs (50% penetration) are to be charged and the charging load is uniformly distributed on Phase A. The PEVs have initial SOC between 10% and 20%, and desired final SOC set to 95%. All PEVs are plugged-in at 5 pm and expect to depart at 8 am the next day.

As a benchmark, a heuristic pattern search method is used to schedule the PEV charging with the objective of minimizing the total circuit losses on three phases. The detailed formulation of the optimization problem is described in [78, 79]. The PEV scheduling optimization involves multiple variables, so the pattern search would take a fairly long time to converge. Since the heuristic method is used here for the purpose of verifying the proposed scheme, instead of attempting to obtain the precisely optimal PEV charging plan, the pattern search terminates when the allowed time limit (72 hours) is exceeded.

Fig. 2.13 shows the system load profiles of Phase A resulted by the proposed scheduling scheme. With ideal forecast on the aggregate system load, the proposed scheme is able to approximately level the system load profile over the night charging period. This shows that utilizing the predetermined constant

PVLF in the scheduling for system load levelling remains effective even when realistic load profiles are considered. When non-ideal forecast on the aggregate system load is fed to the scheduling scheme, some ramps appear in the produced load profile. This shows that the degree of load forecast accuracy is an important factor affecting the effectiveness of the proposed scheduling scheme, and the forecast shall be updated continuously to improve its accuracy.

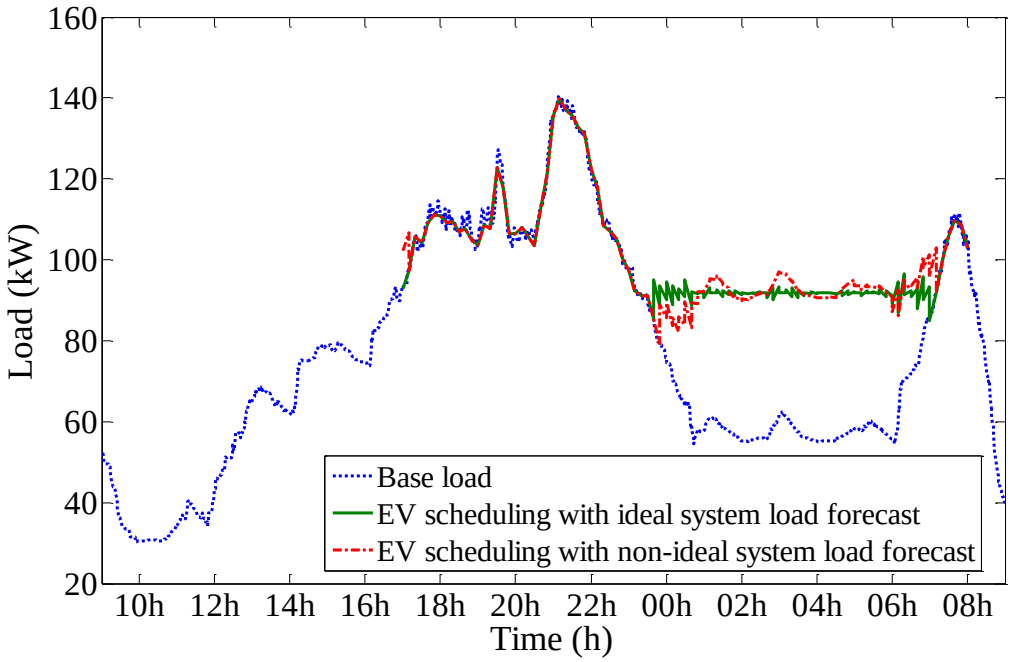

Fig. 2.13 System load profiles resulted by the proposed PEV charging scheduling scheme when practical base loads are considered

The system load profiles resulted by the pattern search and the proposed scheme are compared in Fig. 2.14. As shown in Fig. 2.14(a), the profile of aggregate system load on Phase A obtained from the pattern search is fairly close to that produced by the proposed scheduling scheme. The same observation also applies to load profiles at individual node, as illustrated in Fig. 2.14(b). These two comparisons verify that the proposed scheduling scheme can generate similar charging plan as the conventional optimization solver which requires availability of forecasts on each household load.

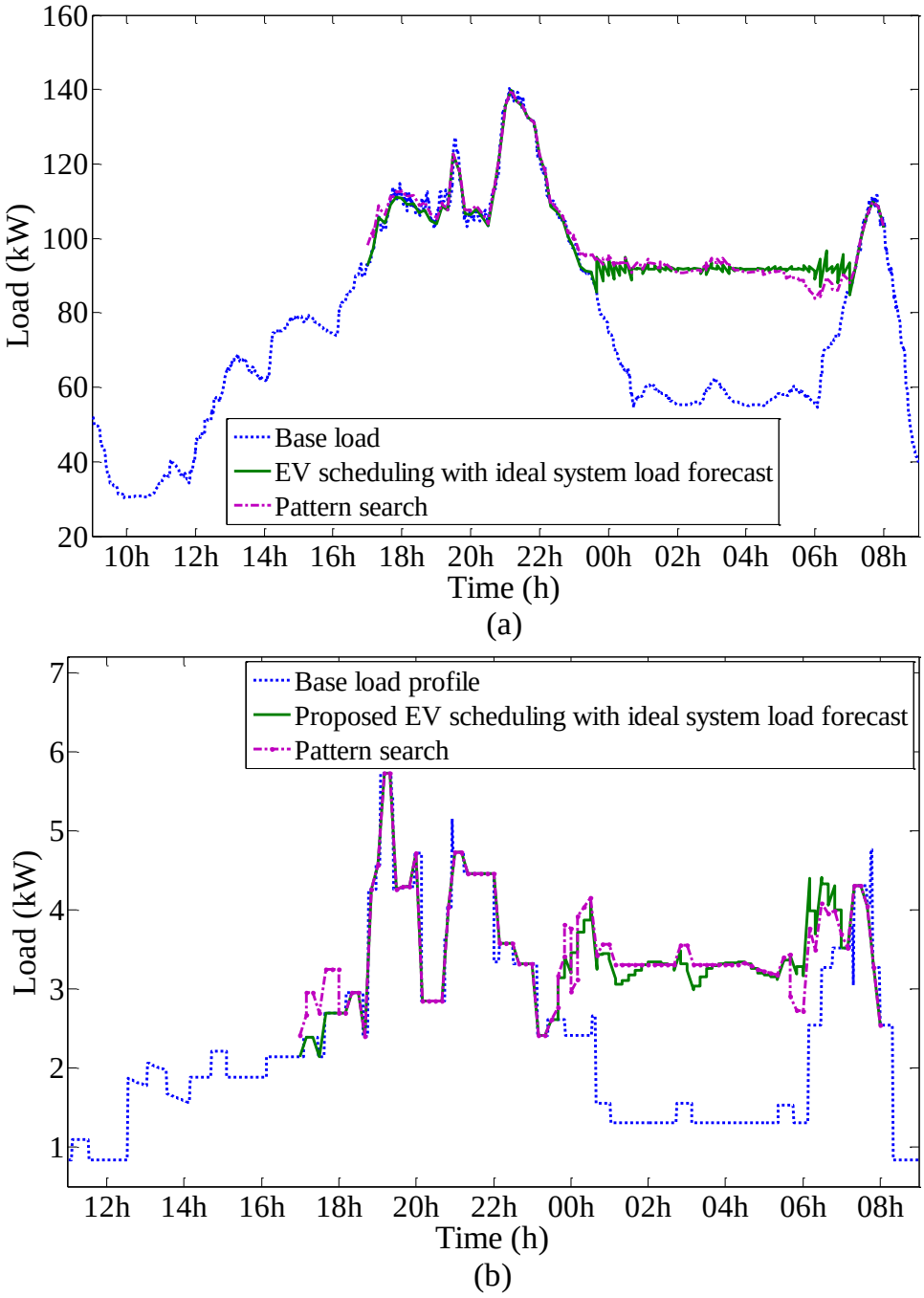

Fig. 2.14 System load profiles resulted by the proposed PEV charging scheduling scheme compared with those produced by pattern search: (a) aggregate system load (Phase A); (b) load profiles at node 22 on Phase A

Fig. 2.15 plots the voltage profiles at node 6 and 20 of Phase A resulted by the proposed scheduling scheme and the pattern search. It is clear that the voltage profiles at these two nodes are similar, though the load profiles at these two

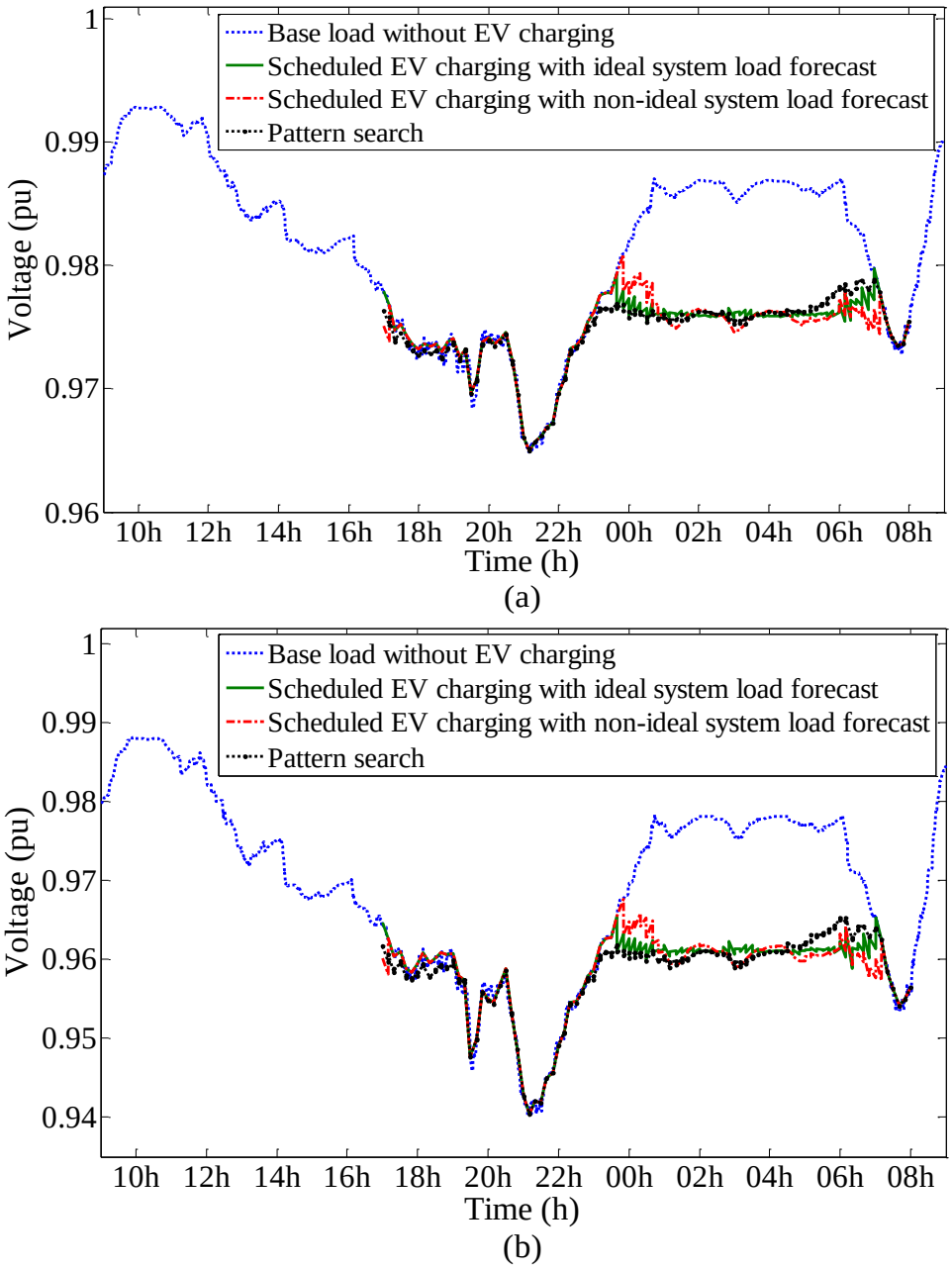

Fig. 2.15 Scheduling with practical base loads: voltage profiles at (a) node 6 and (b) node 20 on phase A

nodes are different. This again verifies that the PEV charging scheduled to level the total voltage deviations of all nodes is also able to approximately level the voltage profile at each of the individual nodes.

Overall, the above results show the adequate effectiveness of the proposed scheduling scheme in dealing with the individual household load uncertainties on the distribution network.

2.5 Summary

As an effort to realize smooth and safe accommodation of PEV charging load at the initial stage of PEV adoption before the upgrade of the network infrastructure, in this chapter, a simple but effective PEV charging scheduling scheme is designed for real-time coordination of randomly arriving or departing PEVs in low-voltage residential networks. Since most often voltage drop would become a binding constraint for a low-voltage residential distribution feeder when subjected to high PEV penetration level, the voltage profile levelling forms the basis of the scheduling scheme. The PVLF is then derived to allow the scheduling to shift seamlessly between being loss-minimization-oriented and voltage-safety-oriented. The proposed scheduling scheme biases PEV charging power according to individual PEV's required amount of energy and expected departure time specified by the PEV owner. Simulations on a low-voltage test feeder in four scenarios have confirmed the effectiveness of the proposed scheduling scheme. Its advantages are summarized as follows:

(1) The proposed scheduling scheme has fast execution speed and is scalable to increased number of PEVs because no computationally intensive optimization algorithms are involved. This is important to handling frequent PEV arrivals and departures.

(2) The proposed scheduling scheme can closely approach the optimal circuit losses when voltage drop is not a blinding constraint. If allowed, the scheduling scheme would avoid increasing the peak load.

(3) When voltage drop becomes a blinding constraint, the proposed scheme can be flexibly adjusted to schedule a charging profile to satisfy the voltage constraint at a proper compromise of system loss optimality.

Chapter III

A Decentralized PEV Charging Control Scheme and Its Application for Mitigating Wind Farm Power Output Intermittency and Enhancing Frequency Regulation

3.1 Introduction

In the scheduling scheme proposed in Chapter II, an intelligent control entity is needed to generate a charging power dispatch signal for each PEV group as dictated by (2.10). Such charging control is centralized and hard to be applied to a large number of dispersedly located PEVs. Inspired by the concept of congestion pricing in Internet traffic control, a decentralized PEV charging control scheme is proposed in this chapter to enable the PEV power to participate in system regulation.

The congestion pricing has been widely adopted in Internet traffic control. Basically, it is a proportionally fair pricing scheme: a user who is willing to pay a higher price would attain a larger share of the scarce network capacity [87-89]. Individual user's willingness to pay and the real-time market price are two important parameters in the congestion pricing scheme. The market price depends on the available network capacity (supply) versus the aggregate flow of users (demand). It will be continuously updated to reflect the changes in demand and supply, and broadcasted to all users in the network. Upon receiving the market price signal, each user will adjust its flow based on the price and the user's willingness to pay. Such iterative process goes on until an equilibrium is

reached, at which the market price and the aggregate flow of users settle to stable values. Mathematically, the market price can be calculated as:

$$MP_t = (\sum_{i=1}^{M} f_{i,t-d} / C_t)^k \tag{3.1}$$

where MP_t is the market price at time *t*; *M* is the number of users; *d* is the size of the time step; $f_{i,t-d}$ is the flow of user *i* at time *t-d*; C_t is the network capacity available at time *t*; and *k* is a positive integer. The flow of individual user is determined as

$$f_{i,t} = f_{i,t-d} + \gamma_i (w_{i,t} - f_{i,t-d} MP_t) \tag{3.2}$$

where $w_{i,t}$ is the willingness to pay parameter of user *i* at time *t*; and γ_i is a parameter affecting the rate of convergence of the algorithm.

At equilibrium, both the market price and the aggregate flow of users settle to stable values, which means

$$\begin{cases} w_i - f_i^{\text{eq}} MP^{\text{eq}} = 0 \\ MP^{\text{eq}} = [\sum_{i=1}^{M} f_i^{\text{eq}} / C_t]^k \end{cases} \tag{3.3}$$

Given f_i^{eq} (for $i = 1, 2, 3, \ldots, M$) and C_t are all positive, it is easy to see from (3.3) that

$$\sum_{i=1}^{M} f_i^{\text{eq}} = (C_t^k \cdot \sum_{i=1}^{M} w_i)^{1/k+1} \tag{3.4}$$

This chapter would focus on utilizing the decentralized response mechanism of the congestion pricing scheme to control PEV charging. Analogous to the Internet user, each PEV in the proposed decentralized charging control scheme would adjust its charging/discharging power autonomously according to a real-time directional signal (DS) and also its own urgency level of charging (ULC). The DS reflects the mismatch between the PEV power requested by the system and the actual PEV power. The ULC will lead to heterogeneous power distribution among PEVs, which would help satisfy the heterogeneous charging requirements specified by PEV owners.

The decentralized charging control scheme is applied to guide the PEV power to compensate undesired fluctuations in a wind farm's power output. A PEV fleet consisting of numerous dispersedly located PEVs is coupled with a wind farm to form a PEV-wind farm (PEV-WF) virtual plant. The PEV fleet acts as an internal power regulator in the virtual plant and the power output of the virtual plant would be the filtered WP. Thus, when participating in power market, the PEV-WF virtual plant will be capable of following the predetermined schedule so as to avoid the imbalance penalty.

3.2 The Proposed Decentralized PEV Charging Control Scheme

3.2.1 Defining the Real-Time Directional Signal

Similar to the market price signal in the congestion pricing scheme, the real-time DS is used to guide the PEV power to approach a desired value. The PEV power shall change in the right direction with the right amount such that at equilibrium:

$$\sum_{i=1}^{N} p_{\mathrm{PEV},i}^{\mathrm{eq}} = DP_{\mathrm{PEV}} \tag{3.5}$$

where $p_{\mathrm{PEV},i}^{\mathrm{eq}}$ is the power of PEV i at equilibrium; DP_{PEV} is the desired aggregate PEV power; and N is the number of PEVs under control. (3.5) is equivalent to the following two conditions:

$$\left|\sum_{i=1}^{N} p_{\mathrm{PEV},i}^{\mathrm{eq}}\right| = \left|DP_{\mathrm{PEV}}\right| \tag{3.6}$$

$$\mathrm{sign}\left(\sum_{i=1}^{N} p_{\mathrm{PEV},i}^{\mathrm{eq}}\right) = \mathrm{sign}(DP_{\mathrm{PEV}}) \tag{3.7}$$

Analogous to the market price in the congestion pricing calculated in (3.1), DS can be defined as $DS_t = (\sum_{i=1}^{N} p_{\mathrm{PEV},i,t-d} / DP_{\mathrm{PEV},t})^k$, where $p_{\mathrm{PEV},i,t}$ is the power of PEV i at time t; and $DP_{\mathrm{PEV},t}$ is the desired aggregate PEV power at time t. Nevertheless, as can be seen in (3.4), the congestion pricing scheme does not

guarantee the scarce resource to be fully exploited by the users at the equilibrium, i.e. $\sum_{i=1}^{M} f_i^{\text{eq}} \neq C_t$. As a result, the condition (3.6) cannot be satisfied.

In order to satisfy the condition (3.6), it is supposed that when the PEV power is guided to approach a value denoted by αDP_{PEV} which deviates from the actual desired value DP_{PEV}, the PEV power will end up approaching DP_{PEV}, where α is a positive scaling factor. With reference to (3.4), the following condition can be formulated.

$$\left|\sum_{i=1}^{N} p_{\text{PEV},i}^{\text{eq}}\right| = \left[(\alpha \cdot DP_{\text{PEV}})^k \cdot \sum_{i=1}^{N} ulc_i\right]^{1/(k+1)} = \left|DP_{\text{PEV}}\right| \tag{3.8}$$

where ulc_i is the ULC of PEV i, which is a positive parameter.

Accordingly, the real-time DS at equilibrium will be calculated as

$$DS^{\text{eq}} = \left(\sum_{i=1}^{N} p_{\text{PEV},i}^{\text{eq}} / (\alpha \cdot DP_{\text{PEV}})\right)^k \tag{3.9}$$

Note that in the design of the proposed charging control scheme, DS is set to be positive and dimensionless. It only reflects the mismatch in magnitude between the PEV power requested by the system and the actual PEV power. Thus, k in (3.9) is set to a positive even number.

Since k is a positive even number, according to (3.8), α can be calculated as

$$\alpha = (\left|DP_{\text{PEV}}\right| / \sum_{i=1}^{N} ulc_i)^{1/k} \tag{3.10}$$

In the dynamic power adjusting process, the scaling factor α and the real-time DS are calculated as

$$\alpha_t = (\left|DP_{\text{PEV},t}\right| / \sum_{i=1}^{N} ulc_{i,t-d})^{1/k} \tag{3.11}$$

$$DS_t = \left(\sum_{i=1}^{N} p_{\text{PEV},i,t-d} / (\alpha_t \cdot DP_{\text{PEV},t})\right)^k \tag{3.12}$$

The sign of the PEV power will automatically be consistent with that of the desired PEV power in the process of PEV power adjustment dictated in (3.14) covered in Section 3.2.3 such that the condition of (3.7) can be satisfied.

3.2.2 Defining Individual PEV's Urgency Level of Charging

In the congestion pricing algorithm, the user's willingness to pay parameter indicates how desirous a user is of the scarce resource. Similarly, in the proposed PEV charging control scheme, the ULC reflects how desirous a PEV is of grid-to-vehicle (G2V) charging power. The ULC parameter is defined as a function of the battery capacity (BC) that can be fulfilled before the planned departure time and the BC to be fulfilled from the current SOC to the desired SOC.

When the G2V power is needed ($DP_{\mathrm{PEV},t} > 0$), the ULC parameter of PEV *i* at *t* is defined as

$$ulc_{i,t} = S_{\mathrm{sys}} \cdot C_i^{\mathrm{batt}} / (\underbrace{P_i^{\mathrm{rated}} \eta_i (T_i - t) / C_i^{\mathrm{batt}}}_{\text{term 1}} - \underbrace{(SOC_i^{\mathrm{desired}} - SOC_{i,t})}_{\text{term 2}}) \qquad (3.13)$$

where C_i^{batt}, P_i^{rated}, and η_i represent the BC, the rated charging power, and the charger efficiency of PEV *i*, respectively; *t* is the present time and T_i is the planned departure time of PEV *i*; SOC_i^{desired} and $SOC_{i,t}$ are the desired SOC at departure and the current SOC, respectively; and S_{sys} is a PEV aggregator-defined scaling factor to prevent α_t in (3.12) from being either over-small or over-large. This is because an over-small α_t could lead to an excessively large DS, responding to which a PEV may encounter the problem of divergent power adjustment, as shown in the analysis in Section 3.2.4; whereas an over-large α_t may result in a very small DS which considerably slows down the PEV power adjustment as indicated in (3.14). Ideally, α_t will be maintained to unity. In (3.13), term 1 is the BC that can be fulfilled before the planned departure time and term 2 represents the BC to be fulfilled from the current SOC to the desired SOC. The difference between them is called the charging margin.

In the implementation of the proposed charging control scheme, tariff schemes could be deployed to establish contractual relation between PEV users and the PEV aggregator. Distinct tariff schemes can be adopted by different consumer groups. One possible tariff scheme is that PEV owners could enjoy

lower price of charging energy if they offer larger schedulability and controllability over their PEVs to the PEV aggregator. For example, a PEV owner can set a loose charging requirement characterized by a late planned departure time and/or a reasonable desired SOC to increase the schedulability, and allow V2G operation to increase the controllability. Another way of integrating tariff schemes into the proposed charging control scheme is that if PEV users already select their favorite tariff schemes, then the PEV ULCs should be modified by weighted values to reflect the different charging priorities granted by the tariff schemes.

In the proposed charging control scheme, one grid-connected PEV is either in responsive state or nonresponsive state. PEV i is in responsive state if its charging margin is greater than a preset threshold value. As time t approaches the planned departure time T_i, the can-be-fulfilled BC of PEV i keeps decreasing at a rate determined by its rated charging power P_i^{rated}, which leads to smaller charging margin over time. If the charging margin drops below the preset threshold value, PEV i will switch to nonresponsive state, in which it will stop responding to the DS signal and adhere to P_i^{rated}. The state transition of a PEV in the proposed charging control scheme is shown in Fig. 3.1.

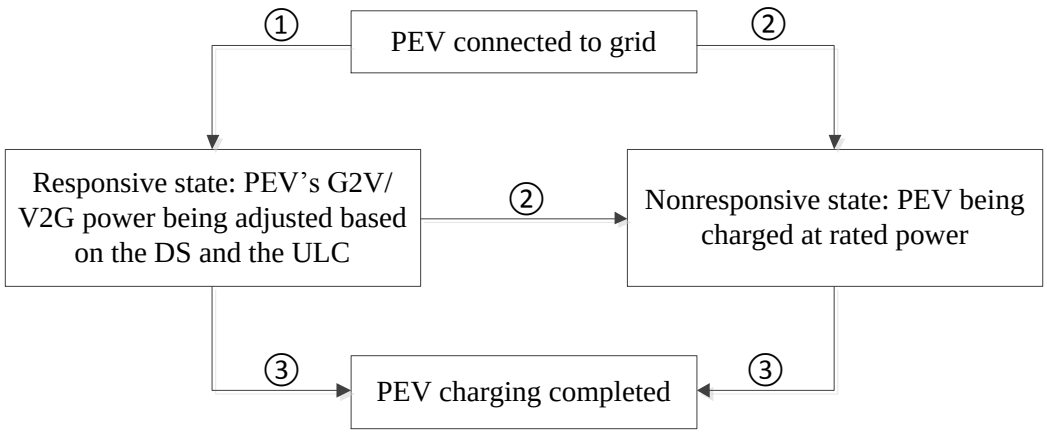

Fig. 3.1 PEV state transition in the proposed decentralized charging control

The three transition conditions are as follows:

$$①: (P_i^{\text{rated}} \eta_i (T_i - t) / C_i^{\text{batt}} - (SOC_i^{\text{desired}} - SOC_{i,t})) > CM_{\text{thld}}$$

$$②: 0 < (P_i^{\text{rated}} \eta_i (T_i - t) / C_i^{\text{batt}} - (SOC_i^{\text{desired}} - SOC_{i,t})) \le CM_{\text{thld}}$$

$$③: T_i - t = 0$$

where CM_{thld} is the predetermined threshold for the charging margin.

3.2.3 Stepwise Power Adjustment of Responsive PEV

The real-time DS is continuously updated as in (3.11) and (3.12), and then broadcasted to all PEVs under control. A responsive PEV will autonomously adjust its power in response to the received DS and based on its own ULC. Stepwise adjustment in PEV power is as follows:

$$p_{\text{PEV},i,t+d} = p_{\text{PEV},i,t} + \gamma (SS_{t+d} \cdot (ulc_{i,t})^{SS_{t+d}} - p_{\text{PEV},i,t} \cdot DS_{t+d}) \tag{3.14}$$

where $p_{\text{PEV},i,t}$ is the power of PEV *i* at time *t*; *d* is the size of the time step; γ is a parameter affecting the rate of convergence of the algorithm; DS_{t+d} is the real-time directional signal at time *t+d*; $ulc_{i,t}$ is the ULC of PEV *i* at time *t*; and SS_{t+d} represents a sign signal (SS) defined as

$$SS_{t+d} = DP_{\text{PEV},t+d} / \left| DP_{\text{PEV},t+d} \right| \tag{3.15}$$

SS is broadcasted together with DS to all PEVs, indicating G2V ($SS_{t+d} = +1$) or V2G ($SS_{t+d} = -1$) power is needed for system regulation. As can be seen from (3.14), when $SS_{t+d} = -1$, ULC would become the reciprocal of its original value calculated in (3.13). The reciprocal of ULC can be viewed as the tolerance level of discharging. The logic underlying the ULC reciprocal is that a PEV which is very desirous of G2V power should be very unwilling to supply V2G power. Thus, a large ULC should correspond to a small tolerance level of discharging, and vice versa. Since ULC and DS are always positive, when $SS_{t+d} = -1$, the minus before $ulc_{i,t}^{-1}$ would lead the PEV power to settle to negative V2G power, and $SS_{t+d} = +1$ would result in positive G2V power. Therefore, the sign of the

actual PEV power will be consistent with that of the desired PEV power, which satisfies the condition (3.7).

3.2.4 Divergent Power Adjustment Caused by PEV Responding to Excessively Large DS and Solution

According to (3.12), an excessively large DS can be produced when there is a sudden significant decrease in the magnitude of $DP_{\mathrm{PEV},t}$. Responding to an excessively large DS can render the PEV power adjustment dictated in (3.14) divergent. The mechanism of the divergent PEV power adjustment is analyzed as follows.

Here, the case of G2V power being requested is taken as an example. A sudden significant decrease in the magnitude of $DP_{\mathrm{PEV},t}$ is usually the trigger. $DP_{\mathrm{PEV},t}$ is updated at time interval *D*, which is often much larger than the time step *d* at which the DS and individual PEV power is updated. Suppose at time *t-d*, $DP_{\mathrm{PEV},t-d}$ is positive, and at time *t*, $DP_{\mathrm{PEV},t}$ is updated and remains positive but with a much smaller magnitude:

$$0 < DP_{\mathrm{PEV},t} \ll DP_{\mathrm{PEV},t-d} \tag{3.16}$$

Since $D \gg d$, it is usually the case that previous desired value $DP_{\mathrm{PEV},t-d}$ has been closely approached by the actual PEV power at *t-d*, i.e. $\sum_{i=1}^{N} p_{\mathrm{PEV},i,t\text{-}d} \approx DP_{\mathrm{PEV},t-d}$. According to (3.12)

$$DS_{t-d} \ll DS_t \tag{3.17}$$

DS_t is then broadcasted to all PEVs and each responsive PEV updates its power for the time *t* according to (3.14). Suppose DS_t is large enough to induce a significant decrease in $p_{\mathrm{PEV},i,t}$ such that $p_{\mathrm{PEV},i,t}$ drops to a negative value with greater magnitude than $p_{\mathrm{PEV},i,t-d}$:

$$0 < p_{\mathrm{PEV},i,t-d} < -p_{\mathrm{PEV},i,t} \tag{3.18}$$

Given $SS_t = +1$, γ and $p_{\mathrm{PEV},i,t-d}$ are positive, the following can be obtained by substituting (3.14) into (3.18):

$$2/\gamma + ulc_{i,t-d} / p_{\mathrm{PEV},i,t-d} < DS_t \tag{3.19}$$

This excessively large DS_t is very likely to cause the majority of responsive PEVs to result in a negative power at time *t* satisfying (3.18). If this is the case, the aggregate PEV power at time *t* would meet the following condition:

$$\sum_{i=1}^{N} p_{\mathrm{PEV},i,t-d} < -\sum_{i=1}^{N} p_{\mathrm{PEV},i,t} \tag{3.20}$$

From *t* to *t+d*, the desired PEV power is not updated, thus $DP_{\mathrm{PEV},t+d} = DP_{\mathrm{PEV},t}$. According to (3.12), $DP_{\mathrm{PEV},t+d} = DP_{\mathrm{PEV},t}$ together with (3.20) indicate that

$$DS_{t+d} > DS_t > 0 \tag{3.21}$$

Moreover, for the small time granularity *d*, ULC would only slightly vary.

$$ulc_{i,t-d} \approx ulc_{i,t} \tag{3.22}$$

Based on (3.18), (3.19), (3.21), and (3.22), the power of PEV *i* at *t+d* satisfies:

$$\begin{aligned}
p_{\mathrm{PEV},i,t+d} &= p_{\mathrm{PEV},i,t} + \gamma(ulc_{i,t} - p_{\mathrm{PEV},i,t} \cdot DS_{t+d}) \\
&> p_{\mathrm{PEV},i,t} + \gamma(ulc_{i,t} - p_{\mathrm{PEV},i,t} \cdot DS_t) \\
&> p_{\mathrm{PEV},i,t} + \gamma(ulc_{i,t} - p_{\mathrm{PEV},i,t} \cdot (2/\gamma + ulc_{i,t-d} / p_{\mathrm{PEV},i,t-d})) \\
&= -p_{\mathrm{PEV},i,t} + \gamma \cdot ulc_{i,t} - \gamma \cdot ulc_{i,t-d} \cdot p_{\mathrm{PEV},i,t} / p_{\mathrm{PEV},i,t-d} \\
&\approx -p_{\mathrm{PEV},i,t} + \gamma \cdot ulc_{i,t}(1 - p_{\mathrm{PEV},i,t} / p_{\mathrm{PEV},i,t-d}) \\
&> -p_{\mathrm{PEV},i,t} + 2\gamma \cdot ulc_{i,t} \\
&> -p_{\mathrm{PEV},i,t}
\end{aligned} \tag{3.23}$$

Inequality (3.23) indicates that DS at time *t+2d* will continue increasing, i.e. $DS_{t+2d} > DS_{t+d}$. From (3.23) and (3.18), it is clear that $0 < p_{\mathrm{PEV},i,t-d} < p_{\mathrm{PEV},i,t+d}$. Also, ULC will only slightly vary from *t* to *t+d*, thus $ulc_{i,t+d} \approx ulc_{i,t} \approx ulc_{i,t-d}$. Together with the condition (3.19) and (3.21), the following inequality can be proven:

$$\begin{aligned}
-p_{\mathrm{PEV},i,t+2d} &= -p_{\mathrm{PEV},i,t+d} - \gamma(ulc_{i,t+d} - p_{\mathrm{PEV},i,t+d} \cdot DS_{t+2d}) \\
&> -p_{\mathrm{PEV},i,t+d} - \gamma(ulc_{i,t+d} - p_{\mathrm{PEV},i,t+d} \cdot DS_{t+d}) \\
&> -p_{\mathrm{PEV},i,t+d} - \gamma(ulc_{i,t+d} - p_{\mathrm{PEV},i,t+d} \cdot DS_t) \\
&> -p_{\mathrm{PEV},i,t+d} - \gamma(ulc_{i,t+d} - p_{\mathrm{PEV},i,t+d} \cdot (2/\gamma + ulc_{i,t-d} / p_{\mathrm{PEV},i,t-d})) \\
&= p_{\mathrm{PEV},i,t+d} - \gamma \cdot ulc_{i,t+d} + \gamma \cdot ulc_{i,t-d} \cdot p_{\mathrm{PEV},i,t+d} / p_{\mathrm{PEV},i,t-d} \\
&\approx p_{\mathrm{PEV},i,t+d} + \gamma \cdot ulc_{i,t+d}(p_{\mathrm{PEV},i,t+d} / p_{\mathrm{PEV},i,t-d} - 1) \\
&> p_{\mathrm{PEV},i,t+d}
\end{aligned} \tag{3.24}$$

Similarly, it is easy to prove that

$$0 < p_{\mathrm{PEV},i,t-d} < -p_{\mathrm{PEV},i,t} < p_{\mathrm{PEV},i,t+d} < -p_{\mathrm{PEV},i,t+2d} < \cdots \leq \left| P_i^{\mathrm{rated}} \right| \tag{3.25}$$

Inequality (3.25) indicates the divergent PEV power adjustment, which makes the power fluctuate between positive and negative values with increasing magnitude until the charger power limit is hit. In the case of V2G power being requested, the divergent PEV power adjustment problem can be proven in a similar way.

Since PEVs responding to excessively large DS is the cause of the divergent power adjustment, a direct solution to this problem is that PEVs should stop responding to DS once it is detected to be dangerously large. From the process of divergent PEV power adjustment, it can be seen that the DS satisfying (3.19) is the trigger of the divergence. Hence, the following condition is selected for PEVs to judge whether the DS is excessively large or not:

$$DS_t \leq 2/\gamma \tag{3.26}$$

This upper limit $2/\gamma$ also applies to the V2G power adjustment. If DS is beyond the upper limit, instead of adjusting power according to (3.14), a responsive PEV would scale down the magnitude of its power until DS satisfies (3.26):

$$p_{\mathrm{PEV},i,t+d} = p_{\mathrm{PEV},i,t} \cdot \varphi \tag{3.27}$$

where φ is a scaling factor in the range $0 < \varphi < 1$.

3.2.5 Dealing with Interrupted Individual PEV Power Adjustment

Individual PEV power adjustment may be interrupted. For example, when a PEV with relatively large ULC is being charged through a charger with small power rating, the power adjustment in (3.14) may attempt to reach a power level higher than the charger's rated power, which causes the PEV power to be constrained. Another example is that when a PEV becomes nonresponsive, it will no longer follow the power adjustment and simply takes its rated charging power. These interruptions to individual PEV power adjustment often lead to a persistent

mismatch between the desired PEV power and the actual PEV power at equilibrium. However, such mismatch can be remedied by increasing the value of the exponent *k* in generating the DS as in (3.12). The proof is as follows.

The case of G2V power being requested is considered as an example. For simplicity, it is assumed that one PEV's power adjustment (PEV *i*) is interrupted. Due to the interruption, the power of PEV *i* is fixed to a value denoted by $p_{\text{PEV},i}^{\text{fixed}}$ and the aggregate PEV power settles to AP_{PEV}, which mismatches the desired PEV power DP_{PEV}, i.e. $AP_{\text{PEV}} \neq DP_{\text{PEV}}$.

The set of PEVs other than PEV *i* is denoted by ***J***. For a PEV *j* belonging to ***J***, its power adjustment is not interrupted. Thus, the power of PEV *j* at equilibrium can be expressed as:

$$\begin{aligned} p_{\text{PEV},j}^{\text{eq}} &= ulc_j / DS^{\text{eq}} \\ &= ulc_j / (AP_{\text{PEV}} / (\alpha \cdot DP_{\text{PEV}}))^k \\ &= ulc_j \alpha^k DP_{\text{PEV}}^k / AP_{\text{PEV}}^k \end{aligned} \tag{3.28}$$

Since $\sum_{j \in J} p_{\text{PEV},j} + p_{\text{PEV},i}^{\text{fixed}} = AP_{\text{PEV}}$,

$$AP_{\text{PEV}} - p_{\text{PEV},i}^{\text{fixed}} = \sum_{j \in J} p_{\text{PEV},j} = \sum_{j \in J} ulc_j \cdot \alpha^k DP_{\text{PEV}}^k / AP_{\text{PEV}}^k \tag{3.29}$$

Hence,

$$\begin{aligned} AP_{\text{PEV}}^k (AP_{\text{PEV}} - p_{\text{PEV},i}^{\text{fixed}}) &= \sum_{j \in J} ulc_j \cdot \alpha^k DP_{\text{PEV}}^k \\ &= (\sum_{e=1}^{N} ulc_e - ulc_i) \cdot DP_{\text{PEV}} / \sum_{e=1}^{N} ulc_e \cdot DP_{\text{PEV}}^k \\ &= (DP_{\text{PEV}} - DP_{\text{PEV}} \cdot ulc_i / \sum_{e=1}^{N} ulc_e) \cdot DP_{\text{PEV}}^k \end{aligned} \tag{3.30}$$

In the ideal situation where the power adjustment of PEV *i* is not interrupted, AP_{PEV} would be able to match DP_{PEV} at equilibrium, and PEV *i* would reach its intended power $p_{\text{PEV},i}^{\text{ideal}}$, which can be expressed as:

$$\begin{aligned} p_{\text{PEV},i}^{\text{ideal}} &= ulc_i / DS^{\text{ideal}} = ulc_i / (DP_{\text{PEV}} / (\alpha \cdot DP_{\text{PEV}}))^k \\ &= ulc_i \alpha^k = DP_{\text{PEV}} \cdot ulc_i / \sum_{e=1}^{N} ulc_e \end{aligned} \tag{3.31}$$

Substituting (3.31) into (3.30), it can be obtained that:

$$AP_{\mathrm{PEV}}^{k}(AP_{\mathrm{PEV}} - p_{\mathrm{PEV},i}^{\mathrm{fixed}}) = DP_{\mathrm{PEV}}^{k}(DP_{\mathrm{PEV}} - p_{\mathrm{PEV},i}^{\mathrm{ideal}}) \tag{3.32}$$

Suppose the mismatch between AP_{PEV} and DP_{PEV} exists in such a way that $AP_{\mathrm{PEV}} > DP_{\mathrm{PEV}} > 0$. Since k is set to a positive even number in (3.12), the following inequality can be obtained:

$$AP_{\mathrm{PEV}}^{k} > DP_{\mathrm{PEV}}^{k} \tag{3.33}$$

Based on (3.32) and (3.33),

$$\frac{DP_{\mathrm{PEV}} - p_{\mathrm{PEV},i}^{\mathrm{ideal}}}{AP_{\mathrm{PEV}} - p_{\mathrm{PEV},i}^{\mathrm{fixed}}} = \frac{AP_{\mathrm{PEV}}^{k}}{DP_{\mathrm{PEV}}^{k}} > 1 \tag{3.34}$$

In the case of G2V power being requested, both $AP_{\mathrm{PEV}} - p_{\mathrm{PEV},i}^{\mathrm{fixed}}$ and $DP_{\mathrm{PEV}} - p_{\mathrm{PEV},i}^{\mathrm{ideal}}$ are positive. Thus, from (3.34),

$$DP_{\mathrm{PEV}} - p_{\mathrm{PEV},i}^{\mathrm{ideal}} > AP_{\mathrm{PEV}} - p_{\mathrm{PEV},i}^{\mathrm{fixed}} > 0 \tag{3.35}$$

As it is supposed that $AP_{\mathrm{PEV}} > DP_{\mathrm{PEV}} > 0$, (3.35) implies the following relation:

$$p_{\mathrm{PEV},i}^{\mathrm{fixed}} > p_{\mathrm{PEV},i}^{\mathrm{ideal}} \tag{3.36}$$

(3.36) corresponds to a possible interruption that PEV *i* became nonresponsive and its power is fixed to its charger's rated power.

When *k* in (3.12) is increased to *k*+2 (as *k* is a positive even number), the following can be obtained similarly:

$$AP'^{k+2}_{\mathrm{PEV}}(AP'_{\mathrm{PEV}} - p_{\mathrm{PEV},i}^{\mathrm{fixed}}) = DP_{\mathrm{PEV}}^{k+2}(DP_{\mathrm{PEV}} - p_{\mathrm{PEV},i}^{\mathrm{ideal}}) \tag{3.37}$$

where AP'_{PEV} is the newly resulted actual aggregate PEV power corresponding to $k' = k + 2$.

If $AP'_{\mathrm{PEV}} \le DP_{\mathrm{PEV}}$, then

$$AP'^{k+2}_{\mathrm{PEV}} \le DP_{\mathrm{PEV}}^{k+2} \tag{3.38}$$

Also, together with (3.36), $AP'_{\mathrm{PEV}} \le DP_{\mathrm{PEV}}$ indicates the following inequality:

$$AP'_{\mathrm{PEV}} - p_{\mathrm{PEV},i}^{\mathrm{fixed}} < DP_{\mathrm{PEV}} - p_{\mathrm{PEV},i}^{\mathrm{ideal}} \tag{3.39}$$

(3.38) and (3.39) will lead to the following inequality:

$$AP'^{k+2}_{\mathrm{PEV}}(AP'_{\mathrm{PEV}} - p^{\mathrm{fixed}}_{\mathrm{PEV},i}) < DP^{k+2}_{\mathrm{PEV}}(DP_{\mathrm{PEV}} - p^{\mathrm{ideal}}_{\mathrm{PEV},i}) \tag{3.40}$$

which is in contradiction to (3.37) and implies that $AP'_{\mathrm{PEV}} \le DP_{\mathrm{PEV}}$ is incorrect. Instead, the following relation must hold:

$$AP'_{\mathrm{PEV}} > DP_{\mathrm{PEV}} \tag{3.41}$$

Next, the relation between AP_{PEV} and AP'_{PEV} is examined. From (3.32),

$$(DP_{\mathrm{PEV}} - p^{\mathrm{ideal}}_{\mathrm{PEV},i}) = AP^{k}_{\mathrm{PEV}} / DP^{k}_{\mathrm{PEV}}(AP_{\mathrm{PEV}} - p^{\mathrm{fixed}}_{\mathrm{PEV},i}) \tag{3.42}$$

then substitute (3.42) into (3.37):

$$\begin{aligned} AP'^{k+2}_{\mathrm{PEV}}(AP'_{\mathrm{PEV}} - p^{\mathrm{fixed}}_{\mathrm{PEV},i}) &= DP^{k+2}_{\mathrm{PEV}} AP^{k}_{\mathrm{PEV}} / DP^{k}_{\mathrm{PEV}}(AP_{\mathrm{PEV}} - p^{\mathrm{fixed}}_{\mathrm{PEV},i}) \\ &= DP^{2}_{\mathrm{PEV}} AP^{k}_{\mathrm{PEV}}(AP_{\mathrm{PEV}} - p^{\mathrm{fixed}}_{\mathrm{PEV},i}) \end{aligned} \tag{3.43}$$

Since $AP_{\mathrm{PEV}} > DP_{\mathrm{PEV}} > 0$ is assumed, the following can be obtained from (3.43):

$$AP'^{k+2}_{\mathrm{PEV}}(AP'_{\mathrm{PEV}} - p^{\mathrm{fixed}}_{\mathrm{PEV},i}) < AP^{k+2}_{\mathrm{PEV}}(AP_{\mathrm{PEV}} - p^{\mathrm{fixed}}_{\mathrm{PEV},i}) \tag{3.44}$$

If $AP'_{\mathrm{PEV}} \ge AP_{\mathrm{PEV}}$, the following can be deduced:

$$AP'^{k+2}_{\mathrm{PEV}} \ge AP^{k+2}_{\mathrm{PEV}} \tag{3.45}$$

$$AP'_{\mathrm{PEV}} - p^{\mathrm{fixed}}_{\mathrm{PEV},i} \ge AP_{\mathrm{PEV}} - p^{\mathrm{fixed}}_{\mathrm{PEV},i} > 0 \tag{3.46}$$

(3.45) and (3.46) will lead to the following inequality:

$$AP'^{k+2}_{\mathrm{PEV}}(AP'_{\mathrm{PEV}} - p^{\mathrm{fixed}}_{\mathrm{PEV},i}) \ge AP^{k+2}_{\mathrm{PEV}}(AP_{\mathrm{PEV}} - p^{\mathrm{fixed}}_{\mathrm{PEV},i}) \tag{3.47}$$

which is in contradiction to (3.44). Therefore, $AP'_{\mathrm{PEV}} \ge AP_{\mathrm{PEV}}$ is incorrect and the following relation must hold:

$$AP'_{\mathrm{PEV}} < AP_{\mathrm{PEV}} \tag{3.48}$$

With (3.41) and (3.48), it can be obtained that

$$AP_{\mathrm{PEV}} > AP'_{\mathrm{PEV}} > DP_{\mathrm{PEV}} > 0 \tag{3.49}$$

Therefore, it is proved that when the mismatch between AP_{PEV} and DP_{PEV} caused by the individual PEV power adjustment being interrupted exists in such a way that $AP_{\mathrm{PEV}} > DP_{\mathrm{PEV}} > 0$, increasing the exponent k in (3.12) can help to reduce the mismatch.

When the mismatch is in the form of $0 < AP_{\text{PEV}} < DP_{\text{PEV}}$, $AP_{\text{PEV}}^{k} < DP_{\text{PEV}}^{k}$. According to (3.32), $0 < DP_{\text{PEV}} - p_{\text{PEV},i}^{\text{ideal}} < AP_{\text{PEV}} - p_{\text{PEV},i}^{\text{fixed}}$. Thus, it can be obtained that

$$p_{\text{PEV},i}^{\text{ideal}} > p_{\text{PEV},i}^{\text{fixed}} \tag{3.50}$$

(3.50) corresponds to a possible interruption that the power adjustment of PEV *i* attempts to reach a high power level but is constrained to the charger's rated power.

To satisfy (3.37), the following inequality must be true:

$$AP'_{\text{PEV}} < DP_{\text{PEV}} \tag{3.51}$$

Otherwise, $AP'_{\text{PEV}} \geq DP_{\text{PEV}}$ will lead to $AP'^{k+2}_{\text{PEV}} \geq DP^{k+2}_{\text{PEV}}$, and together with (3.50) it will also lead to $AP'_{\text{PEV}} - p_{\text{PEV},i}^{\text{fixed}} > DP_{\text{PEV}} - p_{\text{PEV},i}^{\text{ideal}} > 0$. Thus, the inequality $AP'^{k+2}_{\text{PEV}}(AP'_{\text{PEV}} - p_{\text{PEV},i}^{\text{fixed}}) > DP^{k+2}_{\text{PEV}}(DP_{\text{PEV}} - p_{\text{PEV},i}^{\text{ideal}})$ can be resulted, which contradicts (3.37).

Since $0 < AP_{\text{PEV}} < DP_{\text{PEV}}$ is assumed, it can be obtained from (3.43) that:

$$AP'^{k+2}_{\text{PEV}}(AP'_{\text{PEV}} - p_{\text{PEV},i}^{\text{fixed}}) > AP^{k+2}_{\text{PEV}}(AP_{\text{PEV}} - p_{\text{PEV},i}^{\text{fixed}}) \tag{3.52}$$

If $AP'_{\text{PEV}} \leq AP_{\text{PEV}}$, then $AP'^{k+2}_{\text{PEV}} \leq AP^{k+2}_{\text{PEV}}$ and $0 < AP'_{\text{PEV}} - p_{\text{PEV},i}^{\text{fixed}} \leq AP_{\text{PEV}} - p_{\text{PEV},i}^{\text{fixed}}$, which disagrees with (3.52). Therefore, the following inequality must hold:

$$AP'_{\text{PEV}} > AP_{\text{PEV}} \tag{3.53}$$

From (3.51) and (3.53), it can be obtained that

$$0 < AP_{\text{PEV}} < AP'_{\text{PEV}} < DP_{\text{PEV}} \tag{3.54}$$

Therefore, it is proved that when the mismatch between AP_{PEV} and DP_{PEV} exists in such a way that $0 < AP_{\text{PEV}} < DP_{\text{PEV}}$, increasing the exponent *k* in (3.12) can also help to reduce the mismatch.

Moreover, from (3.32), it can be obtained that

$$\frac{1}{k} = \frac{\ln(DP_{\text{PEV}} / AP_{\text{PEV}})}{\ln(\dfrac{AP_{\text{PEV}} - p_{\text{PEV},i}^{\text{fixed}}}{DP_{\text{PEV}} - p_{\text{PEV},i}^{\text{ideal}}})} \tag{3.55}$$

As $k \to +\infty$, $1/k \to 0$, which implies that $\ln(DP_{\text{PEV}} / AP_{\text{PEV}}) \to 0$. Therefore,

$$\lim_{k\to\infty} AP_{\text{PEV}} = DP_{\text{PEV}} \tag{3.56}$$

In summary, the above proof has shown that in the case of G2V power being requested, increasing the value of k is helpful to remedy the mismatch between AP_{PEV} and DP_{PEV} caused by interruptions to individual PEV power adjustments. As k approaches to infinity, the mismatch would be reduced to zero.

The mismatch reduction resulted by increasing exponent k in the case of V2G power being requested can be proved in a similar way.

3.2.6 Overall Process of the Decentralized PEV Charging Control Scheme

The overall process of the proposed decentralized PEV charging control scheme is shown in Fig. 3.2 and 3.3.

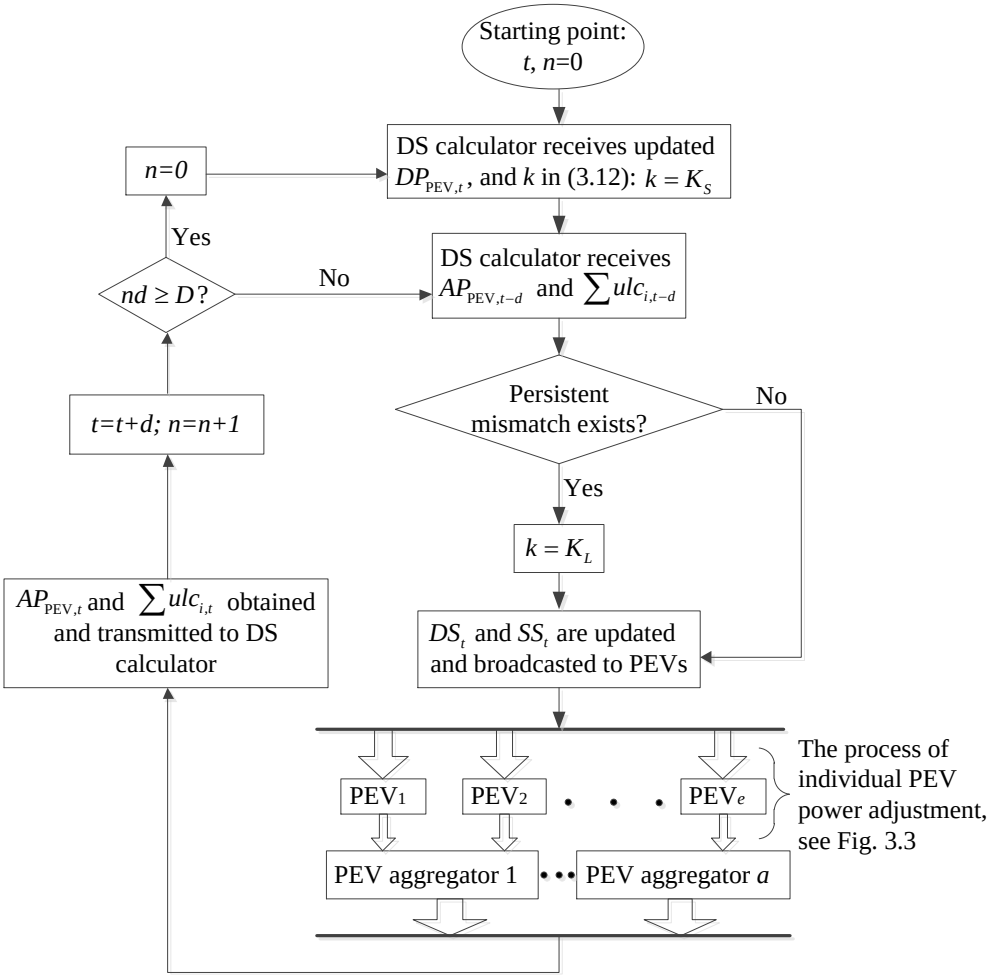

Fig. 3.2 Overall process of the proposed decentralized PEV charging control scheme; the process of individual PEV power adjustment is shown in Fig. 3.3.

When a PEV is connected to grid, the PEV user is allowed to specify the charging requirement in terms of the desired battery SOC and the planned departure time. With the charging requirement, the PEV smart charger will monitor the actual SOC and calculate the ULC parameter based on (3.13).

An information hub, named DS calculator, is needed to calculate the real-time DS. Inputs to the DS calculator include: 1) the desired aggregate PEV power $DP_{\text{PEV},t}$; 2) the power of controllable PEVs ; and 3) the ULC parameters of controllable PEVs for calculating α_t. The DS calculator will broadcast the DS together with the SS to all PEVs.

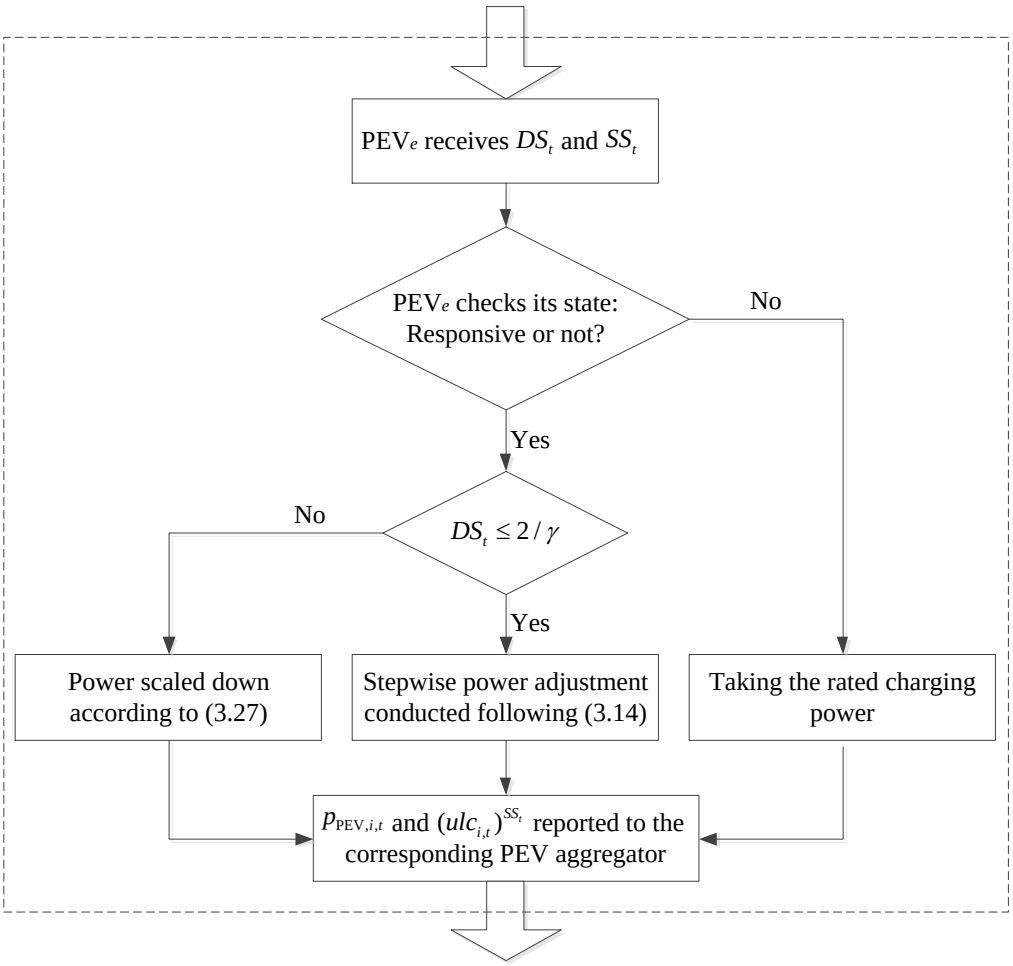

Fig. 3.3 The process of individual PEV power adjustment

For a responsive PEV, if the received DS is equal to or smaller than the upper limit $2/\gamma$, it will respond to the DS and make stepwise adjustment in its power

according to (3.14). If the received DS is greater than $2/\gamma$, the PEV will scale down its power according to (3.27). The updated powers and ULCs are transmitted back to the DS calculator. For a large population of dispersedly located PEVs, there can be regional PEV aggregators between individual PEVs and the DS calculator. A PEV will transmit its power and ULC data to its regional aggregator instead of directly to the DS calculator. Each aggregator summarizes the data of the PEVs and reports the aggregate data to the DS calculator. Such hierarchical communication mechanism can effectively reduce the communication burden on the DS calculator. If the BC margin drops below the preset threshold value, the PEV will enter the nonresponsive state and takes the rated charging power till its desired SOC is fulfilled.

The power and ULC of individual PEV, DS and SS are all updated at regular time interval *d*, while the desired aggregate PEV power $DP_{\mathrm{PEV},t}$ is updated at regular time interval *D*. *D* depends on the rate of change of $DP_{\mathrm{PEV},t}$ and normally it is set to be larger than *d* to allow adequate number of PEV power adjustments to be carried out for each $DP_{\mathrm{PEV},t}$ such that the actual PEV power $AP_{\mathrm{PEV},t}$ can closely follow $DP_{\mathrm{PEV},t}$. For *s* consecutive time steps of *d*, if the mismatch $\left|AP_{\mathrm{PEV},t} - DP_{\mathrm{PEV},t}\right|$ keeps being larger than a preset threshold *PM*, and $\Delta\left|AP_{\mathrm{PEV},t} - DP_{\mathrm{PEV},t}\right|$ between any two adjacent time steps is smaller than a threshold *PMV*, then the mismatch is considered as persistent. Two values, K_S and K_L, can be assigned to the exponent *k* in (3.12), where $K_S < K_L$. Normally, *k* is equal to K_S to prevent the DS from being oversensitive to the changes in the actual or the desired PEV power. When a persistent mismatch is detected, however, *k* will be set to K_L. When $DP_{\mathrm{PEV},t}$ is updated, *k* will be reset to K_S.

3.3 Modeling of the Test System

A PEV fleet is coupled with a wind farm to form a PEV-WF virtual plant. The decentralized charging control scheme is applied to guide the PEV power to

compensate the undesired fluctuations in the wind farm power output. Thus, the power output of the virtual plant will be the filtered, less fluctuating WP, which helps to maintain the balance between generation and demand and enhance the system frequency regulation.

3.3.1 Wind Farm Power Output and System Load Profile

A wind speed model which consists of four components including the base component, the ramp component, the gust component, and the turbulence [90, 91] is adopted to generate a series of wind speed data. A wind turbine power output model is then used to generate a WP profile based on the wind speed data. These models are outlined in Appendix B.

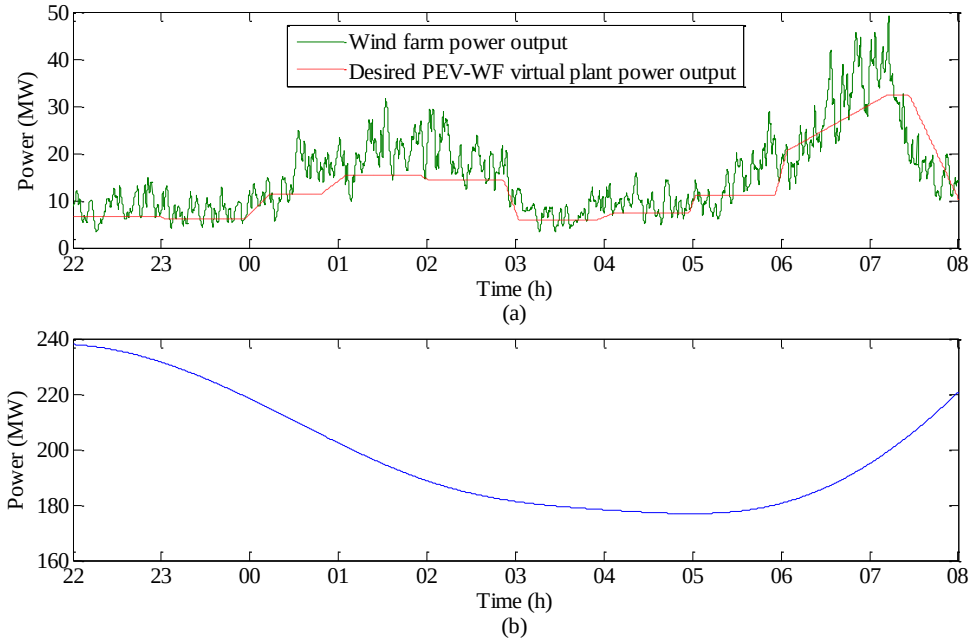

Fig. 3.4 (a) Wind farm power output profile and the desired power output of the PEV-WF virtual plant; (b) system load profile

The resulted wind farm power output profile is shown in Fig. 3.4(a). The desired power output from the PEV-WF virtual plant can be determined by the operator of the virtual plant (e.g. to satisfy certain ramp rate limit) or the system dispatch center (e.g. to help economic dispatch). The decision making should

take into account the forecasted WP and the PEV charging requirement. Any deviations of the actual WP from the desired value will be counterbalanced by the controlled PEV power. In this simulation, the desired power output of the virtual plant, which is shown in Fig. 3.4(a), is set to be smaller than the actual WP for most of the time so the surplus power can be used for PEV charging. To highlight the effect of neutralizing WP fluctuations on improving load frequency control, a smooth system load profile excluding PEV charging load is used in the simulation, as shown in Fig. 3.4(b).

3.3.2 Power System Model and Parameter Settings

A single-area system is used to investigate to what extent the load frequency control can benefit from the WP fluctuations being counterbalanced by the PEV power guided by the proposed control scheme. The block diagram of the single-area system is shown in Fig. 3.5. There are conventional thermal units, fast-reacting diesel generators (DGs) and a wind farm in the system. The thermal units provide both primary and secondary frequency regulation, whereas the DGs only conduct primary load frequency control. The parameters of the single-area power system model are summarized in Table 3.1 [92, 93].

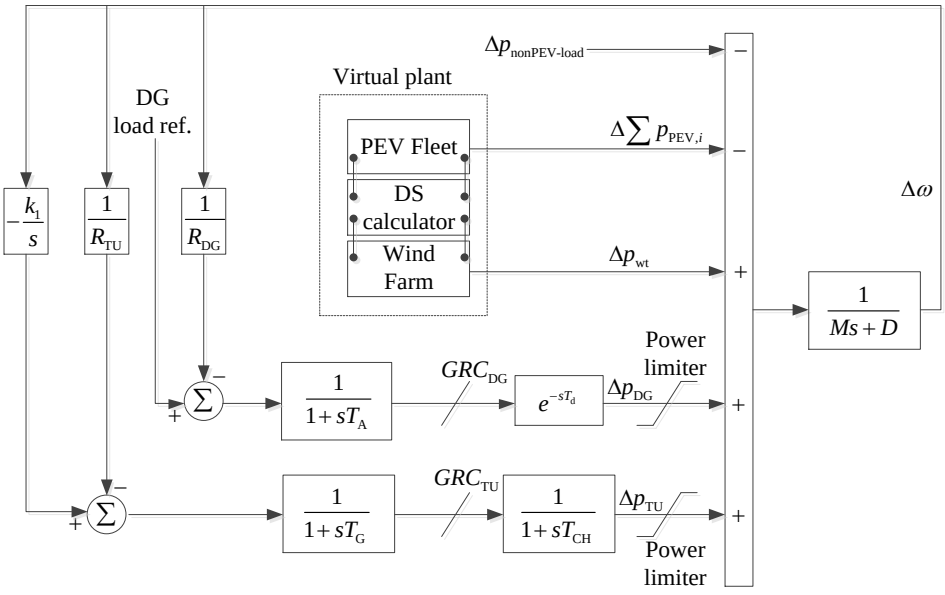

Fig. 3.5 Block diagram of the single-area power system model

Table 3.1 Parameters of the single-area power system model

Parameters	Values
Nominal frequency	50 Hz
Thermal units capacity	3×125 MW
Wind power capacity	25×2 MW
DG capacity	6×2 MW
No. of PEVs	2000
AGC execution frequency	every 2 s
M	10 s
D	9.375 MW/Hz
T_G, T_{CH}	0.2 s, 0.3 s
T_A, T_d	0.1 s, 0.1 s
$1/R_{TU}$, $1/R_{DG}$	150 MW/Hz, 60 MW/Hz
GRC_{TU}, GRC_{DG}	3×6.25 MW/min, 6×1.8 MW/min
k_1	1.5 MW/Hz/s

The investigation period is from 10 p.m. to 8 a.m. the next day, during which the system load is relatively low and the wind power may take a large share of the total generation. Besides, PEVs are normally parked and charged during this period for the next trip in the morning. The PEV is assumed to have a 24.15 kWh battery capacity with 5.06 kW rated charging power and 95% charging efficiency. For simplicity, the total 2000 PEVs are divided into 16 groups. PEVs in each group have the same initial SOC, desired SOC, and planned departure time. The initial SOC is between 25% and 50%, and the desired SOC is assumed to be either 90% or 95%. The planned departure time is distributed between 5 am and 8:30 am.

Frequency detection delay is modeled as a first-order lag with time constant 0.1 s. Wireless communication delay between PEV and the VMP calculator, and VMP calculation delay are modeled as dead time of 2 s and 1 s, respectively [94]. Thus, the time step d is 5 s. Percentage error in measuring the wind farm power output is modeled by a zero-mean white noise with standard deviation of 3%. The smaller value K_S for the exponent k in (3.12) is set to 2 and the larger value

K_L is set to 6. The parameter γ in (3.14), which affects the step size of individual PEV power adjustment, depends on the rate of change of the desired PEV power and the size of the PEV fleet. For the PEV-WF virtual plant described in Table 3.1, simulation studies showed that a value in the range of 0.01–0.08 is acceptable. Here, γ is set to 0.04. The scaling factor φ in (3.27) is set to 0.8. The charging margin threshold CM_{thld} for a PEV to stay responsive is set to 4%. In this study, for 3 consecutive time steps of d, if the mismatch $\left|AP_{\text{PEV},t} - DP_{\text{PEV},t}\right|$ is larger than $0.1\left|DP_{\text{PEV},t}\right|$ and $\Delta\left|AP_{\text{PEV},t} - DP_{\text{PEV},t}\right|$ between any two adjacent time steps is smaller than $0.01\left|DP_{\text{PEV},t}\right|$, then the mismatch is regarded as a persistent one. The wind farm power output is normally measured once every 30 seconds, so the time interval D at which the requested PEV power $DP_{\text{PEV},t}$ is updated is 30 s. Yet, if the average rate of change of WP is larger than 1.5 MW/min, D will be set to 8 s.

3.4 Simulation Results

3.4.1 Wind Power Fluctuation Compensation

With the proposed decentralized charging control scheme, the aggregate power of responsive PEVs is guided to counterbalance the wind power fluctuations. Relevant results are presented in Fig. 3.6.

From Fig. 3.6(a), it can be observed that with the proposed charging control, the aggregate power of responsive PEVs can track and neutralize the WP fluctuations timely and accurately. Thus, compared with the original WP profile, the power output from the PEV-WF virtual plant is much less fluctuating, as shown in Fig. 3.6(b). As time passes, an increasing number of responsive PEVs become nonresponsive or are plugged-out, as indicated in Fig. 3.6(c). Therefore, the fluctuation compensation provided by PEVs becomes insufficient after 6 a.m. and the virtual plant's power output begins to fluctuate again as a result.

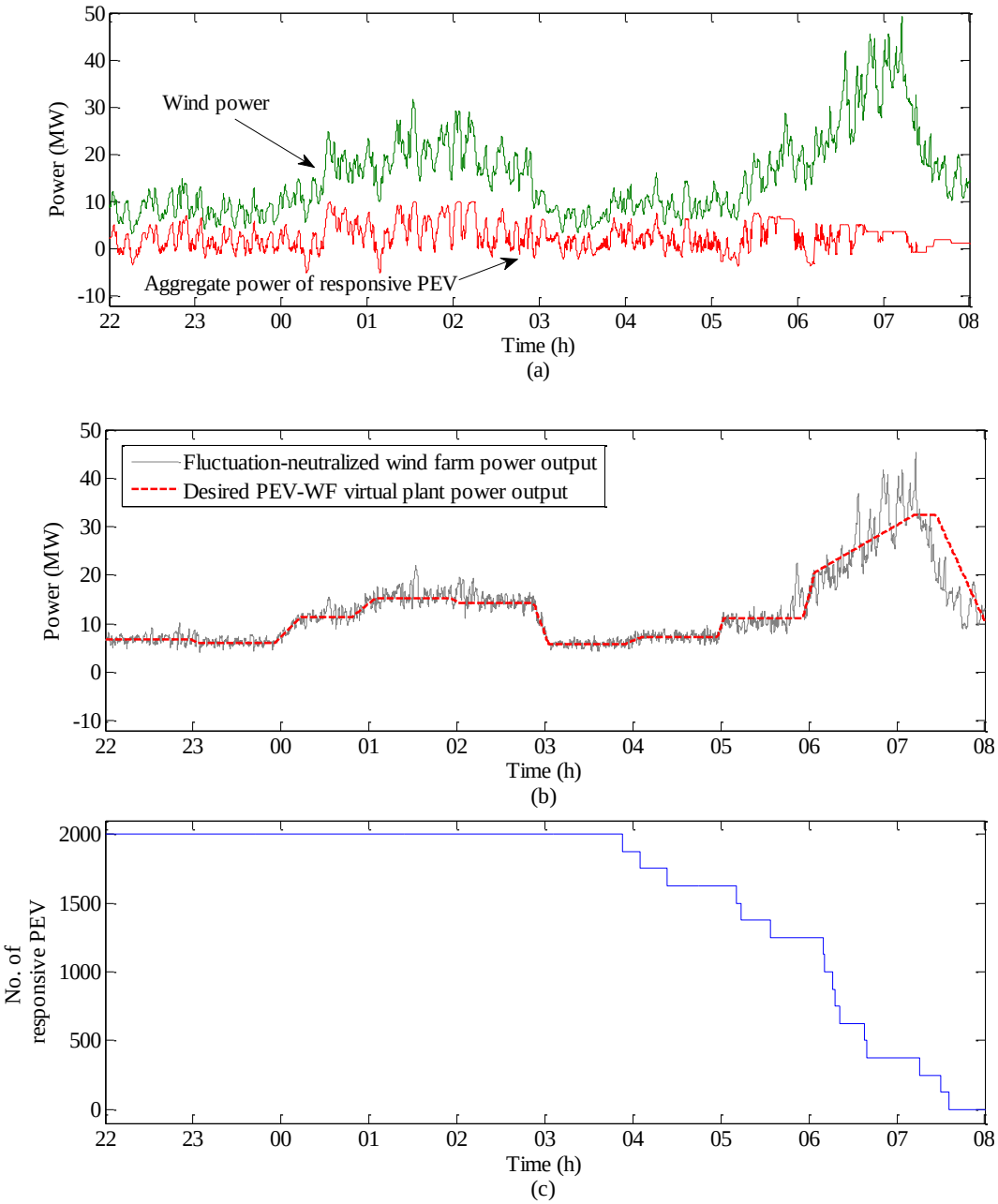

Fig. 3.6 PEV power guided by proposed charging control scheme to compensate the WP fluctuations: (a) the aggregate power of responsive PEVs; (b) the smoothed WP; (c) the number of responsive PEVs

3.4.2 Effect on System Frequency Regulation

In a system highly penetrated by WP, neutralizing WP fluctuations can effectively enhance the load frequency control. Here, the frequency regulation performance is examined under four scenarios for comparison purpose: 1)

frequency control by thermal units only; 2) frequency control by thermal units and DGs, where DGs provide fast-reacting reserve; 3) frequency control by thermal units and WP fluctuations compensated by the PEV power guided by the proposed charging control scheme; 4) frequency control by thermal units and PEVs, where the PEV power responds to frequency deviation based on a power-frequency droop controller [60]. Details of this controller are given in Appendix C.

In Scenario 2, six 2-MW DGs are half-loaded to provide equal amount of regulation up/down capacity. In Scenario 3 and 4, if the responsive PEVs account for less than 60% of the total PEVs under control, then some DGs would be turned on and half-rated to maintain the total fast-reserve capacity in the system higher than 6 MW. In Scenario 4, when the power-frequency droop controller described in [60] is applied, the maximum V2G gain (K_{max}) and the minimum frequency deviation (Δf_{min}) are set to 50 kW/Hz and -0.12 Hz, respectively, and all other parameters are kept the same. The accuracy of frequency measurements is affected by two factors: one is frequency estimation error, which can be controlled within 0.01−0.02 Hz [95], and the other is noise with noise strength from several to tens of mHz [62]. In this study, the frequency estimation error and noise is considered bindingly by superposing a zero-mean white noise with standard deviation of 0.02 Hz on the actual frequency. The frequency deviations in each of the four scenarios are shown in Fig. 3.7. Table 3.2 summarizes the maximum magnitudes and root mean square (RMS) values of the frequency deviations.

As can be seen from Fig. 3.7 and Table 3.2, the frequency regulation by thermal units alone underperforms the others. This is because the relatively slow generation rate constraints of the thermal units prevent them from catching up with fast WP ramps. The use of fast-reacting DGs effectively improves frequency regulation performance in Scenario 2. Comparing the results in Scenario 3 with those in Scenario 2, it can see that in a system with high WP

penetration level, compensating WP fluctuations can effectively enhance the system load frequency control, resulting in a frequency regulation even better than that with the use of fast-reacting generators. In Scenario 4, PEVs equipped with power-frequency droop controllers give the best regulation performance when frequency measurements are accurate. The regulation performance is considerably degraded, however, in the presence of frequency estimation errors and noise.

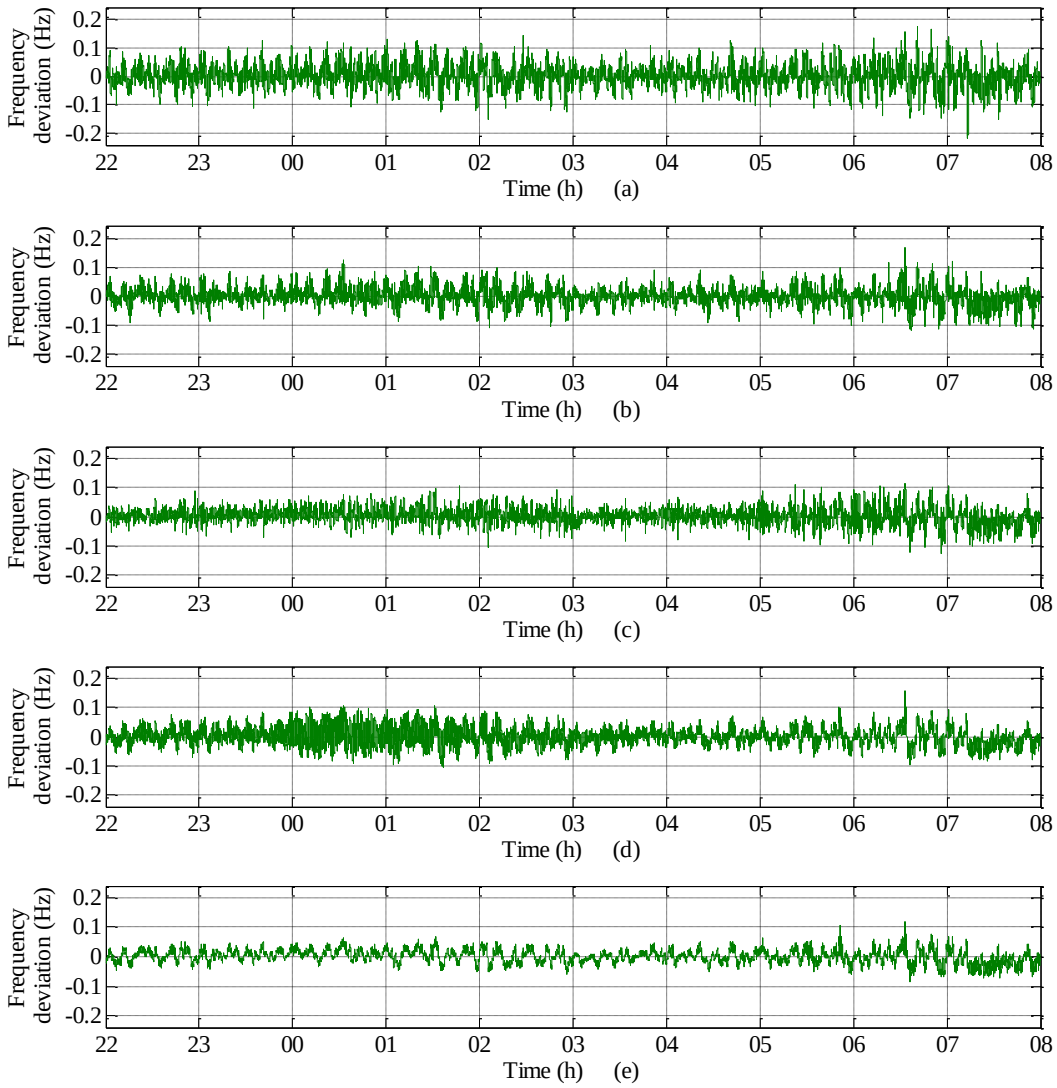

Fig. 3.7 Frequency deviation in (a) Scenario 1; (b) Scenario 2; (c) Scenario 3; (d) Scenario 4 with frequency estimation errors and noise; and (e) Scenario 4 without frequency estimation errors or noise

Table 3.2 Frequency deviation evaluation indices

Scenario	1	2	3	4 (w. errors and noise)	4 (w/o. errors or noise)
Max (Hz)	0.2144	0.1670	0.1256	0.1582	0.1183
RMS (Hz)	0.0394	0.0289	0.0251	0.0281	0.0220

3.4.3 Satisfaction of PEV User's Charging Requirement

Though the charging process of PEV is controlled for system regulation purpose, the PEV charging requirement should be satisfied without compromising the convenience of PEV owner. In the proposed charging control scheme, a PEV with higher ULC shall receive more G2V power when the desired PEV power is positive ($DP_{\mathrm{PEV},t} > 0$), or supply less V2G power when $DP_{\mathrm{PEV},t} < 0$.

The SOC variations of two representative PEVs are examined. Both PEVs have equal initial SOC (40%) and desired SOC (90%). Two cases are considered. In the first case, PEV_1 is planned to depart at 07:00 and PEV_2 at 05:30, whereas in the second case their planned departure times are exchanged at 03:00. The SOC variations in Case 1 and 2 are shown in Fig. 3.8(a) and 3.8(b), respectively.

It can be seen from Fig. 3.8(a) that PEV_2 receives more charging power than PEV_1 due to its earlier planned departure time. PEV_1, however, obtains more charging power than PEV_2 after 03:00 in Case 2, as shown in Fig. 3.8(b). Consequently, the SOC of PEV_1 exceeds that of PEV_2 soon after resetting their planned departure times. Both PEVs manage to achieve the desired SOC upon their planned departure times. This example confirms the ability of the proposed charging control scheme to recognize and satisfy the heterogeneous PEV charging requirements specified by PEV users.

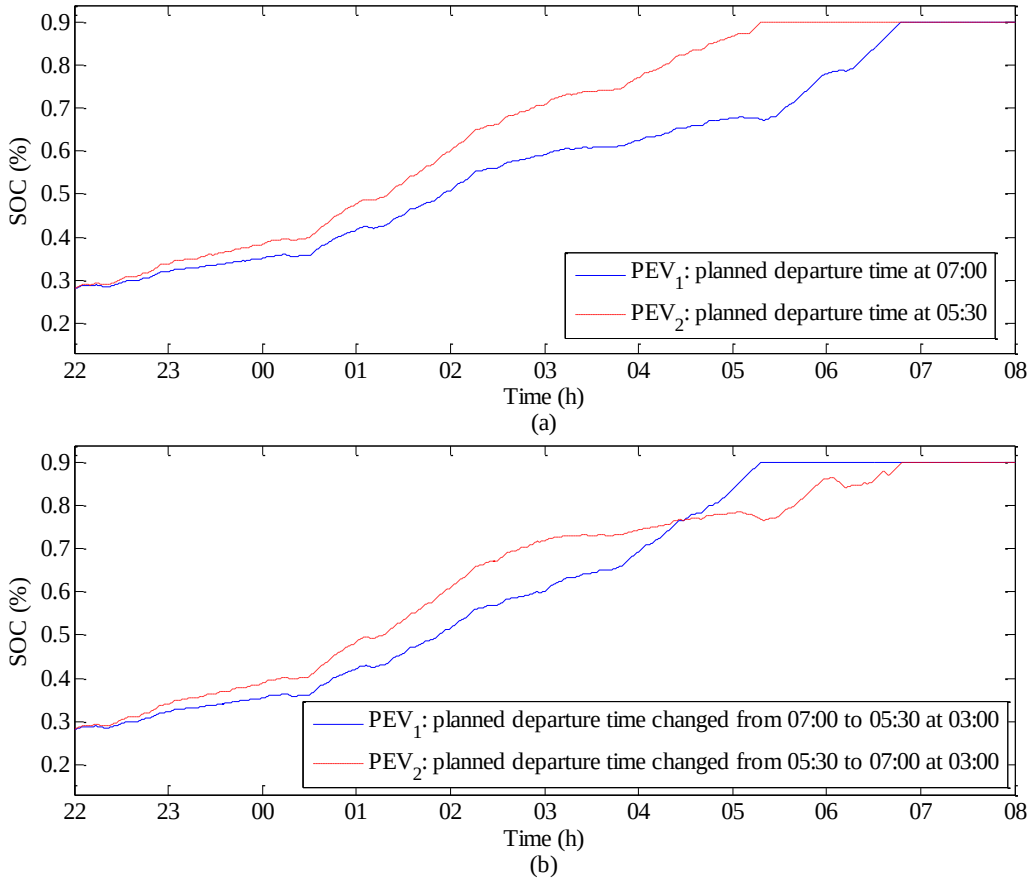

Fig. 3.8 SOC variations of two representative PEVs: (a) earlier planned departure time for PEV_2; (b) planned departure time reset during charging

3.5 Summary

In this chapter, a decentralized PEV charging control scheme based on the congestion pricing mechanism is designed and then applied to guide the PEV power to compensate WP fluctuations. Each PEV can be responsive or nonresponsive, depending on its charging margin. A responsive PEV will autonomously adjust its charging/discharging power according to the received DS, SS and its own ULC, while a nonresponsive PEV simply absorbs its rated charging power. The DS and SS are updated at the DS calculator and broadcasted to all PEVs. Since no central control entity would be needed to determine the power for each of the individual PEVs, the proposed scheme is scalable to a large population of dispersedly located PEVs. Also, the communication between PEV

and the DS calculator is unsophisticated without needing any special communication network and/or protocol.

Simulation results verify that with the proposed decentralized charging control scheme, the PEV power can respond to undesired WP fluctuations timely and accurately. The resultant power output from the PEV-WF virtual plant is much less fluctuating compared with the original WP. As a result, the system load frequency control is greatly enhanced. Besides, differential charging power distribution among PEVs consistent with their ULCs is realized, which is important to satisfying the heterogeneous PEV charging requirements specified PEV users.

Chapter IV

A Hierarchical Scheme for Utilizing PEV Power to Hedge against Unit Ramp Cycling Operations in a System with High Wind Power Penetration Level

4.1 Introduction

With increasing WP capacity added to the power system, the conventional thermal units will face more and greater net load variations. Also, the number of thermal units online will decrease as the system load is increasingly supplied by WP. As a result, the thermal units will incur more frequent and significant cycling operations.

Unit cycling is defined as a generator being loaded at varying levels, including on/off cycling, ramp cycling (significant load following), and minimum load operations [96]. Generator components such as the boiler, gas pipes, and turbine will have to go through considerable thermal transient and pressure stress during cycling operations, which causes accelerated thermal fatigue, blade erosion and chemical deposit, among many other damaging mechanisms. Over time, the accumulated wear and tear to unit components will be translated into higher equivalent forced outage rates, higher maintenance and replacement costs, and ultimately shortened service life of the generator [63, 96, 97].

In this chapter, a hierarchical scheme is proposed to schedule, dispatch and control the PEV power to hedge against the URC operations in a system with considerable WP. The objective is to minimize the URC operations without sacrificing too much PEV charging energy. This hierarchical scheme consists of

3 levels. At the top level, a variation range of the system net load is determined first to capture the WP uncertainty. Then, the PEV power is scheduled day-ahead to reshape the net load variation range (NLVR) to minimize the number of URC operations that can be caused by the possible net load realizations in the NLVR. The reshaped NLVR will be much more resistant to WP fluctuations than the original NLVR with regard to avoiding the URC operation. Yet, the reshaped NLVR is usually at the cost of excessive interruptions to PEV charging. As a result, significant charging energy will be lost. Based on the latest update of WP predictions, the middle-level dispatch model will exempt over-scheduled anti-URC regulation onus on PEVs such that PEV charging power can be restored to various degrees to promote PEV charging. To ensure effective URC mitigation and avoid over-restoring the PEV charging power, the actual net load determined in the middle-level dispatch model is restricted in the reshaped NLVR produced by the top-level scheduling model. At the bottom-level, the decentralized charging control scheme proposed in Chapter III is adopted to implement the PEV power dispatch instruction from the middle-level dispatch model.

4.2 Formulation of the 3-Level Hierarchical Scheme

The proposed hierarchical scheme aims to minimize the URC operation. Though the scheme can also be applied to reduce the on/off cycling operations, such application, however, usually causes prolonged and intense interruptions to PEV charging, which is likely to render PEVs severely undercharged. Here, it is assumed that a UC problem has been solved before the start of the proposed hierarchical scheme, and the generator on-off statuses in the hierarchical scheme are fixed based on the UC solution.

4.2.1 Construction of Wind Power Uncertainty Interval

In the proposed scheme, the PEV power is coordinated to reshape the NLVR which is obtained by superposing the WP uncertainty interval onto the system load profile. In each timeslot of the scheduling horizon, the WP uncertainty interval is a range of possible values for the actual WP in that timeslot. Given a WP forecast, the associated WP uncertainty interval can be attained by consulting the historical data of actual WP corresponding to that particular forecast. The procedures are summarized as follows [98].

First, all WP data shall be normalized to per unit values based on the installed WP capacity. Second, the range of WP output from 0 to 1 p.u. is equally divided into K smaller intervals, where K is a user-specified integer. Each interval is referred to as a forecast grouping interval (FGI). For FGI k ($k = 1, 2, \ldots, K$), the actual WP data whose corresponding forecast values belong to FGI k will be collected. Thus, K datasets of actual WP can be obtained, in one-to-one correspondence with the K FGIs. Next, a probability histogram (PH) is constructed from the kth actual WP dataset, which represents the conditional probability density function of the actual WP for a WP forecast belonging to FGI k. Then, the cumulative distribution functions (CDF) can be calculated accordingly.

Here, the historical data of predicted and actual WP in 2013 from Elia [99], the transmission system operator of Belgium, are used to construct the WP uncertainty intervals. With K = 40, the PHs and CDFs of the actual WP data corresponding to the 10th and 30th FGIs are illustrated in Fig. 4.1.

In timeslot t, if the WP forecast w_t^{f} belongs to FGI k and the WP uncertainty interval is required to cover Q% of the possible values for the actual WP suggested by the historical data, the bounds of the uncertainty interval are determined as follows:

$$\bar{W}_t^{\mathrm{UI}} = F_k^{-1}\left((1+Q\%)/2\right) \tag{4.1}$$

$$\underline{W}_t^{\mathrm{UI}} = F_k^{-1}\left((1-Q\%)/2\right) \tag{4.2}$$

where $\overline{W}_t^{\mathrm{UI}}$ and $\underline{W}_t^{\mathrm{UI}}$ are the upper and lower bounds of the WP uncertainty interval in timeslot *t*, respectively; and F_k^{-1} is the inverse CDF of the *k*th actual WP dataset.

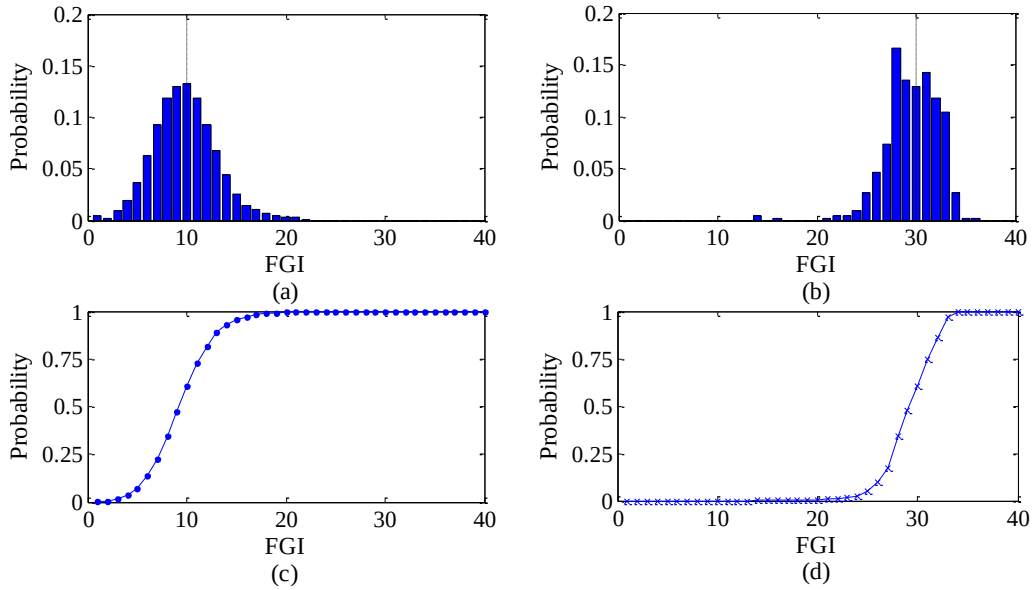

Fig. 4.1 PH and CDF of the actual WP dataset associated with FGI *k*. Subfigure (a) and (c): k = 10; (b) and (d): k = 30.

4.2.2 Representation of Unit Ramp Cycling Operations

Whether a generator power output change is counted as a URC operation depends on the magnitude and duration of that change. In [63], if a change in generator power output between two consecutive timeslots is greater than a preset threshold and the change is not caused by unit start-up or shut-down, then it is regarded as a URC operation. In this study, the URC operation is defined within a time window which consists of more than 2 consecutive timeslots. The URC representation in [63] is extended to a more general form as follows:

$$\begin{aligned} &g_{i,t} - g_{i,t-1} - LN \cdot rc_{i,t} \le RCTHR_i + LN \cdot \left(2 - U_{i,t} - U_{i,t-1}\right), \\ &\forall i \in I, \forall t \in T \end{aligned} \tag{4.3}$$

$$g_{i,t} - g_{i,t-k} - LN \cdot rc_{i,t} \le RCTHR_i + LN \cdot \left((k+1) - \sum_{r=0}^{k} U_{i,t-r} \right) + LN \sum_{h=1}^{k-1} rc_{i,t-h}, \ \forall i \in I, \forall t \in T, \forall k = 2 \ldots WS - 1 \quad (4.4)$$

$$g_{i,t-1} - g_{i,t} - LN \cdot rc_{i,t} \le RCTHR_i + LN \cdot \left(2 - U_{i,t} - U_{i,t-1}\right), \ \forall i \in I, \forall t \in T \quad (4.5)$$

$$g_{i,t-k} - g_{i,t} - LN \cdot rc_{i,t} \le RCTHR_i + LN \cdot \left((k+1) - \sum_{r=0}^{k} U_{i,t-r} \right) + LN \sum_{h=1}^{k-1} rc_{i,t-h}, \ \forall i \in I, \forall t \in T, \forall k = 2 \ldots WS - 1 \quad (4.6)$$

where $g_{i,t}$ is the power output of unit i in timeslot t; $rc_{i,t}$ is the binary URC indicator for unit i in timeslot t; $RCTHR_i$ is the unit i's threshold of ramp cycling operation; $U_{i,t}$ is the indicator for on/off (1/0) status of unit i in timeslot t; LN is a large positive number; I is the set of indexes for generators; T is the set of indexes for timeslots; and WS is the number of timeslots of the time window in which the URC operation is defined.

Inequalities (4.3) and (4.4) identify the upward URC operations while (4.5) and (4.6) flag the downward ones. $rc_{i,t}$ will be set to 1 if the change in unit i's power output developed between timeslot t and t-k exceeds $RCTHR_i$. According to [96], the threshold is selected to be 20% of the generator's dependable capacity. The above formulation shows that a URC operation can be developed between any two timeslots within the WS-slot time window. The second terms on the right-hand side of (4.3)–(4.6) ensure that a URC operation is a power output change of an online generator so as to distinguish URC operations from on/off cycling operations. The third terms on the right-hand side of (4.4) and (4.6) are used to avoid double-counting the URC operation. That is, the unit output change between timeslot t and t-k, even if greater than the ramp cycling threshold, should not be regarded as a URC operation if there has been a URC operation already formed in an intermediate timeslot t-h (t-k < t-h < t). Thus, the unit power output variations which have accounted for one URC operation will not repeatedly contribute to the formation of another.

Fig. 4.2 illustrates the identification of URC operations, where $RCTHR_i$ is set to 50 MW and a URC operation shall be within a 4-slot time window (i.e. $WS = 4$). As can be seen from Fig. 4.2, the maximum unit output change ($\Delta P_{\max}$) in a time window may be different from the amount of output change that form the URC operation (ΔP_{URC}). In the four time windows shown in Fig. 4.2, $\Delta P_{\max}$ = 52, 60, 52, 66 MW while correspondingly ΔP_{URC} = 22, 60, 10, 28 MW. Therefore, even if $\Delta P_{\max}$ exceeds the 50 MW ramp cycling threshold in all of the four windows, there is only one URC operation formed in the second window.

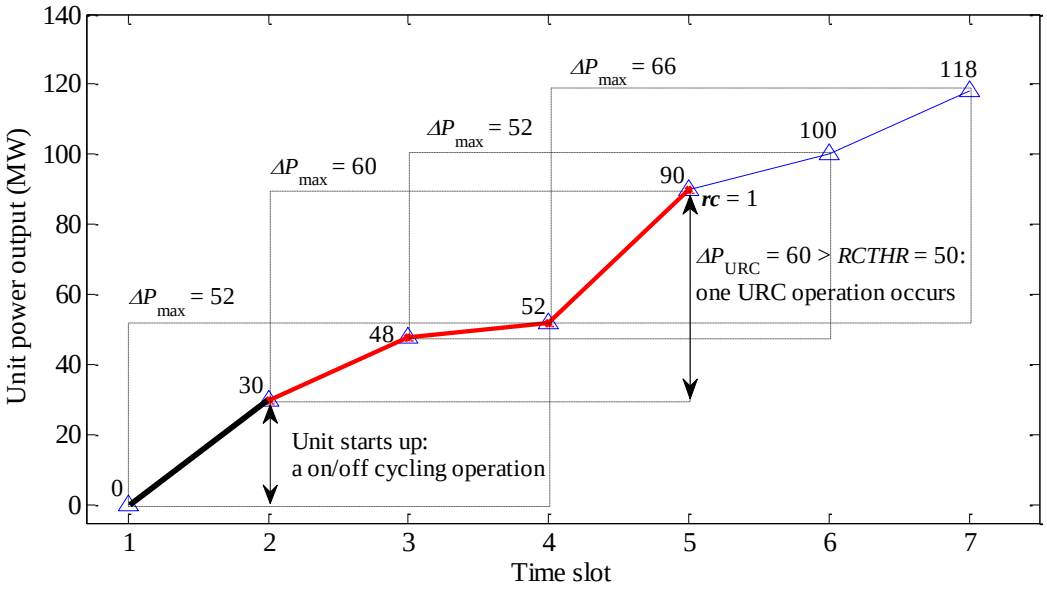

Fig. 4.2 Illustration of identifying the URC operation, $RCTHR_i$ = 50 MW and the URC operation is defined in a 4-slot time window (shown as the rectangles).

4.2.3 Top-Level Scheduling Model

The NLVR contains numerous possible net load realizations. In response to a possible realization, the generators may incur some URC operations which cannot be avoided by properly distributing the cycling onus among the generators. The top-level scheduling model of the proposed scheme aims to minimize such URC operations by reshaping the NLVR via PEV power coordination. Fig. 4.3 illustrates a NLVR and its reshaped counterpart. It can be

seen that the reshaped NLVR is less varying. For an example of WP realization, the correspondingly realized net load profile in the reshaped NLVR is also seen to be much less varying than that in the original NLVR. Since the top-level scheduling model takes into account all possible net load scenarios in the NLVR including those extremely varying ones, the PEV demand response can be intensely used to reshape the NLVR, which may lead to a considerable loss of the PEV charging energy.

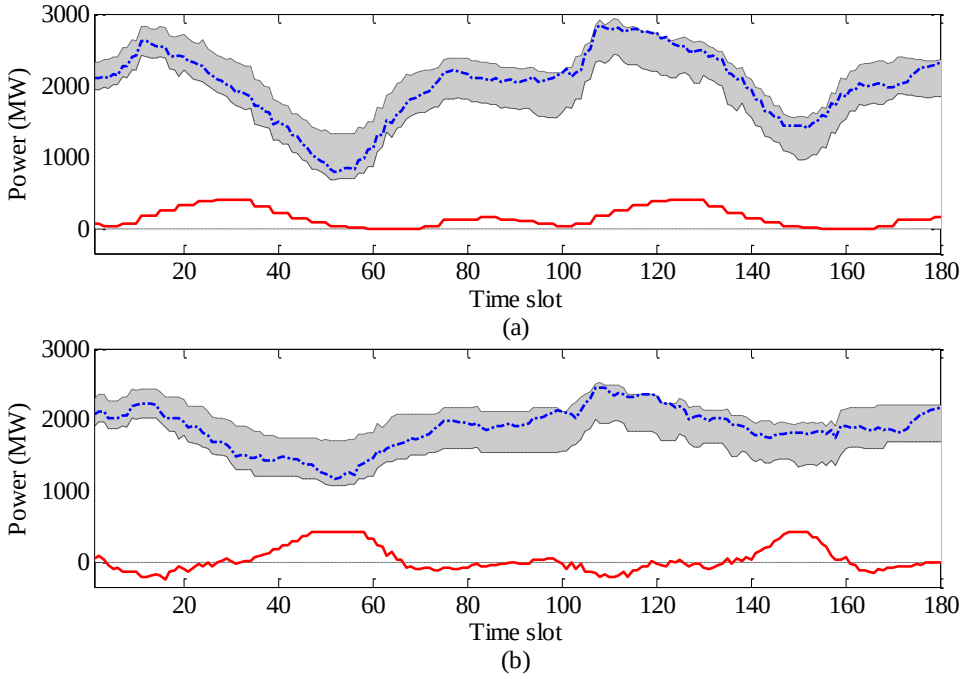

Fig. 4.3 (a) the original NLVR (grey shaded area) with uncontrolled PEV power (the red solid line); (b) the reshaped NLVR with coordinated PEV power. For an example WP realization, the correspondingly realized net load profiles are represented by the blue dash lines within the NLVRs

The detailed formulation of the top-level scheduling model is as follows:

$$\min \sum_{t\in T}\Bigg\{\sum_{i\in I}\theta_{rc}\left[rc_{i,t}^{\text{up}}+rc_{i,t}^{\text{down}}\right] + \sum_{i\in I}\theta_{fc}SW\left[fc_{i,t}(\bar{g}_{i,t})+fc_{i,t}(\underline{g}_{i,t})\right]-p_t^{\text{PEV}}SW\Bigg\} \tag{4.7}$$

subject to

1) Power balance constraints:

$$\sum_{i\in I}\bar{g}_{i,t} = L_t + p_t^{\text{PEV}} - \underline{W}_t^{\text{UI}},\ \forall t \in T \tag{4.8}$$

$$\sum_{i\in I}\underline{g}_{i,t} = L_t + p_t^{\text{PEV}} - \bar{W}_t^{\text{UI}},\ \forall t \in T \tag{4.9}$$

2) Generator power output range:

$$U_{i,t}\underline{G}_i \le \bar{g}_{i,t} \le U_{i,t}\bar{G}_i,\ \forall t \in T, \forall i \in I \tag{4.10}$$

$$U_{i,t}\underline{G}_i \le \underline{g}_{i,t} \le U_{i,t}\bar{G}_i,\ \forall t \in T, \forall i \in I \tag{4.11}$$

3) 3-segment piecewise linear approximation of the quadratic generator fuel cost function [100]:

$$fc_{i,t}(g_{i,t}) = fc_i^{\min}U_{i,t} + \sum_{l=1}^{3} SL_{l,i}\kappa_{l,i,t},\ \forall t \in T, \forall i \in I \tag{4.12}$$

$$fc_i^{\min} = a_i + b_i\underline{G}_i + c_i\underline{G}_i^2,\ \forall i \in I \tag{4.13}$$

$$g_{i,t} = \sum_{l=1}^{3}\kappa_{l,i,t} + U_{i,t}\underline{G}_i,\ \forall t \in T, \forall i \in I \tag{4.14}$$

$$0 \le \kappa_{1,i,t} \le G_{1,i} - \underline{G}_i,\ \forall t \in T, \forall i \in I \tag{4.15}$$

$$0 \le \kappa_{2,i,t} \le G_{2,i} - G_{1,i},\ \forall t \in T, \forall i \in I \tag{4.16}$$

$$0 \le \kappa_{3,i,t} \le \bar{G}_i - G_{2,i},\ \forall t \in T, \forall i \in I \tag{4.17}$$

4) Identification of URC operations:

$$\bar{g}_{i,t} - \underline{g}_{i,t-k} - LN \cdot rc_{i,t}^{\text{up}} \le RCTHR_i + LN \cdot \left((k+1) - \sum_{r=0}^{k} U_{i,t-r}\right), \quad \forall t \in T, \forall i \in I, \forall k = 1 \ldots WS - 1 \tag{4.18}$$

$$\bar{g}_{i,t-k} - \underline{g}_{i,t} - LN \cdot rc_{i,t}^{\text{down}} \le RCTHR_i + LN \cdot \left((k+1) - \sum_{r=0}^{k} U_{i,t-r}\right), \quad \forall t \in T, \forall i \in I, \forall k = 1 \ldots WS - 1 \tag{4.19}$$

5) Start-up and shut-down ramp rate constraints

$$\bar{g}_{i,t} \le SURL_i\left(U_{i,t} - U_{i,t-1}\right) + \bar{G}_i\left(1 - U_{i,t} + U_{i,t-1}\right), \forall t \in T, \forall i \in I \tag{4.20}$$

$$\bar{g}_{i,t} \le SDRL_i \left(U_{i,t} - U_{i,t+1}\right) + \bar{G}_i \left(1 - U_{i,t} + U_{i,t+1}\right), \forall t \in T, \forall i \in I \tag{4.21}$$

$$\underline{g}_{i,t} \le SURL_i \left(U_{i,t} - U_{i,t-1}\right) + \bar{G}_i \left(1 - U_{i,t} + U_{i,t-1}\right), \forall t \in T, \forall i \in I \tag{4.22}$$

$$\underline{g}_{i,t} \le SDRL_i \left(U_{i,t} - U_{i,t+1}\right) + \bar{G}_i \left(1 - U_{i,t} + U_{i,t+1}\right), \forall t \in T, \forall i \in I \tag{4.23}$$

6) System-level PEV power and energy constraints

$$P_t^{\text{PEV\_dch}} \le p_t^{\text{PEV}} \le P_t^{\text{PEV\_ch}}, \forall t \in T \tag{4.24}$$

$$E_t^{\text{PEV\_dch}} \le \sum_{t_n=1}^{t} p_{t_n}^{\text{PEV}} SW \le E_t^{\text{PEV\_ch}}, \forall t \in T \tag{4.25}$$

7) Binary variable constraints

$$rc_{i,t}^{\text{up}}, rc_{i,t}^{\text{down}} \in \{0,1\}, \ \forall t \in T, \forall i \in I \tag{4.26}$$

A URC operation is most likely to occur between two timeslots if the net load varies from the upper bound of the NLVR in one timeslot to the lower bound in the other, and vice versa. Thus, the generator power output in each timeslot of the scheduling horizon is represented by $\bar{g}_{i,t}$ and $\underline{g}_{i,t}$ which correspond to the upper and lower bounds of the NLVR, respectively. In (4.7)–(4.26), $\bar{G}_i$ and $\underline{G}_i$ are the maximum and minimum power output of unit i, respectively; SW is the width of timeslot, which is 15 min in this study; $rc_{i,t}^{\text{up}}$ and $rc_{i,t}^{\text{down}}$ are binary indicators for the upward and downward URC operation of unit i in timeslot t, respectively; p_t^{PEV} is the PEV power in timeslot t; $P_t^{\text{PEV\_ch}}$ and $P_t^{\text{PEV\_dch}}$ are the aggregate charging and discharging power capacity of all connected and controllable PEVs in timeslot t, respectively; $E_t^{\text{PEV\_ch}}$ and $E_t^{\text{PEV\_dch}}$ are the maximum amount of energy that can be charged to and discharged from the controllable PEVs from the first timeslot to the tth timeslot of the scheduling horizon, respectively; L_t is the non-PEV load in timeslot t; $SL_{l,i}$ is the slope of segment l of the piecewise linear fuel cost function of unit i; $\kappa_{l,i,t}$ represents the power output within the range of segment l of the piecewise linear fuel cost function of unit i in timeslot t; a_i, b_i, and c_i are the coefficients of the quadratic fuel cost function of unit i; $G_{1,i}$ and $G_{2,i}$ are the upper limits of segment 1 and 2 of

the piecewise linear fuel cost function of unit *i*, respectively; and $SURL_i$ and $SDRL_i$ are the start-up and shut-down ramp rate limits of unit *i*, respectively.

The objective function (4.7) contains three objectives: to minimize the number of URC operations (the primary objective) with the least sacrifice of PEV charging energy (the secondary objective) while the generators are dispatched economically (the tertiary objective). Coefficients θ_{rc} and θ_{fc} are used to prioritize these three objectives and their ranges are as follows:

$$\theta_{rc} > \max\left\{P_t^{\text{PEV\_ch}} - P_t^{\text{PEV\_dch}} : t \in T\right\} \tag{4.27}$$

$$0 < \theta_{fc} < 0.5 \Big/ \max\left\{ifc_i(\bar{G}_i) :\ i \in I\right\}. \tag{4.28}$$

where $ifc_i(\bar{G}_i)$ represents the incremental fuel cost of unit *i* at its maximum power output $\bar{G}_i$. $P_t^{\text{PEV\_ch}} - P_t^{\text{PEV\_dch}}$ represents the PEV power range in timeslot *t*. With θ_{rc} set to be greater than the maximum PEV power range in the scheduling horizon, eliminating a URC operation will outweigh any possible increases in the PEV power. Thus, the primary objective is prioritized over the secondary one. With θ_{fc} satisfying (4.28), an increase in the PEV power will have an overwhelming effect on minimizing the objective function though it will lead to a higher generator fuel cost. Hence, the secondary objective is prioritized over the tertiary one.

The system level PEV power and energy in constraints (4.24) and (4.25) can be determined by aggregating the information of individual PEVs. Here, the information reporting mechanism proposed in [101] is adopted to realize the information aggregation. Each PEV user will report his/her anticipated charging activities to his/her regional PEV aggregator. The reported information includes the expected plug-in and plug-out time, the rated charging power, the normal uncontrolled charging power profile leading to the desired SOC, and the normal uncontrolled discharging power profile leading to minimum allowable SOC. Note that the reported charging plans do not have to be very accurate. In fact, routine charging schedule is already good enough to approximate charging plan

for most of the commuter PEVs. The system level PEV power and energy are determined as follows:

$$\begin{cases} P_t^{\text{PEV\_ch}} = \sum_{A_k \in AI} \sum_{e \in A_k} P_e^{\text{rated}} C_{e,t} \\ P_t^{\text{PEV\_dch}} = -\sum_{A_k \in AI} \sum_{e \in A_k} \eta_e P_e^{\text{rated}} C_{e,t} \end{cases} \tag{4.29}$$

$$E_t^{\text{PEV\_ch}} = \sum_{t_n=1}^{t} \sum_{A_k \in AI} \sum_{e \in A_k} P_{e,t_n}^{\text{unctl\_ch}} SW \tag{4.30}$$

$$E_t^{\text{PEV\_dch}} = \sum_{t_n=1}^{t} \sum_{A_k \in AI} \sum_{e \in A_k} P_{e,t_n}^{\text{unctl\_dch}} SW \tag{4.31}$$

where AI is the set of indexes for PEV aggregators; A_k is set of indexes for PEVs affiliated to the kth PEV aggregator; P_e^{rated} and η_e are the rated charging power and charger efficiency of PEV e, respectively; $P_{e,t_n}^{\text{unctl\_ch}}$ and $P_{e,t_n}^{\text{unctl\_dch}}$ represent the normal uncontrolled charging and discharging power of PEV e in timeslot t, respectively; and $C_{e,t}$ is the binary indicator for plug-in/-out (1/0) status of PEV e in timeslot t. Note that $P_{e,t_n}^{\text{unctl\_ch}}$ and $P_{e,t_n}^{\text{unctl\_dch}}$ are the charging/discharging power measured at the grid end of the PEV charger.

There are two things worth noting about the top-level scheduling model. First, the term $LN\sum_{h=1}^{k-1} rc_{i,t-h}$, which is included in (4.4) and (4.6) to avoid double-counting the URC operation, is absent from the URC conditions (4.18) and (4.19). This is because in the top-level scheduling model, all net load scenarios in the NLVR are considered possible. Thus, a URC operation caused by a net load scenario should not deny the possibilities of the URC operations caused by the other net load scenarios. The term will be re-included in the URC conditions in the middle-level dispatch model to ensure correct counting of the URC operation.

Second, no ramp rate constraints are imposed on the power output of an online generator. In fact, ramp rate constraints established between $\overline{g}_{i,t-1}$ and $\underline{g}_{i,t}$ as well as $\underline{g}_{i,t-1}$ and $\overline{g}_{i,t}$ are unnecessary, since they would force a lot more generators to be committed to provide sufficient ramping capacity for handling the steepest possible net load ramp between two adjacent timeslots. The steepest

possible net load ramps, in fact, rarely occur. According to the historical data used in this study, 99.95% of the actual net load ramps between two adjacent slots are not as half steep as their corresponding steepest possible ramps. Ramp rate constraints will be engaged in the middle-level dispatch model to ensure actual generator dispatches satisfy the ramp rate limits.

4.2.4 Middle-Level Dispatch Model

The dispatch model resembles the process of receding horizon control. That is, when determining the PEV and generator dispatches for the current timeslot *t*, the dispatch model will optimize the entire dispatch horizon $[t,\ t+OH-1]$. Then the dispatch horizon is shifted one slot forward to determine the dispatches for the new current timeslot. The dispatch model adopts the latest update of WP forecasts. If the updated forecasts indicate less varying WP, then the unnecessary interruptions to PEV charging power scheduled by the top-level model would be exempted to promote PEV charging.

As the dispatch model rolls forward and approaches future timeslots, the WP forecasts are assumed to be iteratively updated with gradually diminished uncertainties. Specifically, when the dispatch model is solved for the current timeslot t_c, it is assumed that the actual WP in t_c is revealed and the WP uncertainty intervals in the subsequent *NUF* slots will shrink, depending on how far the timeslot is into the future [102]. The WP uncertainty intervals are updated as follows:

$$\overline{W}^{\text{UI\_upd}}_{t_c+n} = W^{\text{a}}_{t_c+n} + n/\left(NUF+1\right)\left(\overline{W}^{\text{UI}}_{t_c+n} - W^{\text{a}}_{t_c+n}\right) \tag{4.32}$$

$$\underline{W}^{\text{UI\_upd}}_{t_c+n} = W^{\text{a}}_{t_c+n} + n/\left(NUF+1\right)\left(\underline{W}^{\text{UI}}_{t_c+n} - W^{\text{a}}_{t_c+n}\right) \tag{4.33}$$

where $\overline{W}^{\text{UI\_upd}}_{t_c+n}$ and $\underline{W}^{\text{UI\_upd}}_{t_c+n}$ represent the updated upper and lower bounds of the WP uncertainty interval in timeslot t_c+n, respectively; $W^{\text{a}}_{t_c+n}$ is the actual WP in timeslot t_c+n; and $n=1\ldots NUF$. Beyond timeslot t_c+NUF, the WP uncertainty intervals remain the same as those considered in the top-level scheduling.

The dispatch horizon is shown in Fig. 4.4. From the current timeslot t_c to t_c+*OH*-1 is the optimization horizon. When the PEV and generator dispatches in t_c are optimized, the dispatches in each of the remaining *OH*-1 timeslots of the optimization horizon will be optimized as well. *OH* is set to *NUF*+1 such that the mid-level dispatch model will take all updated WP forecasts into consideration.

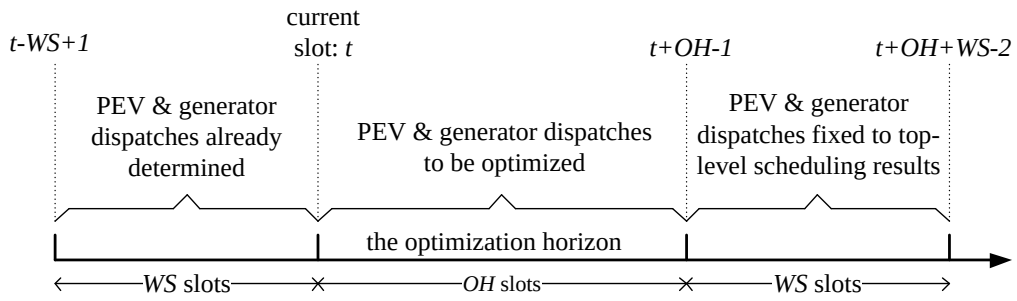

Fig. 4.4 Schematic of the dispatch horizon of the mid-level dispatch model

It should be noted that URC operations can be formed across the boundaries of the optimization horizon, e.g. between t_c-1 and t_c+1 across t_c, or between t_c+*OH*-2 and t_c+*OH* across t_c+*OH*-1. To consider such cross-boundary URC operations in the dispatch model, two *WS*-slot time windows are attached to the optimization horizon: one from the current slot t_c back to t_c-*WS*+1, the other from t_c+*OH*-1 to t_c+*WS*+*OH*-2. Dispatches in the past timeslots will be fixed to the earlier solutions of the dispatch model, while dispatches in the timeslots beyond the optimization horizon will adhere to the results generated by the top-level scheduling, i.e.:

$$\begin{aligned} &p_t^{\text{PEV}} = P_t^{\text{PEV\_disp}}, g_{i,t} = P_{i,t}^{\text{gen\_disp}}, \\ &\forall t \in \left[t_c - WS + 1,\ t_c - 1\right], \forall i \in I \end{aligned} \tag{4.34}$$

$$\begin{aligned} &p_t^{\text{PEV}} = P_t^{\text{PEV\_sched}}, \overline{g}_{i,t} = \overline{P}_{i,t}^{\text{gen\_sched}}, \underline{g}_{i,t} = \underline{P}_{i,t}^{\text{gen\_sched}}, \\ &\forall t \in \left[t_c + OH,\ t_c + OH + WS - 2\right], \forall i \in I \end{aligned} \tag{4.35}$$

The middle-level dispatch model has similar formulation to the top-level scheduling model, comprising objective function (4.7) and constraints (4.8)–(4.26). For simplicity, only their differences are outlined here. There are four

differences. First, in the current timeslot t_c, the dual generator power output variables $\overline{g}_{i,t_c}$ and $\underline{g}_{i,t_c}$ used in the top-level scheduling model would coincide and become a single variable g_{i,t_c} in the mid-level dispatch model. This is because the actual WP in t_c is assumed to be revealed when the dispatch model is solved for t_c, thus the system net load in t_c is deterministic.

Second, between timeslots *t-k* and *t*, if there are some intermediate timeslots *t-h* (*t-k* < *t-h* < *t*) in which generator power outputs are deterministic, the URC condition regarding to *t-k* and *t* will have the term $LN\sum_{h=1}^{k-1} rc_{i,t-h}$ included. The URC conditions in the dispatch model are summarized as follows:

1) between the current timeslot t_c and a past timeslot:

$$g_{i,t_c} - g_{i,t_c-1} - LN \cdot rc_{i,t_c}^{\text{up}} \le RCTHR_i + LN \cdot \left(2 - U_{i,t_c} - U_{i,t_c-1}\right), \quad \forall i \in I \tag{4.36}$$

$$g_{i,t_c} - g_{i,t_c-k} - LN \cdot rc_{i,t_c}^{\text{up}} \le RCTHR_i + LN \cdot \left((k+1) - \sum_{r=0}^{k} U_{i,t_c-r}\right) + LN \sum_{h=1}^{k-1} (rc_{i,t_c-h}^{\text{up}} + rc_{i,t_c-h}^{\text{down}}), \quad \forall i \in I, \forall k = 2 \ldots WS-1 \tag{4.37}$$

$$g_{i,t_c-1} - g_{i,t_c} - LN \cdot rc_{i,t_c}^{\text{down}} \le RCTHR_i + LN \cdot \left(2 - U_{i,t_c} - U_{i,t_c-1}\right), \quad \forall i \in I \tag{4.38}$$

$$g_{i,t_c-k} - g_{i,t_c} - LN \cdot rc_{i,t_c}^{\text{down}} \le RCTHR_i + LN \cdot \left((k+1) - \sum_{r=0}^{k} U_{i,t_c-r}\right) + LN \sum_{h=1}^{k-1} (rc_{i,t_c-h}^{\text{up}} + rc_{i,t_c-h}^{\text{down}}), \quad \forall i \in I, \forall k = 2 \ldots WS-1 \tag{4.39}$$

2) between the current timeslot t_c and a future timeslot:

$$\overline{g}_{i,t_c+k} - g_{i,t_c} - LN \cdot rc_{i,t_c+k}^{\text{up}} \le RCTHR_i + LN \cdot \left(k + 1 - \sum_{r=0}^{k} U_{i,t_c+r}\right), \quad \forall i \in I, \forall k = 1 \ldots WS-1 \tag{4.40}$$

$$g_{i,t_c} - \underline{g}_{i,t_c+k} - LN \cdot rc^{\text{down}}_{i,t_c+k} \le RCTHR_i + LN \cdot \left(k+1-\sum_{r=0}^{k} U_{i,t_c+r} \right), \quad (4.41)$$
$$\forall i \in I, \forall k = 1 \ldots WS-1$$

3) between a future timeslot and a past timeslot:

$$\bar{g}_{i,t} - g_{i,t-k} - LN \cdot rc^{\text{up}}_{i,t} \le RCTHR_i + LN \cdot \left(k+1-\sum_{r=0}^{k} U_{i,t-r} \right)$$
$$+LN \sum_{h=t-t_c}^{k-1} (rc^{\text{up}}_{i,t_c-h} + rc^{\text{down}}_{i,t_c-h}), \quad (4.42)$$
$$\forall i \in I, \forall t \in \left[t_c+1, t_c+WS-2 \right], \forall k \in \left[t-t_c+1, WS-1 \right]$$

$$g_{i,t-k} - \underline{g}_{i,t} - LN \cdot rc^{\text{down}}_{i,t} \le RCTHR_i + LN \cdot \left(k+1-\sum_{r=0}^{k} U_{i,t-r} \right)$$
$$+LN \sum_{h=t-t_c}^{k-1} (rc^{\text{up}}_{i,t_c-h} + rc^{\text{down}}_{i,t_c-h}), \quad (4.43)$$
$$\forall i \in I, \forall t \in \left[t_c+1, t_c+WS-2 \right], \forall k \in \left[t-t_c+1, WS-1 \right]$$

4) between two future timeslots:

$$\bar{g}_{i,t} - \underline{g}_{i,t-k} - LN \cdot rc^{\text{up}}_{i,t} \le RCTHR_i + LN \cdot \left(k+1-\sum_{r=0}^{k} U_{i,t-r} \right),$$
$$\forall i \in I, \forall t \in \left[t_c+2, t_c+OH+WS-2 \right], \quad (4.44)$$
$$\forall k \in \left[1, \min\left\{ t-(t_c+1), WS-1 \right\} \right]$$

$$\bar{g}_{i,t-k} - \underline{g}_{i,t} - LN \cdot rc^{\text{down}}_{i,t} \le RCTHR_i + LN \cdot \left(k+1-\sum_{r=0}^{k} U_{i,t-r} \right),$$
$$\forall i \in I, \forall t \in \left[t_c+2, t_c+OH+WS-2 \right], \quad (4.45)$$
$$\forall k \in \left[1, \min\left\{ t-(t_c+1), WS-1 \right\} \right]$$

Third, ramp rate limits will be imposed on generator power outputs in some of the timeslots in the optimization horizon of the dispatch model. Denote two adjacent timeslots in the optimization horizon by t_c+g and t_c+g+1, where $0 \le g \le OH-2$. The condition for the ramp rate limits to be imposed on the generator power outputs in t_c+g and t_c+g+1 is that the WP uncertainties in both of the timeslots have been sufficiently diminished. In this study, the WP uncertainty in a timeslot is regarded to have been sufficiently diminished if the

updated WP uncertainty interval in that timeslot has shrunk to an extent that its width is smaller than or equal to half of the width of the original WP uncertainty interval in that timeslot considered in the top-level scheduling model. That is, if $\overline{W}_{t_c+g}^{\text{UI\_upd}} - \underline{W}_{t_c+g}^{\text{UI\_upd}} \le 0.5(\overline{W}_{t_c+g}^{\text{UI}} - \underline{W}_{t_c+g}^{\text{UI}})$ and $\overline{W}_{t_c+g+1}^{\text{UI\_upd}} - \underline{W}_{t_c+g+1}^{\text{UI\_upd}} \le 0.5(\overline{W}_{t_c+g+1}^{\text{UI}} - \underline{W}_{t_c+g+1}^{\text{UI}})$, the ramp rate limits will be added between $\overline{g}_{i,t_c+g}$ and $\underline{g}_{i,t_c+g+1}$ as well as $\underline{g}_{i,t_c+g}$ and $\overline{g}_{i,t_c+g+1}$. To integrate the ramp rate limits, (4.20)–(4.23) will be transformed into the following constraints:

$$\begin{aligned} &\overline{g}_{i,t} - \underline{g}_{i,t-1} \le \overline{G}_i + \left(RUL_i - SURL_i\right)U_{i,t-1} + \left(SURL_i - \overline{G}_i\right)U_{i,t}, \\ &\forall t \in \left[t_c, t_c + NS_{\text{half\_NRW}}\right], \forall i \in I \end{aligned} \tag{4.46}$$

$$\begin{aligned} &\overline{g}_{i,t-1} - \underline{g}_{i,t} \le \overline{G}_i + \left(SDRL_i - \overline{G}_i\right)U_{i,t-1} + \left(RDL_i - SDRL_i\right)U_{i,t}, \\ &\forall t \in \left[t_c, t_c + NS_{\text{half\_NRW}}\right], \forall i \in I \end{aligned} \tag{4.47}$$

$$\underline{g}_{i,t} \le \overline{g}_{i,t}, \forall t \in \left[t_c, t_c + NS_{\text{half\_NRW}}\right], \forall i \in I \tag{4.48}$$

where RUL_i and RDL_i are the upward and downward ramp rate limits of unit i, respectively; and $NS_{\text{half\_NRW}}$ is the number of future timeslots in which the WP uncertainty has been sufficiently diminished.

Forth, the dispatch model runs the risk of overly restoring the PEV charging power because the dispatch decision-making only takes into account the limited number of timeslots of the dispatch horizon. The over restoration of PEV charging power may leave insufficient anti-URC regulation capacity of PEVs for the future timeslots beyond the dispatch horizon, thus jeopardizing the overall effectiveness of the PEV-aided URC mitigation. To avoid the over restoration, the reshaped NLVR from the top-level scheduling model, which has strong mitigating effect on URC operations, is used in the dispatch model to confine the updated NLVR resulted by the dispatch model:

$$\begin{aligned} &L_t + P_t^{\text{PEV\_sched}} - \underline{W}_t^{\text{UI}} \ge L_t + p_t^{\text{PEV}} - \underline{W}_t^{\text{UI\_disp}}, \\ &\forall t \in \left[t_c, t_c + OH - 1\right] \end{aligned} \tag{4.49}$$

$$L_t + P_t^{\text{PEV\_sched}} - \bar{W}_t^{\text{UI}} \le L_t + p_t^{\text{PEV}} - \bar{W}_t^{\text{UI\_disp}}, \quad \forall t \in [t_c, t_c + OH - 1] \tag{4.50}$$

4.2.5 Bottom-Level Decentralized PEV Power Control

The decentralized PEV charging control scheme proposed in Chapter III is adopted here to guide numerous dispersedly located PEVs to implement the PEV power dispatch instruction issued by the middle-level dispatch model. Note that in this study, though it would be perfect if the PEVs can reach the target SOCs specified by their owners while the PEV power is controlled to help mitigate URC operations, some charging energy usually have to be compromised to alleviate the URC operation most effectively, thus it is not a must for the PEVs to be charged to their target SOCs and the PEVs in this study will stay responsive during their entire charging periods.

The PEVs are divided into two groups: the responsive PEV group and the spare PEV group. The power of responsive PEVs is controlled to follow the dispatch instruction. However, there often exists a mismatch between the dispatch instruction and the power of responsive PEVs, which is referred to as a control inaccuracy. The control inaccuracy can be remedied by increasing the value of the exponent *k* in generating the DS as in (3.12). If the control inaccuracy still persists after the largest value of *k* is applied, the power of spare PEVs will be altered to further compensate the control inaccuracy. Normally, a spare PEV is charged at the power level

$$R_{\text{min-avg},e} = C_e^{\text{batt}} (SOC_e^{\text{desired}} - SOC_e^{\text{initial}}) \big/ \big(\eta_e (DT_e - AT_e)\big) \tag{4.51}$$

which is the minimum average charging power for the spare PEV *e* to achieve its desired SOC before its planned departure time. In (4.51), C_e^{batt} is the battery capacity of PEV *e*; SOC_e^{initial} and SOC_e^{desired} are the initial and desired SOC of PEV *e*, respectively; η_e is the charger efficiency; and AT_e and DT_e are the arrival and departure time of PEV *e*, respectively. From this power level, the

spare PEV can adjust its power up or down when needed to offset the control inaccuracy. The decentralized charging control method is also used to control the power of spare PEVs.

4.3 A Benchmark Scheme

A benchmark scheme is developed from the BESS control methods proposed in [65, 69] to control the PEV power to hedge against the URC operation. In the benchmark scheme, PEVs reserve upward and downward regulation capacities by being charged at power levels lower than their rated charging power. The partial charging power level is termed as the PEV base power level and represented as a fraction of the rated power.

At the scheduling stage of the benchmark scheme, a series of simulations are conducted to search through different PEV base power levels to find the one at which PEVs reserve sufficient anti-URC regulation capacity. Point predictions of WP are considered in the simulations. The procedures are as follows. For a PEV base power level $\delta \in [0,1]$, the corresponding base charging power is $\delta P_e^{\text{rated}}$. The scheduling model of the benchmark scheme is solved to determine the minimum amount of anti-URC regulation power required in each timeslot. The model is formulated as follows:

$$\min \sum_{t\in T}\left[\sum_{i\in I}\theta_{rc} rc_{i,t} + \sum_{i\in I}\left(\theta_{fc}\cdot fc_{i,t}(g_{i,t})\right) + p_t^{\text{reg\_up}} - p_t^{\text{reg\_down}}\right] \tag{4.52}$$

subject to

1) Power balance constraints

$$\sum_{i\in I} g_{i,t} = L_t + P_{\text{base},\delta,t}^{\text{PEV}} + p_t^{\text{reg\_up}} + p_t^{\text{reg\_down}} - W_t^{\text{PP}},\ \forall t \in T \tag{4.53}$$

2) Range of regulation power

$$0 \le p_t^{\text{reg\_up}} \le P_t^{\text{PEV\_ch}},\ \forall t \in T \tag{4.54}$$

$$P_t^{\text{PEV\_dch}} \le p_t^{\text{reg\_down}} \le 0,\ \forall t \in T \tag{4.55}$$

together with the generator output range constraints (deterministic version of (4.10) and (4.11)), generator fuel cost function ((4.12)–(4.17)), URC constraints ((4.3)–(4.6)), generator ramp rate constraints (deterministic version of (4.46) and (4.47)), and the binary variable constraint $rc_{i,t} \in \{0,1\}$. In (4.53), $p_t^{\text{reg\_up}}$ and $p_t^{\text{reg\_down}}$ are the upward and downward anti-URC regulation power required in timeslot *t*, respectively; $P_{\text{base},\delta,t}^{\text{PEV}}$ is the aggregate PEV base power corresponding to the base power level δ in timeslot *t*; and W_t^{PP} represents the point prediction of WP in timeslot *t*.

Next, the determined anti-URC regulation power $p_t^{\text{reg\_up}}$ and $p_t^{\text{reg\_down}}$ are added to the base power $P_{\text{base},\delta,t}^{\text{PEV}}$ to obtain the initial anti-URC PEV power profile, denoted by $P_{\text{pre-adj},\delta,t}^{\text{PEV}}$. Then, $P_{\text{pre-adj},\delta,t}^{\text{PEV}}$ is adjusted as follows to satisfy the PEV power and energy constraints (4.24) and (4.25):

$$P_{\text{adj},\delta,t}^{\text{PEV}} = \max\left\{\min\left\{P_{\text{pre-adj},\delta,t}^{\text{PEV}},\ P_t^{\text{PEV\_ch}}\right\},\ P_t^{\text{PEV\_dch}}\right\},\ \forall t \in T \tag{4.56}$$

$$P_{\text{adj},\delta,t}^{\text{PEV}} = \begin{cases} P_{\text{adj},\delta,t}^{\text{PEV}}, & \text{if } E_t^{\text{PEV\_dch}} \le \sum_{t_n=1}^{t} P_{\text{adj},\delta,t_n}^{\text{PEV}} SW \le E_t^{\text{PEV\_ch}} \\ 0, & \text{otherwise} \end{cases},\ \forall t \in T \tag{4.57}$$

where $P_{\text{adj},\delta,t}^{\text{PEV}}$ is the anti-URC power profile that can be actually implemented by the PEVs with base power level δ. Finally, how many URC operations still persist after implementing $P_{\text{adj},\delta,t}^{\text{PEV}}$ is checked by re-solving the scheduling model with $P_{\text{base},\delta,t}^{\text{PEV}}$ in (4.53) substituted by $P_{\text{adj},\delta,t}^{\text{PEV}}$, and $p_t^{\text{reg\_up}}$ and $p_t^{\text{reg\_down}}$ fixed to zero.

Following the above procedures, the values of δ from 0 to 1 at a step of 0.05 are searched through to find the one corresponding to the least number of persistent URC operations, which is denoted by $\delta_{\text{least\_URC}}$. $\delta_{\text{least\_URC}}$ will be adopted by PEVs to reserve anti-URC regulation capacity. If more than one $\delta_{\text{least\_URC}}$ can be found, the one that gives the least sacrifice of PEV charging energy will be chosen.

The dispatch process is similar to the scheduling. The dispatch model takes into account the latest update of the WP forecast and rolls forward through each timeslot to determine $p_t^{\text{reg\_up}}$ and $p_t^{\text{reg\_down}}$. The anti-URC PEV power profile is calculated as $\delta_{\text{least\_URC}} P_t^{\text{PEV\_ch}} + p_t^{\text{reg\_up}} + p_t^{\text{reg\_down}}$ and then adjusted according to (4.56) and (4.57) to satisfy the PEV power and energy constraints. The adjusted charging power profile is the one to be actually implemented by PEVs to hedge against the URC operations. It is assumed that the anti-URC regulation onus is distributed among individual PEVs in proportion to their regulation capacities.

The differences between the benchmark scheme and the proposed 3-level hierarchical scheme are summarized in Table 4.1.

Table 4.1 Comparison of the proposed 3-level hierarchical scheme and the benchmark scheme

	Proposed scheme	Benchmark scheme
Wind power	Wind power uncertainty intervals	Wind power point predictions
Objective of the scheduling stage	To minimize the URC operations that can be caused by the possible net load realizations within the NLVR	To reserve sufficient anti-URC regulation capacity in PEVs
Outcome of the scheduling stage	A reshaped NLVR	A PEV base power level
PEV charging promotion	To exempt the over-scheduled anti-URC regulation onus on PEVs	Not considered
Individual PEV power	Autonomous PEV power adjustment based on the real-time DS, SS and ULC	Regulation onus distributed among PEVs in proportion to their regulation capacities

4.4 Simulation Setting

The proposed scheme and the benchmark scheme are tested in a 16-unit system over an 81-hour scheduling horizon. The horizon contains 324 15-min timeslots (SW = 0.25 hr.), and in each of them the WP and system load are assumed to be unchanged.

4.4.1 Generator Data

9 coal-fired units and 7 gas-fired units are considered in the simulation. The parameters of the coal-fired units are obtained from [103] and those of the gas-fired units are given in [104]. For quick reference, the generator parameters are summarized in Table 4.2.

Table 4.2 Generator parameters

	Unit type		
	Coal-fired	Coal-fired	Gas-fired
No. of unit	5	4	7
$\overline{G}_i$ (MW)	350	155	150
$\underline{G}_i$ (MW)	140	56	42
RUL_i (MW/min)	4	3	2.5
RDL_i (MW/min)	4	3	2.5
$SURL_i$ (MW)	150	65	90
$SDRL_i$ (MW)	150	65	90
$RCTHR_i$ (MW)	70	31	30

The coefficients of the quadratic generator fuel cost functions are presented in Table 4.3, which are calculated by using the generator heat rate curves and fuel prices. The adopted fuel prices of coal and natural gas are 2.41 $/MMBtu and 5.34 $/MMBtu, respectively, which are the US average costs of coal and natural gas for electricity generation in April 2014 [105].

Table 4.3 Generator cost data

	Unit type		
	350 MW Coal-fired	155 MW Coal-fired	150 MW Gas-fired
a_i ($/MW^{2}h)	0.00786	0.01341	0.01426
b_i ($/MW)	17.91	18.19	49.67
c_i ($/h)	779.7	444.5	1013
Estimated cost of URC operation, lower limit ($/operation)	490	296.1	45

The threshold $RCTHR_i$ for a change in generator power output to be regarded as a damaging URC operation is set to 20% of the generator's dependable capacity [96]. The time window for checking the URC operation may differ in width for different generators, depending on specific generator type, design, operating history, etc [96]. As no explicit results have been found in the accessible literature, it is assumed that the time window spans a period of 3 hours, i.e. WS = 12, for all units considered in this study. The large constant LN in the URC conditions is set to 1000.

4.4.2 Wind Power and Non-PEV Load

The historical data of forecasted and actual WP from aggregate Belgian wind farms in 2013 [99] are used to construct the WP uncertainty intervals. With the number of FGIs set to 40 (K = 40), 40 WP uncertainty intervals are extracted. For each of the 40 FGIs, its corresponding WP uncertainty interval covers 96% of the values of the actual WP dataset associated with that FGI, i.e. Q% = 96%.

The forecasted and actual WP profiles of aggregate Belgian wind farms from 15:15 6/3/2014 to 00:15 10/3/2014 are used in the simulation, as shown in Fig. 4.5(a). To further investigate the performance of the proposed scheme in an extreme scenario of WP intermittency, a hypothetical WP profile containing severe fluctuations is also considered in the simulation, which is shown in Fig.

4.5(b). In the dispatch process, the updated WP forecasts are assumed to be available in 23 timeslots ahead (*NUF* = 23).

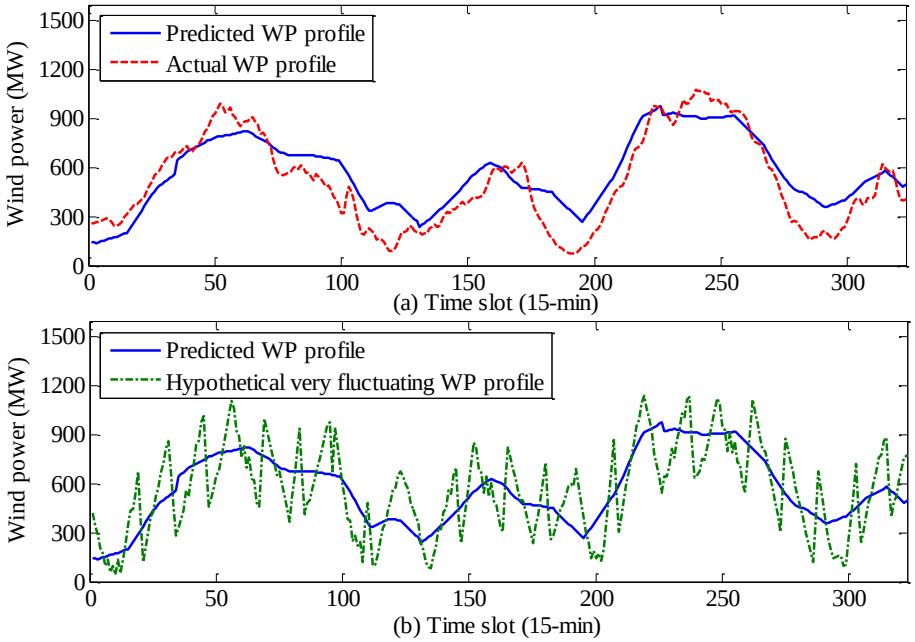

Fig. 4.5 WP profiles used in the simulation

As this research focuses on examining to what extent the WPUnV would aggravate the URC operation, the non-PEV load is assumed to be deterministic in the simulation, which is shown in Fig. 4.6. This load profile is the downscaled version of the load profile of New South Wales from 15:15 1/June/2014 to 00:15 5/June/2014 [106]. The wind energy accounts for about 20% of the non-PEV load, which represents a situation of high WP penetration.

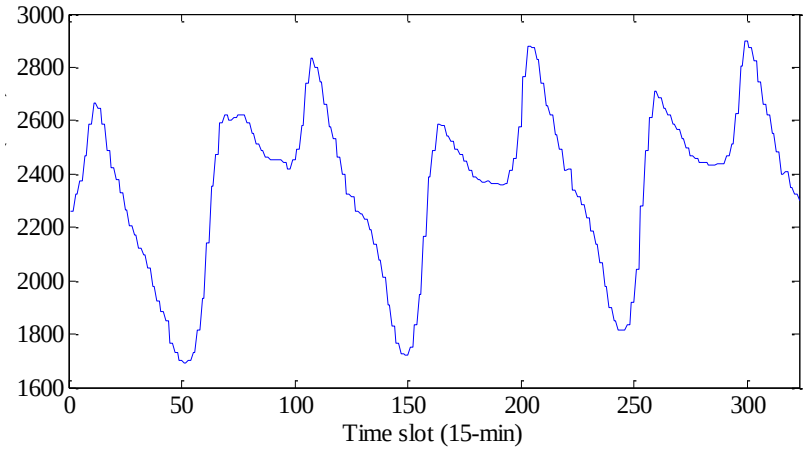

Fig. 4.6 Non-PEV load profile

4.4.3 PEV Load Data

16.5 kWh, 24 kWh, and 60 kWh PEV batteries are considered in the simulation. Each of these three battery capacities accounts for 1/3 of the fleet. It is assumed that PEVs with 16.5 kWh or 24 kWh batteries adopt AC Level 1 Charging with 1.8 kW rated charging power, and those having 60 kWh batteries adopt AC Level 2 Charging with 6.6 kW rated charging power [107]. The charger efficiency is set to 90%.

The total number of PEVs is assumed to be 240 000, among which 70% are responsive PEVs and 30% are spare PEVs. Plug-in and plug-out times are sampled from the distribution models which characterize the daily start time of the first trip and the end time of the last trip of USA household vehicles, as presented in [101]. The initial SOC is uniformly distributed between 20% and 50%, and the desired SOC is assumed to be 90%.

4.4.4 Other Data

With the given simulation setting of PEV load in Section 4.4.3, the maximum PEV power range in the scheduling horizon (i.e. $\max\{P_t^{\text{PEV\_ch}} - P_t^{\text{PEV\_dch}} : t \in T\}$) amounts to 758.9 MW. According to (4.27), θ_{rc} is set to 1000. The generators considered in this simulation have the maximum $ifc_i(\bar{G}_i)$ equal to 53.95 \$/MWh. According to (4.28), θ_{fc} is set to 0.005.

4.5 Simulation Results and Discussions

4.5.1 Determining the PEV Base Power Level in the Benchmark Scheme

At the scheduling stage of the benchmark scheme, the PEV base power level δ is determined for PEVs to reserve sufficient anti-URC regulation capacity. Following the procedures in Section 4.3, a series of simulations is conducted to search through the values of δ from 0 to 1 at a step of 0.05. The results are

shown in Fig. 4.7, where the PEV charging energy loss is expressed as a percentage of the desired charging energy.

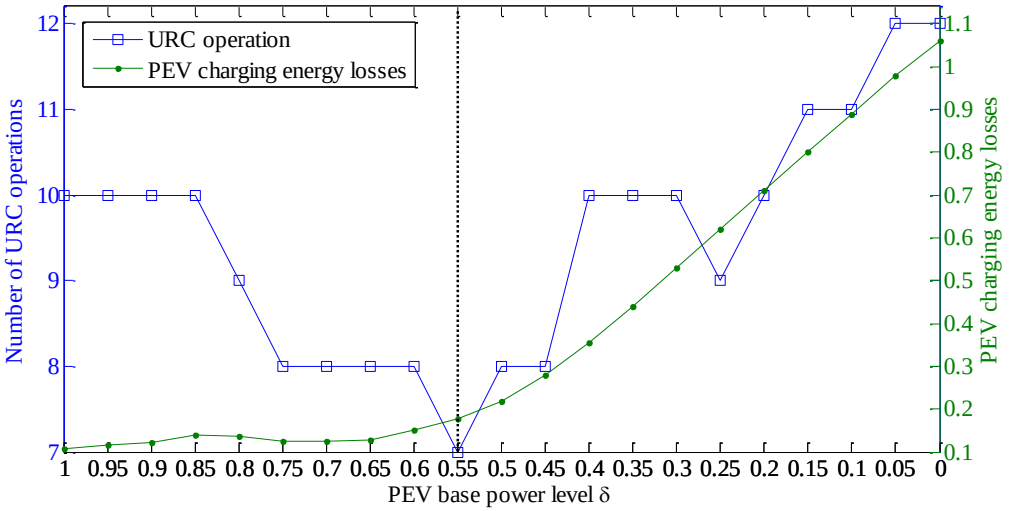

Fig. 4.7 Results of searching through different PEV base power levels

It can be seen that when the PEV base power level is equal to 0.55, the regulation capacity in PEVs results in the least number of URC operations. Thus, $\delta_{\text{least\_URC}} = 0.55$, which means the PEVs under the control of the benchmark scheme will be normally charged at 55% of their rated power, from which the PEV power will be adjusted up or down according to the requested anti-URC regulation during dispatch.

4.5.2 Simulation with Realistic Wind Power Profiles

In this section, the proposed hierarchical scheme is compared with the benchmark scheme with respect to the effectiveness in coordinating PEV power to hedge against the URC operations while preserving the PEV charging energy. The simulation is conducted with the realistic WP profiles recorded in Fig. 4.5(a). For comparison purpose, another two schemes are also tested. The first one assumes uncontrolled PEV charging. It helps to evaluate to what extent proper generator dispatches alone can avoid the URC operations. The second scheme is the deterministic version of the proposed hierarchical scheme, in which point

predictions of WP are adopted and accordingly the NLVR is replaced by a deterministic net load profile. The deterministic scheme will indicate how the lack of consideration for WP uncertainties would influence URC operation mitigation.

All optimizations are solved by Gurobi Optimizer 5.6.3 [108].

Results of Scheduling

The scheduled NLVRs of the four schemes are shown in Fig. 4.8, among which the one generated by the top-level scheduling model of the proposed scheme (referred to as the reshaped NLVR) is apparently the least varying. When a WP profile is realized, there will be four net load profiles correspondingly realized in each of the four NLVRs. Take the predicted WP shown in Fig. 4.5(a) as an example. The four corresponding net load realizations are displayed in Fig. 4.8 and their standard deviations are recorded in Table 4.4. As expected, the net load realization in the reshaped NLVR is less varying than the others, which proves that the reshaped NLVR is more resistant to WP variations. This is because the top-level scheduling of the proposed scheme reshapes the NLVR to minimize the URC operations that can be caused by any possible net load realization in the NLVR, including those extremely varying scenarios. As a result, the conservative top-level scheduling imposes a strong smoothing effect on its reshaped NLVR.

Table 4.4 Results of scheduling: standard deviations of the example net load realizations and the scheduled PEV charging energy losses

	Standard deviation (MW)	PEV charging energy losses
Uncontrolled scheme	470.96	0%
Proposed scheme	267.42	53.72%
Benchmark scheme	380.83	17.59%
Deterministic scheme	382.33	1.62%

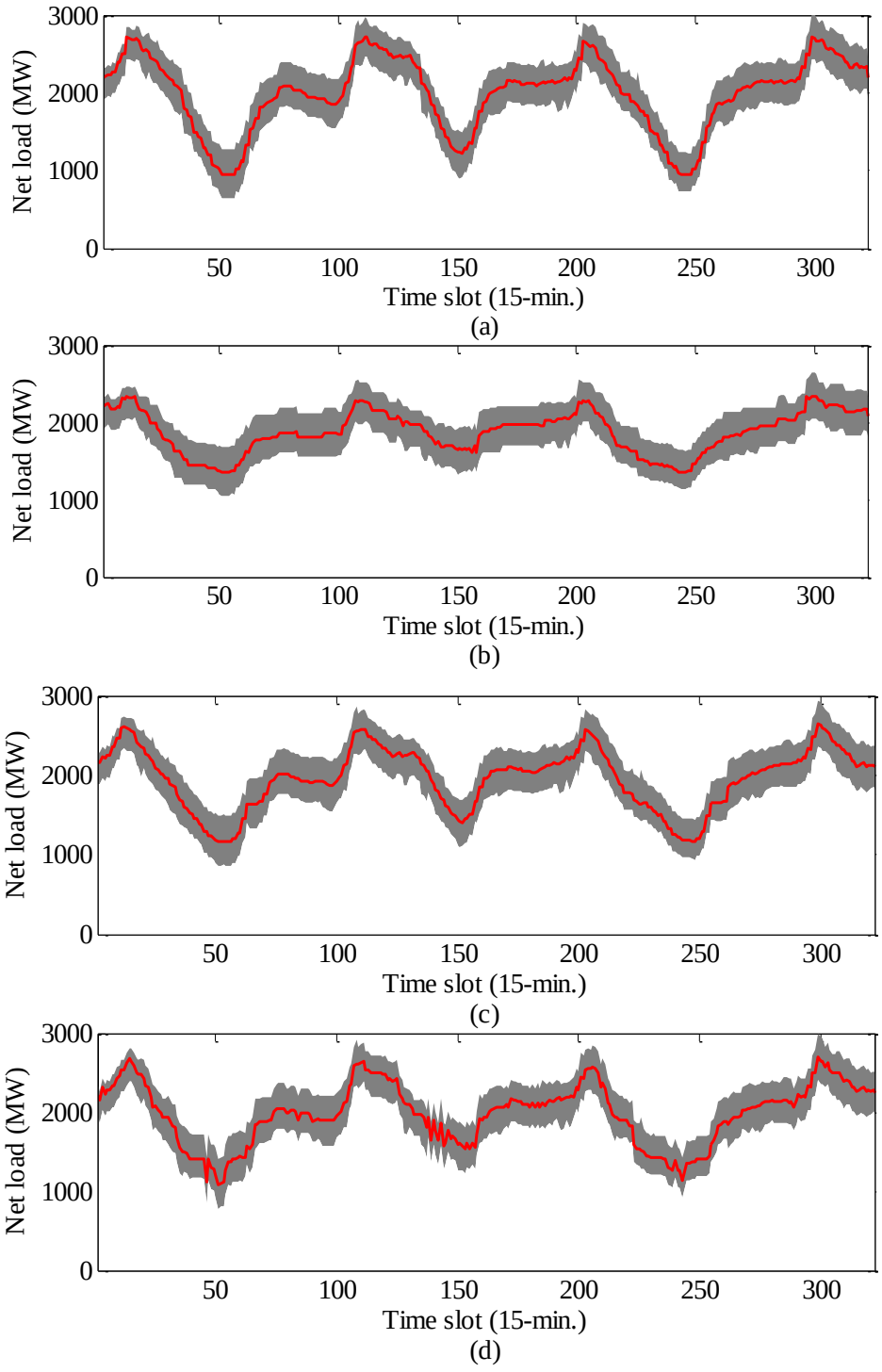

Fig. 4.8 The scheduled NLVRs of the four schemes investigated in this study, represented by the grey shaded areas; the red solid lines are the realized net load profiles corresponding to the predicted WP profile in Fig. 4.5(a). Subfigure (a) uncontrolled PEV charging; (b) the proposed scheme; (c) the benchmark scheme; (d) the deterministic scheme

The reshaped NLVR, however, comes with a significant scheduled sacrifice of the desired PEV charging energy, as can be observed from the results in Table 4.4, where charging energy losses are expressed as percentages of the desired charging energy. Nevertheless, the scheduled charging energy loss can be reduced at the dispatch stage of the proposed scheme. The relevant results are presented in the following section.

Results of Dispatch: URC Operation Mitigation

Given the updated WP forecasts, the middle-level dispatch model of the proposed scheme can exempt the unnecessary interruptions to PEV charging scheduled by the conservative top-level model so as to promote PEV charging. The dispatched net load profiles and their standard deviations are shown in Fig. 4.9. The number of URC operations is summarized in Table 4.5.

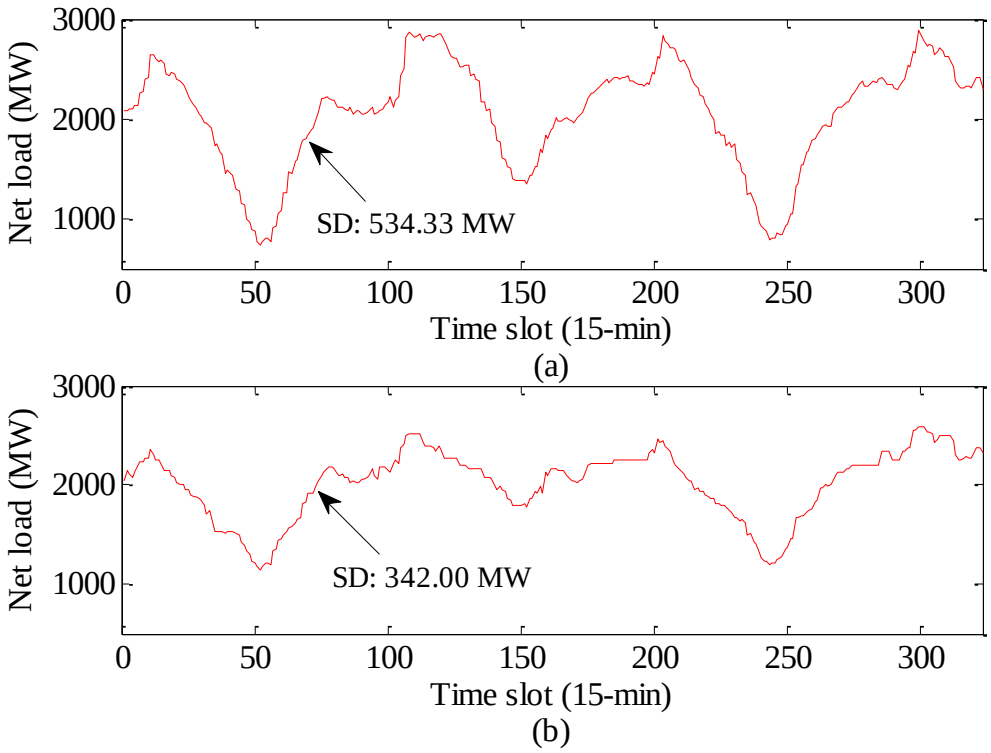

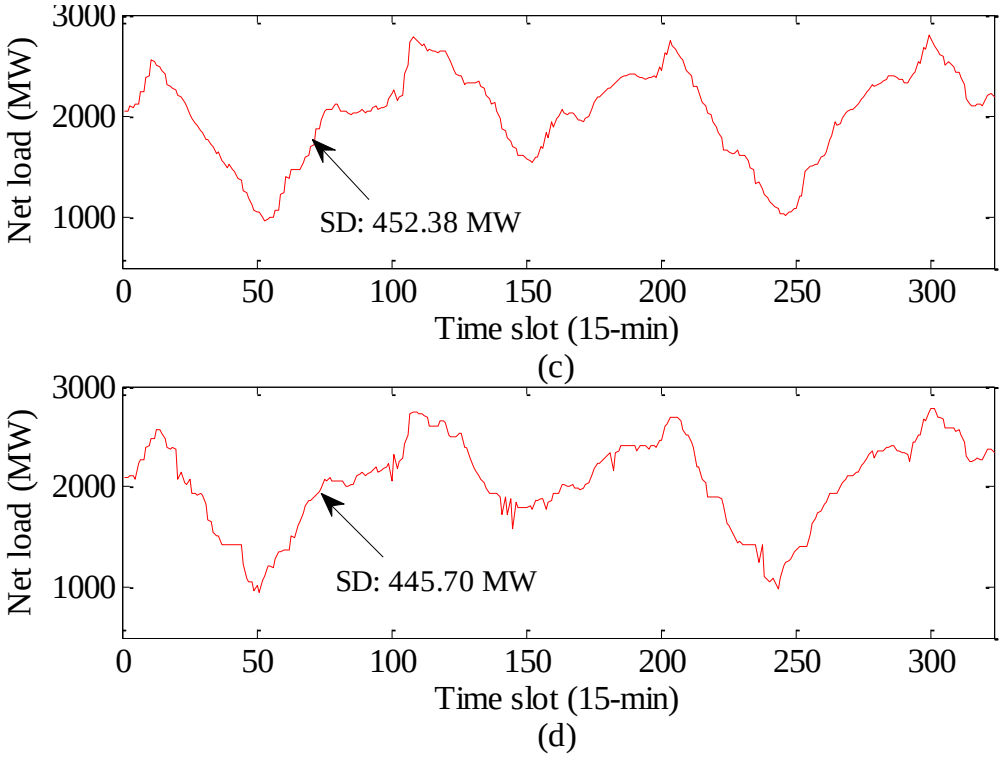

Fig. 4.9 Dispatched net load profiles (a) the scheme with uncontrolled PEV charging; (b) the proposed scheme; (c) the benchmark scheme; (d) the deterministic scheme. SD stands for standard deviation

Table 4.5 URC operations

	Upward URC operations	Downward URC operations	Total URC operations
Uncontrolled scheme	21	20	41
Proposed scheme	0	0	0
Benchmark scheme	3	6	9
Deterministic scheme	1	2	3

With uncontrolled PEV charging, the generators undergo dozens of URC operations, much more than that in any of the three schemes with controlled PEV charging. Thus, it is proved that generator dispatch alone only has fairly limited effect on URC operation mitigation. On the other hand, with controlled PEV charging, the majority of the URC operations are alleviated by the benchmark scheme and the deterministic scheme, and the proposed scheme even manages to avert the URC operations completely.

The benchmark scheme fails to mitigate multiple URC operations because of the insufficient anti-URC regulation capacity reserved in the PEVs. The insufficiency is caused by the lack of consideration for the WP uncertainty at the scheduling stage of the benchmark scheme. The consequence of the insufficient anti-URC regulation capacity can be seen in Fig. 4.10(a).

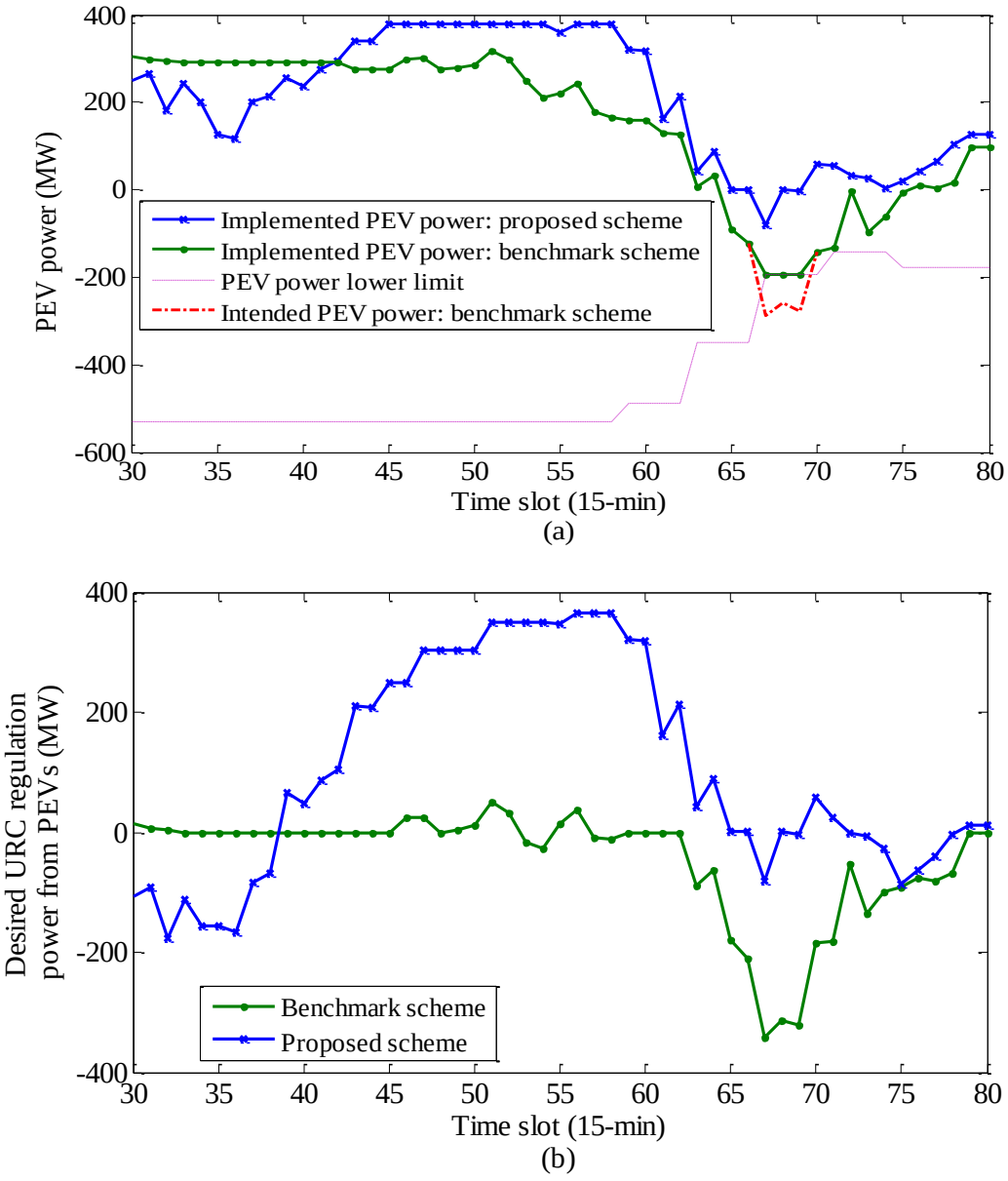

Fig. 4.10 Zoomed-in comparison between the dispatch results of the benchmark scheme and those of the proposed scheme. (a) implemented and intended PEV power dispatch; (b) desired anti-URC regulation power from PEVs

In timeslots 67–69 where two upward URC operations have occurred, the PEV power controlled by the benchmark scheme hits its lower limit while the intended PEV power dispatch is actually beyond that limit. This exemplifies that the intended PEV power dispatch of the benchmark scheme cannot be completely implemented at times as a result of the insufficient anti-URC regulation capacity reserved in the PEVs. Therefore, the expected URC operation mitigation via PEV power control may not be fully attained.

Moreover, when determining the required anti-URC regulation power, the benchmark scheme does not consider the amount of regulation capacity reserved in the PEVs. Thus, the determined regulation power can be concentrated in a short period, which could easily saturate the PEV power range. As shown in Fig. 4.10(b), the anti-URC regulation power determined by the benchmark scheme is mainly concentrated in timeslots 62–79, while that determined by the proposed scheme spreads over the entire selected period from timeslot 30 to 80. By increasing the PEV power in the valley period of the net load (i.e. timeslots 35–60), the proposed scheme expands the PEVs' downward regulation capacity. Therefore, when the PEV power needs to be decreased later in timeslot 60–67 to counterbalance the rapidly increasing net load, there is sufficient downward regulation capacity available in the PEVs controlled by the proposed scheme and the PEV power avoids hitting its lower limit.

For the deterministic scheme, the lack of consideration for WP uncertainty accounts for the scheme's failure to completely mitigate the URC operation. Without considering the WP uncertainty, the deterministic scheme may underestimate the required anti-URC regulation power. When underestimating the required upward regulation power, the deterministic scheme can over-restore the PEV charging power. Over restoration of PEV charging power is demonstrated in Fig. 4.11. The two downward URC operations which the deterministic scheme has failed to mitigate occur in timeslot 222 and 223, respectively. From Fig. 4.11(a), it can be seen that the deterministic scheme

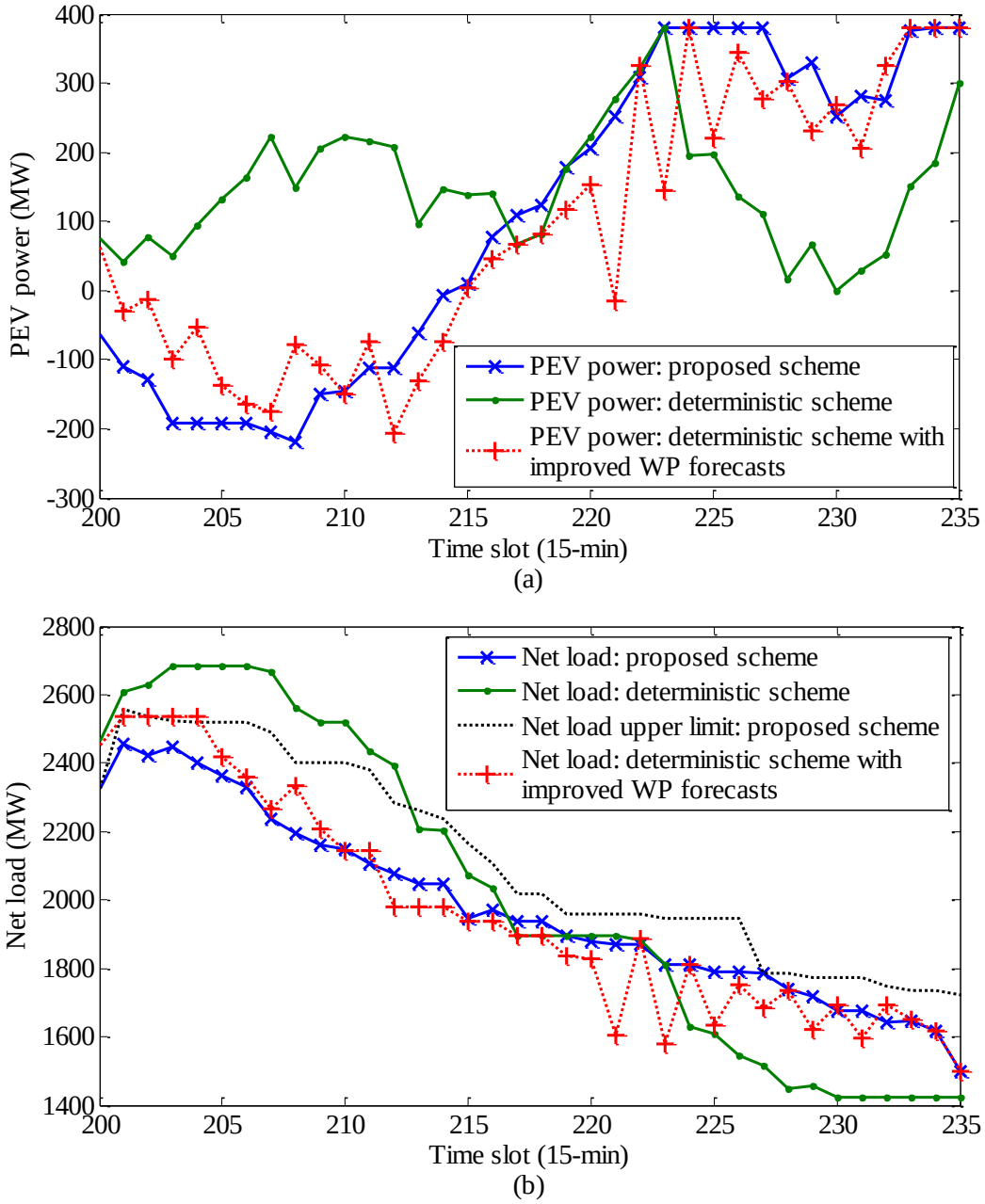

Fig. 4.11 Zoomed-in comparison between the dispatch results of the deterministic scheme and those of the proposed scheme. (a) PEV power; (b) system net load

attempts to avoid the downward URC operations by increasing the PEV power in timeslots 217–223. The high-level charging power in the antecedent timeslots 200–216, however, has made the upward regulation capacity of PEVs insufficient to help the generators avoid the downward URC operations. The PEV power is thus said to be overly restored. Conversely, the PEV power

controlled by the proposed scheme remains at a relatively low level during timeslots 200–216, which leaves sufficient upward regulation capacity for the upcoming net load decrease.

To further illustrate the lack of consideration for WP uncertainty being responsible for the over restoration of PEV power in the deterministic scheme, the scheme is re-simulated with *NUF* increased from 23 to 35, which represents reduced WP uncertainty. The simulation shows that the deterministic scheme manages to mitigate all URC operations. The resulted PEV power profile and net load profile are presented in Fig. 4.11(a) and 4.11(b), respectively. It can be observed that with reduced WP uncertainty, the deterministic scheme has noticeably altered its PEV power dispatch. The PEV power in timeslots 200–216 is significantly decreased to reserve more upward regulation capacity for later use. Thus, the original PEV power over restoration is prevented. The PEV power profile resulted by the deterministic scheme with reduced WP uncertainty turns out to be similar to that produced by the proposed scheme. Therefore, with respect to the effectiveness in controlling PEV power to mitigate URC operations, the proposed scheme is equivalent to the deterministic scheme using more advanced WP forecasting techniques.

Results of Dispatch: PEV Charging Energy Losses

The results of actual PEV charging energy loss are presented in Table 4.6.

Table 4.6 Actual PEV charging energy losses

	PEV charging energy losses
Uncontrolled scheme	0%
Proposed scheme	10.90%
Benchmark scheme	19.80%
Deterministic scheme	3.54%

The scheduled and actually dispatched PEV power profiles of the proposed scheme are compared in Fig. 4.12.

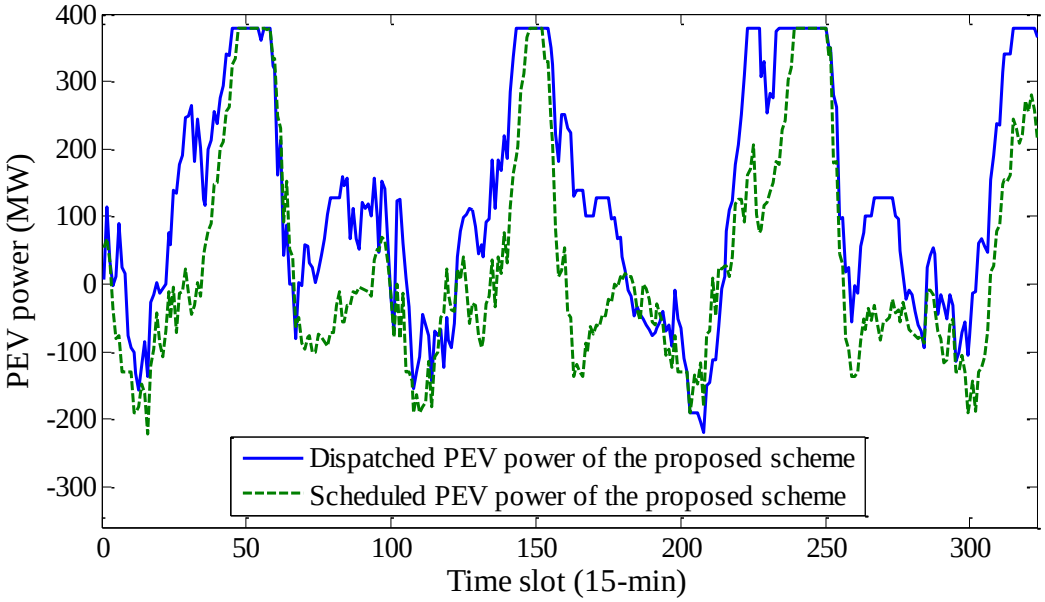

Fig. 4.12 Comparison of the scheduled and dispatched PEV power of the proposed scheme

It can be seen that different degrees of PEV power restorations have occurred in most of the timeslots. These restorations have considerably reduced the charging energy loss from the scheduled 53.72% to the 10.9% in the actual dispatch. Without any mechanism to promote PEV charging, the benchmark scheme incurs a 19.8% charging energy loss, which is nearly twice as much as that caused by the proposed scheme. The deterministic scheme is the best with regard to minimizing charging energy loss.

The proposed hierarchical scheme deploys the decentralized charging control scheme introduced in Chapter III to guide individual PEV power. The statistics of PEV battery SOC are summarized in Table 4.7. With the desired SOC set to 100%, here, PEVs are broadly categorized as adequately charged ($SOC \geq 80\%$) or undercharged ($SOC < 80\%$). Especially, a PEV with SOC $\geq$ 90% is considered to have satisfied its charging requirement. It can be seen that 74.29% of the PEVs controlled by the proposed scheme have satisfied their charging

requirements, which is prominently better than the 61.31% resulted by the benchmark scheme. On the other hand, 12.34% of the total PEVs are undercharged with the benchmark scheme, versus 6.84% with the proposed scheme. These results indicate that the heterogeneous PEV charging requirements can be better satisfied by the bottom-level decentralized charging control scheme.

Table 4.7 PEV SOC statistics

	Proposed scheme	Benchmark scheme
Maximum SOC	100%	100%
Minimum SOC	58.90%	55.16%
% of PEVs with SOC in [90%, 100%]	74.29%	61.31%
% of PEVs with SOC in [80%, 90%)	18.87%	26.35%
% of PEVs with SOC in [70%, 80%)	5.49%	9.46%
% of PEVs with SOC in [60%, 70%)	1.18%	2.47%
% of PEVs with SOC in [50%, 60%)	0.17%	0.41%
Adequately charged	93.16%	87.66%
Undercharged	6.84%	12.34%

Overall, the proposed scheme achieves complete avoidance of URC operations with an acceptable PEV charging energy loss. Thus, the proposed scheme is effective at coordinating PEV power to mitigate the URC operations while it is able to preserve most of the desired charging energy. The benchmark scheme results in more URC operations and larger charging energy loss than the proposed scheme and the deterministic scheme. Since the benchmark scheme is developed based on typical ESS control methods, the results indicate that designing a tailor-made control scheme for PEV charging, such as the proposed hierarchical scheme, is necessary and important as it may not be a good choice to directly apply ESS control methods to control PEV charging. Incurring only 3 URC operations with the minimum sacrifice of PEV charging energy, the deterministic scheme achieves the overall effectiveness comparable to that of the

proposed scheme. Nevertheless, the proposed scheme is more robust to WP forecast errors than the deterministic scheme, which is shown in Section 4.5.3.

The case study is conducted on a computer with Intel I5-3337U CPU @ 1.8GHz and 4GB RAM. The required computation time for the top-level scheduling model is usually 1-2 hours and that for the middle-level dispatch model is usually up to several minutes. The top-level scheduling model is slow. However, since it only needs to be solved once a day, the computational speed should not be an issue. The middle-level dispatch model only considers a limited number of timeslots. Hence, it achieves relatively fast computational speed and is suitable to be solved in a rolling fashion. The bottom level decentralized charging control is proven to be usable for real-time controlling. Therefore, the proposed 3-level hierarchical scheme can be used for real-time application.

4.5.3 Simulation with Hypothetical Wind Power Profile Containing Severe Fluctuations

This section investigates the performances of the four schemes when subject to severe WP fluctuations in unstable fast-moving weather. The hypothetical WP described in Fig. 4.5(b) is adopted in the simulation. The resultant net load profiles and their standard deviations are shown in Fig. 4.13. The number of URC operations and the associated PEV charging energy losses are summarized in Table 4.8.

Table 4.8 URC operations and PEV charging energy losses

	Upward URC operations	Downward URC operations	PEV charging energy losses
Uncontrolled scheme	73	70	0%
Proposed scheme	14	7	3.68%
Benchmark scheme	22	16	20.41%
Deterministic scheme	15	16	1.17%

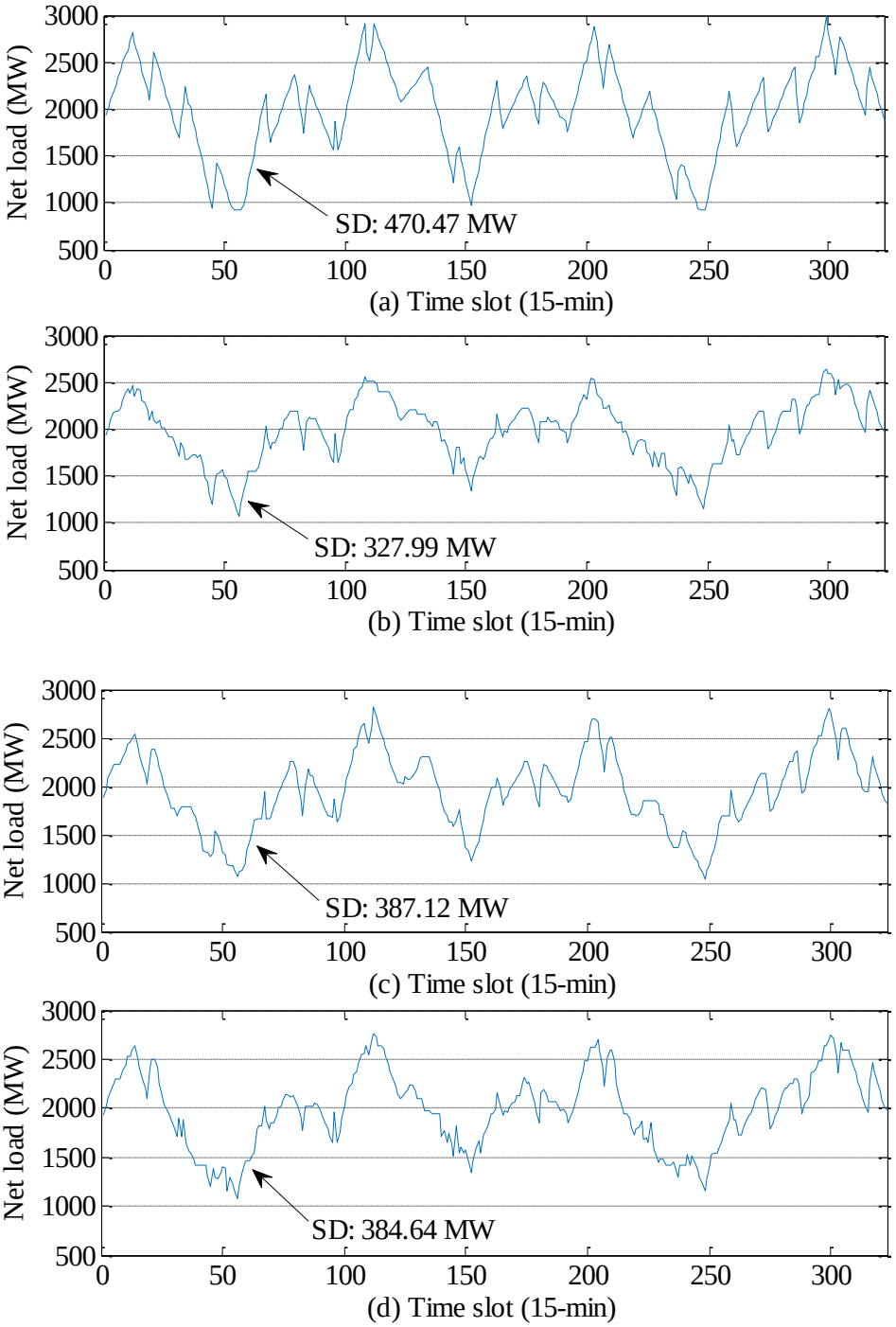

Fig. 4.13 Net load profiles produced by the four schemes in the very fluctuating WP scenario; (a) uncontrolled PEV charging; (b) the proposed scheme; (c) the benchmark scheme; (d) the deterministic scheme

From Fig. 4.13, it can be seen that the net load profile generated by the proposed scheme is the least varying. As expected, a number of URC operations are incurred in the case of uncontrolled PEV charging. Among the other three

schemes, the proposed scheme achieves the best URC operation mitigation. PEV charging energy losses resulted by the proposed scheme and the deterministic scheme are comparably small. These results show that the proposed scheme is more robust to severe WP fluctuations than the deterministic scheme and the benchmark scheme. This means the proposed scheme is more capable of withstanding WP forecast errors. For future smart grids with significant WP where WP may vary frequently and to various extents, the proposed scheme can be particularly helpful due to its guaranteed effectiveness in buffering the conventional units from the impact of WP variation.

4.5.4 Brief Ex Post Facto Cost Analysis

A brief ex post facto cost analysis is conducted on the dispatch results of the proposed scheme and the scheme with uncontrolled PEV charging. The cost results are then compared to evaluate the economic viability of the proposed scheme. Two types of cost are considered in the analysis, namely the generator fuel cost and the PEV battery degradation cost.

The battery degradation cost (C_{BD}) is proportional to the amount of V2G energy supplied by the PEV. This cost can be roughly evaluated as follows:

$$C_{BD} = C_{BC} C_{\text{batt}} / (L_C C_{\text{batt}} DoD) \tag{4.58}$$

where C_{BC} is the battery capital cost; C_{batt} is the battery capacity; L_C is the battery life in number of cycles at a certain depth of discharge; and DOD is the depth of discharge at which L_c is determined. Several studies show that the PEV battery cost has declined rapidly in recent years [109-111], from above 1000 US$/kWh in 2007 to around 300 US$/kWh in 2014 accomplished by some market-leading automakers. As the proposed scheme implicitly assumes the availability of a large population of PEVs in the system, the cost of 150 US$/kWh is selected in this analysis, since it is the value that supposedly makes PEVs cost competitive with internal combustion cars [111] thereby paving the way for mainstream

adoption of PEVs. 20% loss of initial capacity is assumed to be the end-of-life threshold for PEV battery. Our simulation results indicate that the maximum DOD in the PEVs controlled by the proposed scheme is less than 40%. Hence, L_c is evaluated at 50% DOD and amounts to 6500 cycles before 20% capacity fade, according to the dynamic stress test results on Li-Ion cells [112]. With all these data, C_{BD} is calculated to be 46.15 US$/MWh.

Table 4.9 and 4.10 summary the calculated costs. The proposed scheme achieves generator fuel cost saving in both scenarios of realistic and hypothetical WP.

Table 4.9 Costs (US$), in the scenario of realistic WP

	Uncontrolled PEV charging	Proposed scheme	ΔCost
Generator fuel cost	4583871	4477028	-106843
C_{BD}	0	78139	+78139
Total	4583871	4555167	-28704

Table 4.10 Costs (US$), in the scenario of hypothetical very fluctuating WP

	Uncontrolled PEV charging	Proposed scheme	ΔCost
Generator fuel cost	4491750	4432014	-59736
C_{BD}	0	97863	+97863
Total w/o URC related cost	4491750	4529877	+38127
URC related cost (lower limit)	51210	9845	-41365
Total with URC related cost	4542960	4539722	-3238

The fuel cost saving stems from the less varying system net load resulted by the proposed scheme. In the scenario of realistic WP, the saved fuel cost is sufficient to offset the battery degradation cost for 1693 MWh V2G energy. Thus, a net payoff is yielded by the proposed scheme, which proves the scheme's economic viability. The net payoff can be used as financial compensation for PEV owners. Thus, deploying the proposed scheme can be mutually beneficial to both the utility and the PEV owner.

In the hypothetical WP scenario, the PEV battery degradation cost increases a lot because of the increased use of V2G energy (2120 MWh). The saved fuel cost is not enough to cover the incurred battery degradation cost in this case. Hence, there exists a net loss for deploying the proposed scheme, which appears to make the economic viability of the proposed scheme questionable. Nevertheless, it is worth noting that the benefit of URC operation mitigation achieved by the proposed scheme is not counted in this cost analysis because noticeable variations have been found in the URC operation related cost for different units, depending on specific unit type, age, operating history, etc. [63, 96]. If this cost is included, even just at its lower limit (refer to Table 4.3), the combined benefit of fuel cost saving and URC operation mitigation would reach approximate parity with the battery degradation cost, as can be seen from Table 4.10. Therefore, the proposed scheme still remains economically viable in this scenario.

From the resultant costs, it is clear that the battery degradation cost is an important factor affecting whether the proposed scheme would create a net payoff, cost parity or net loss. Since the degradation cost is proportional to the discharged energy from PEV batteries, an effective way of improving the proposed scheme's economic viability is to reduce the use of V2G power. In fact, this can be readily achieved by recruiting more PEVs such that sufficient downward anti-URC regulation power can be provided by lowering PEV power within the positive power range.

4.6 Summary

Increasing WP integration is notably changing the way conventional generators are operated. An important but somehow overlooked issue is the unit cycling, whose damaging effects are recognized but difficult to be quantified since they may widely vary from one unit to another. Unlike most of the existing literature whose primary concern is on the scarcity of unit ramping capabilities,

this study presents a scheme specifically designed to coordinating PEV power to address the URC operations in the presence of high-penetration WP.

As essential building blocks for the proposed scheme, the construction of WP uncertainty intervals and explicit formulation of URC operations are firstly introduced. The hierarchical structure of the proposed scheme consists of scheduling, dispatch, and control layers, which form a complete full-package solution for coordinating PEV power to hedge against the URC operation. The top-level scheduling model produces a conservatively reshaped NLVR to minimize the URC operations that can be caused by the possible net load realizations in the NLVR. With updated WP forecasts, the middle-level dispatch model exempts over-scheduled anti-URC regulation onus on the PEVs to promote PEV charging. Meanwhile, the actually dispatched net load is confined in the conservatively reshaped NLVR from the top-level scheduling in order to avoid over restoration of PEV charging power to ensure the effective URC mitigation. The bottom-level decentralized charging control method implements the PEV dispatch instruction and enables differentiated charging power distribution among PEVs in accordance with their individual ULC to cater to heterogeneous charging requirements.

The proposed scheme is compared with its deterministic version and the benchmark scheme. Simulation results show that with the uncertainty in WP forecasts taken into account, the proposed scheme is more effective in mitigating URC operations while able to preserve most of the desired PEV charging energy and satisfy the charging requirements for the majority of PEVs. Moreover, the proposed scheme is shown to be more robust to severe WP fluctuations in unstable fast-moving weather condition, which indicates its greater capability to withstand WP forecast errors. Buffering the conventional units from the impact of WP variations, the proposed scheme can be very helpful to future smart grids with high-penetration WP. As shown in the ex post facto cost analysis, the proposed scheme creates a net payoff in the normal WP scenario and cost parity

in the case of very fluctuating WP. Therefore, the economic viability of the proposed scheme can be confirmed.

It is worth noting that though the proposed scheme is designed to realize PEV-aided URC operation mitigation, the overall framework for avoiding URC operations is generally applicable to other reserve sources.

Chapter V

Effect of Controlled PEV Charging on Wind Power Uncertainty Cost

5.1 Introduction

Besides the technical aspects, large-scale WP integration also has a noticeable impact on power system economics. To accommodate WPUnV in power systems, additional cost will be incurred, which is referred to as the WPUC.

In order to compensate WPUnV, frequent unscheduled use of expensive fast-reacting units is often needed and base-load units will be forced into longer periods of part-load operations. Thus, cost per MWh generated by the thermal units will be increased. This fuel cost increase induced by WPUnV is the primary component of the WPUC. The other important, but often overlooked component of the WPUC is the cycling costs of conventional units raised by WPUnV. The unit cycling operation results in accelerated wear and tear to unit components, thus causing higher maintenance and replacement costs.

In future smart grid, DR will be an important tool to mitigate the WPUC, and therefore, in this chapter the focus is to investigate to what extent the controlled PEV charging would help reduce the WPUC. A comprehensive WPUC model is proposed in which generator cycling costs are included. WPUnV is decomposed into two components, namely forecast errors on hourly WP and sub-hourly WP fluctuations. The WPUC raised by each of the two components will be evaluated. System operating costs in ideal and non-ideal WP situations are computed and then compared to reveal the WPUC.

5.2 Methodology

5.2.1 Unit Cycling Costs

Two types of unit cycling costs are considered here, namely on/off cycling cost and ramp cycling cost. The on/off cycling cost is incurred each time when a generator is started up. It is modeled as follows:

$$\begin{cases} c_{i,t}^{\text{on/off}} \geq C_i^{\text{ON/OFF}} \left(u_{i,t} - u_{i,t-1} \right) \\ c_{i,t}^{\text{on/off}} \geq 0 \end{cases}, \ \forall i \in I, \forall t \in T \tag{5.1}$$

where $C_i^{\text{ON/OFF}}$ is the cost of one on/off cycling operation in unit *i*; $c_{i,t}^{\text{on/off}}$ is the on/off cycling cost of unit *i* in timeslot *t*; $u_{i,t}$ is the binary indicator for on/off (1/0) status of unit *i* in timeslot *t*; *I* is set of indexes for generators; and *T* is the set of indexes for the timeslots in the scheduling horizon.

The ramp cycling cost is calculated based on the identification of URC operation presented in Section 4.2.2:

$$c_{i,t}^{\text{RC}} \geq C_i^{\text{RC}} rc_{i,t}, \ \forall i \in I, \forall t \in T \tag{5.2}$$

where $rc_{i,t}$ is the binary indicator for the URC operation in unit *i* in timeslot *t*, which is determined using (4.3)-(4.6); C_i^{RC} is the cost of one URC operation in unit *i*; and $c_{i,t}^{\text{RC}}$ represents the ramp cycling cost of unit *i* in timeslot *t*.

5.2.2 Evaluating Approach of the WPUC

The evaluating approach for the WPUC used in this study is based on the approach proposed in [102]. System operating costs in ideal and non-ideal WP situations are calculated and then compared to reveal the amount induced by WPUnV. In this study, it is assumed that WP predictions are made at hourly resolution. Three WP situations are considered. The ideal WP situation refers to perfect forecasts on hourly WP without sub-hourly WP fluctuations. The first non-ideal WP situation is with imperfect forecasts on hourly WP yet still

assumes the inexistence of sub-hourly WP fluctuations. The second non-ideal WP situation represents the actual situation, where both imperfect hourly WP forecasts and sub-hourly WP fluctuations are considered. These three WP situations are illustrated in Fig. 5.1.

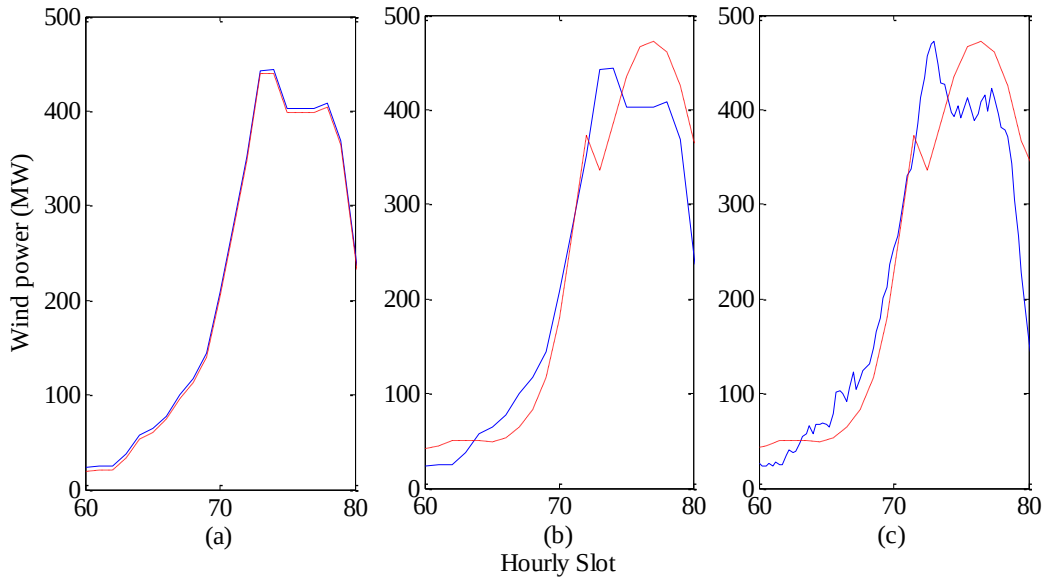

Fig. 5.1 Illustration of the three considered WP situations. Sub-figure (a): the ideal WP situation; (b): the first non-ideal WP situation; (c): the second non-ideal WP situation. The blue solid lines are the actual WP and the red dashed lines represent the WP forecasts on hourly scale.

The model for system operations consists of three levels. At the top level is a day-ahead UC model on hourly scale which spans over a period of 36 hours. The generator commitments will be determined and fixed to the day-ahead UC solution, except for the fast-reacting units.

At the middle level is a smaller scale UC model, which is solved in a rolling fashion for each hour of the day taking into account the latest update of WP forecasts. When solved for the current hour *h*, this model determines the commitments of fast-reacting units in *h*.

Finally, with the generator commitments fixed to the top-level and middle-level solutions, the bottom-level dispatch model is solved for each of the 15-min

timeslots in *h* to dispatch the online generators with the sub-hourly WP fluctuations considered.

After the bottom-level dispatch model is solved for the last 15-min timeslot in the current hour *h*, the middle-level UC model will roll to the next hour. Once this rolling process reaches the last hour of the day, the top-level day-ahead UC will be launched again for the next day.

Top-Level Day-Ahead UC Model

The top-level day-ahead UC model is formulated as a mix-integer linear programming. It is at hourly resolution and spans over a period of 36 hours. The detailed formulation is as follows:

$$\min \sum_{t\in T}\left\{\sum_{i\in I}\left(c_{i,t}^{\text{fuel}}+c_{i,t}^{\text{SU}}+c_{i,t}^{\text{on/off}}+c_{i,t}^{\text{RC}}\right)+c_{t}^{\text{V2G}}\right\} \tag{5.3}$$

subject to

1) 3-segment piecewise linear approximation of the quadratic generator fuel cost function: refer to (4.12)–(4.17).
2) Start-up fuel cost:

$$c_{i,t}^{\text{SU}} \ge C_{i}^{\text{SU}}\left(u_{i,t}-u_{i,t-1}\right),\ \forall i\in I,\forall t\in T \tag{5.4}$$

$$c_{i,t}^{\text{SU}} \ge 0,\ \forall i\in I,\forall t\in T \tag{5.5}$$

3) On/off cycling cost: refer to (5.1)
4) Ramp cycling cost: refer to (4.3)–(4.6) and (5.2)
5) PEV V2G cost:

$$c_{t}^{\text{V2G}} \ge -p_{\text{dch},t}^{\text{PEV}} C_{\text{V2G}} \big/ \eta,\ \forall t\in T \tag{5.6}$$

6) Power balance constraint:

$$\sum_{i\in I} g_{i,t} = L_t + p_{\text{ch},t}^{\text{PEV}} + p_{\text{dch},t}^{\text{PEV}} - w_t,\ \forall i\in I,\forall t\in T \tag{5.7}$$

7) WP range constraint:

$$0 \le w_t \le W_t^{\text{f}},\ \forall t\in T \tag{5.8}$$

8) Generator power output range:

$$\underline{G}_i u_{i,t} \le g_{i,t} \le \bar{g}_{i,t},\ \forall i \in I, \forall t \in T \tag{5.9}$$

$$\underline{G}_i u_{i,t} \le \bar{g}_{i,t} \le \bar{G}_i u_{i,t},\ \forall i \in I, \forall t \in T \tag{5.10}$$

9) Generator ramp-up rate and start-up rate constraint:

$$\begin{aligned} &\bar{g}_{i,t} - g_{i,t-1} \le RUL_i \cdot u_{i,t-1} + SURL_i \left(u_{i,t} - u_{i,t-1}\right) + \bar{G}_i \left(1 - u_{i,t}\right), \\ &\forall i \in I, \forall t \in T \end{aligned} \tag{5.11}$$

10) Generator ramp-down rate and shut-down rate constraint:

$$\begin{aligned} &g_{i,t-1} - g_{i,t} \le RDL_i \cdot u_{i,t} + SDRL_i \left(u_{i,t-1} - u_{i,t}\right) + \bar{G}_i \left(1 - u_{i,t-1}\right), \\ &\forall i \in I, \forall t \in T \end{aligned} \tag{5.12}$$

11) Reserve requirement:

$$\sum_{i \in I} \left(\bar{g}_{i,t} - g_{i,t} + NSR_i \left(1 - u_{i,t}\right)\right) \ge 0.06 L_t + 0.1 w_t,\ \forall t \in T \tag{5.13}$$

$$\sum_{i \in I} \left(\bar{g}_{i,t} - g_{i,t}\right) \ge 0.04 L_t + 0.05 w_t,\ \forall t \in T \tag{5.14}$$

12) Minimum up time constraint:

$$\sum_{t=1}^{UT_i^{\text{init}}} \left(1 - u_{i,t}\right) = 0,\ \forall i \in I, \forall t \in T \tag{5.15}$$

where $UT_i^{\text{init}} = \min\left\{NS, \left(UT_i - UT_i^{\text{prior}}\right) \cdot U_i^{\text{prior}}\right\}$.

If $UT_i^{\text{init}} < NS$, the following constraint will be used together with (5.15):

$$\begin{aligned} &NSO\left(u_{i,t} - u_{i,t-1}\right) + \sum_{k=t}^{t+NSO-1} \left(-u_{i,k}\right) \le 0, \\ &\forall i \in I, \forall t = UT_i^{\text{init}} + 1, \cdots, NS \end{aligned} \tag{5.16}$$

where $NSO = \min\{NS - t + 1, UT_i\}$.

13) Minimum down time constraint:

$$\sum_{t=1}^{DT_i^{\text{init}}} u_{i,t} = 0,\ \forall i \in I, \forall t \in T \tag{5.17}$$

where $DT_i^{\text{init}} = \min\left\{NS, \left(DT_i - DT_i^{\text{prior}}\right) \cdot \left(1 - U_i^{\text{prior}}\right)\right\}$.

If $DT_i^{\text{init}} < NS$, the following constraint will be used together with (5.17):

$$NSD\left(u_{i,t-1}-u_{i,t}\right)+\sum_{k=t}^{t+NSD-1}\left(u_{i,k}-1\right)\le 0,$$
$$\forall i\in I,\forall t=DT_i^{\text{init}}+1,\cdots,NS \tag{5.18}$$

where $NSD=\min\{NS-t+1,DT_i\}$.

14) System level PEV power and energy constraints:

$$P_t^{\text{PEV\_dch}}\le p_{\text{dch},t}^{\text{PEV}}\le 0,\ \forall t\in T \tag{5.19}$$

$$0\le p_{\text{ch},t}^{\text{PEV}}\le P_t^{\text{PEV\_ch}},\ \forall t\in T \tag{5.20}$$

$$E_t^{\text{PEV\_dch}}\le\sum_{t_n=1}^{t}\left(p_{\text{ch},t_n}^{\text{PEV}}+p_{\text{dch},t_n}^{\text{PEV}}\right)\le E_t^{\text{PEV\_ch}},\ \forall t\in T \tag{5.21}$$

$$\sum_{t_n=1}^{t}\left(p_{\text{ch},t_n}^{\text{PEV}}+p_{\text{dch},t_n}^{\text{PEV}}\right)\ge E_t^{\text{target}},\ \forall t\in T \tag{5.22}$$

15) Binary variable constraint:

$$u_{i,t},\ rc_{i,t}\in\{0,1\},\ \forall i\in I,\forall t\in T \tag{5.23}$$

In (5.3), $c_{i,t}^{\text{fuel}}$ and $c_{i,t}^{\text{SU}}$ are the generation fuel cost and start-up fuel cost of unit *i* in timeslot *t*, respectively; c_t^{V2G} is the V2G cost in timeslot *t*, which consists of the payment for V2G energy and the compensation for PEV battery degradation. In (5.4), C_i^{SU} is the fuel cost for one start-up of unit *i*. $p_{\text{ch},t}^{\text{PEV}}$ and $p_{\text{dch},t}^{\text{PEV}}$ in (5.6) and (5.7) are the system-level PEV charging and discharging power in timeslot *t*, respectively. In (5.6), C_{V2G} is the cost for one MWh V2G energy and η is the PEV charger efficiency. In (5.7), L_t is the non-PEV load in timeslot *t*; in (5.8), w_t is the scheduled WP in timeslot *t*, and W_t^{f} represents the forecasted available WP in *t*. In (5.9) and (5.10), $\overline{g}_{i,t}$ is the highest possible power output of unit *i* in timeslot *t*. In (5.11) and (5.12), RUL_i, RDL_i, $SURL_i$ and $SDRL_i$ are the ramp-up limit, ramp-down limit, start-up ramp limit and shut-down ramp limit of unit *i*, respectively. NSR_i in (5.13) is the non-spinning reserve that can be provided by unit *i*. In (5.15) and (5.16), *NS* is the number of timeslots in the scheduling horizon; UT_i and DT_i are the minimum up time and minimum down time of unit *i*, respectively; UT_i^{prior} and DT_i^{prior} are the number of timeslots unit *i* has been

online or offline prior to the first timeslot of the current scheduling horizon; and U_i^{prior} represents the initial on/off state of unit *i*. In (5.19)–(5.21), $P_t^{\text{PEV\_ch}}$ and $P_t^{\text{PEV\_dch}}$ are the aggregate charging and discharging power capacities of all controlled PEVs in timeslot *t*, respectively; $E_t^{\text{PEV\_ch}}$ and $E_t^{\text{PEV\_dch}}$ are the maximum amount of energies that can be charged to and discharged from the PEVs from the first timeslot to the *t*th timeslot of the scheduling horizon, respectively; and E_t^{target} in (5.22) is the required charging energy from the first timeslot to the *t*th timeslot of the scheduling horizon to satisfy the charging requirements of the PEVs whose expected departure times are within [1, *t*].

Objective function (5.3) aims to minimize the overall cost of system operations. Constraint (5.8) allows the scheduled WP to be less than the forecasted available WP such that WP curtailment is enabled which makes the system more capable of handling WP underestimation. The spinning reserve provided by unit *i* in timeslot *t* can be readily calculated as $\bar{g}_{i,t} - g_{i,t}$ as in constraints (5.13) and (5.14). Since $\bar{g}_{i,t}$ is limited by the generator ramp rate in constraint (5.11), the spinning reserve carried by unit *i* will automatically satisfy the generator ramp rate. Constraint (5.13) defines the required amount of reserve in the system including spinning and non-spinning reserves. The lower limit for spinning reserve is specified in (5.14).

Middle-Level Intra-Day UC Model

The middle-level UC model is on hourly scale. It has the same formulation as the day-ahead UC model except that its optimization horizon is shorter (12 hours in this study). The objective of this intra-day UC model is to continuously re-optimize the commitments of the fast-reacting generators, the PEV power and the scheduled WP, based on the latest updates of WP forecasts. Those generators other than the fast-reacting ones will adhere to their commitment schedules determined by the top-level model.

The intra-day UC model is solved in a rolling fashion for each hour of the day. It is assumed that as this model rolls forward, the WP forecasts will be continuously updated with gradually diminished inaccuracies. Specifically, when this model is solved for the current hour t_c, it is assumed that the WP forecast in t_c will be equal to the actual hourly WP, and the forecasts in some subsequent timeslots will improve upon the day-ahead forecasts. The degree of improvement depend on how far the timeslot is into the future [102]. The boundaries for the system-level PEV power and energy (i.e. $P_t^{\text{PEV\_ch}}$, $P_t^{\text{PEV\_dch}}$, $E_t^{\text{PEV\_ch}}$, $E_t^{\text{PEV\_dch}}$, E_t^{target}) will also be updated as the intra-day model rolls forward to reflect the latest change in PEV charging load. When the intra-day UC model is solved for t_c, though the commitments of fast-reacting generators in each hour of the optimization horizon will be determined, only the commitments in t_c will be applied to the generators.

Bottom-Level Intra-Hour Dispatch Model

After the intra-day UC model is solved for the current hour t_c, the intra-hour dispatch model will be used to determine generator dispatches in each 15-min timeslot of t_c, with the sub-hourly WP fluctuations taken into account. The commitments of slow-reacting units in t_c will be fixed to the solution of the top-level model, while the commitments of fast-reacting units, the PEV power, and the scheduled WP in t_c will adhere to the solution of the middle-level model. This intra-hour dispatch model aims to minimize the generation fuel cost and ramp cycling cost in each 15-min timeslot of t_c. The objective function is presented as follows:

$$\min \sum_{i \in I} \left(c_{i,qh\_t_c}^{\text{fuel}} + c_{i,qh\_t_c}^{\text{RC}} \right) \tag{5.24}$$

where $qh\_t_c = 1,2,3,4$ is the index of the 15-min timeslots in t_c. (5.24) is subject to: 1) the generator ramp cycling cost: (4.3)–(4.6) and (5.2); 2) the generator fuel cost definition (4.12)–(4.17); 3) the power balance constraint (5.7) with $p_{\text{ch},t_c}^{\text{PEV}}$ and

$p_{\mathrm{dch},t_c}^{\mathrm{PEV}}$ fixed to the middle-level UC solution and the sub-hourly WP fluctuations added to w_{t_c} ; 4) the generator power output range (5.9) and (5.10); 5) the generator ramp-up rate and start-up rate constraint (5.11); 6) the generator ramp-down rate and shut-down rate constraint (5.12); and 7) the binary variable constraint in (5.23) with fixed $u_{i,t}$.

PEVs are obligated to meet their charging requirements. Thus, it is possible that the responsive PEV load fail to precisely implement the desired PEV power dispatch because some PEVs may have to withdraw from the system regulation to fulfill their charging requirements. This study does not assume ideal demand response from PEVs. Instead, the decentralized charging control scheme proposed in Chapter III is adopted to guide individual PEV power, such that a realistic response of the PEV load to the system dispatch instruction can be modeled, which facilitate more accurate evaluation of the effect of controlled PEV charging on WPUC.

5.3 Simulation Setting

The simulation is conducted in a 29-unit system over a 30-day period.

5.3.1 Generator Data

The generators consist of 17 coal-fired units and 12 gas-fired units. The parameters of the coal-fired units are attained from [103] and those of the gas-fired units are given in [104]. For quick reference, the generator parameters are summarized in Table 5.1. The 30-MW gas-fired units, which can be brought online quickly when needed, are regarded as non-spinning reserve providers.

Table 5.1 Generator parameters

	Unit type				
	Coal-fired	Coal-fired	Coal-fired	Gas-fired	Gas-fired
No. of unit	7	6	4	6	6
$\overline{G}_i$ (MW)	350	155	76	150	30
$\underline{G}_i$ (MW)	140	56	16	42	10
RUL_i (MW/min)	4	3	2	2.5	3
RDL_i (MW/min)	4	3	2	2.5	3
$SURL_i$ (MW)	150	65	35	90	30
$SDRL_i$ (MW)	150	65	35	90	30
$RCTHR_i$ (MW)	70	31	15	30	15
NSR_i (MW)	0	0	0	0	30
UTi (h)	14	10	7	3	1
DTi (h)	14	10	7	3	1

The coefficients of the quadratic generator fuel cost functions are presented in Table 5.2. The threshold $RCTHR_i$ for a generator output change to be regarded as a damaging RC operation is set to 20% of the generator's dependable capacity [96] for the 350/155/76 MW coal-fired units and the 155 MW gas-fired units, and to 50% for the 30 MW gas-fired units since they are built for fast ramping. Noticeable variations have been found in the cycling operation related costs [63, 96]. This study uses the median estimates of the on/off cycling cost and the ramp cycling cost reported in [96]. These costs are shown in Table 5.2. The time window for defining the URC operation may differ in width for different generators. As no explicit results have been found in the accessible literature, it is assumed that the time window spans over a period of 18 hours for all generators. This time window is sufficient to cover the URC operations caused by normal system load changes in each WP scenario. Thus, the change in ramp cycling cost from ideal WP situation to non-ideal WP situation can more accurately reflect the amount induced by the WPUnV.

Table 5.2 Generator cost data

	Unit type				
	Coal-fired	Coal-fired	Coal-fired	Gas-fired	Gas-fired
a_i ($/MW^{2}h)	0.00786	0.01341	0.07457	0.03140	0.01426
b_i ($/MWh)	17.91	18.19	18.95	59.17	49.67
c_i ($/h)	779.7	444.5	323.2	692.9	1013
C_i^{SU} ($/start-up)	4615	627	1436	1440	214
C_i^{RC} ($/operation)	857.5	517.7	253.8	96	18.9
$C_i^{\mathrm{ON/OFF}}$ ($/start-up)	20650	14570	7144	5250	570

5.3.2 Wind Power and Non-PEV Load Data

The WP data used in the simulation are based on the historical data of forecasted and actual WP in June 2014 from TenneT, a European transmission system operator [113]. The original data is downscaled first. As the original data is at 15-min resolution, the mean value of the 15-min data in each hour is used as the hourly WP. The differences between the 15-min data and the hourly data are the sub-hourly WP fluctuations. The WP profiles are shown in Fig. 5.2(a).

The middle-level intra-day UC model will utilize the continuously updated WP forecasts. Similar to (4.32) and (4.33), the WP updating rule is assumed as follows

$$W_{t_c+n}^{\mathrm{f\_updt}} = W_{t_c+n}^{\mathrm{a}} + n/\left(NFH+1\right)\left(W_{t_c+n}^{\mathrm{f}} - W_{t_c+n}^{\mathrm{a}}\right) \tag{5.25}$$

where $W_{t_c+n}^{\mathrm{f\_updt}}$ is the updated WP forecast for the nth hour subsequent to t_c; $W_{t_c+n}^{\mathrm{a}}$ is the actual WP in t_c+n; and $n = 0 \ldots NFH+1$. In the simulation, NFH is set to 4.

The non-PEV load profile is shown in Fig. 5.2(b), which is the downscaled load profile of New South Wales in May 2014 [114]. The wind energy accounts for approximately 20% of the non-PEV load.

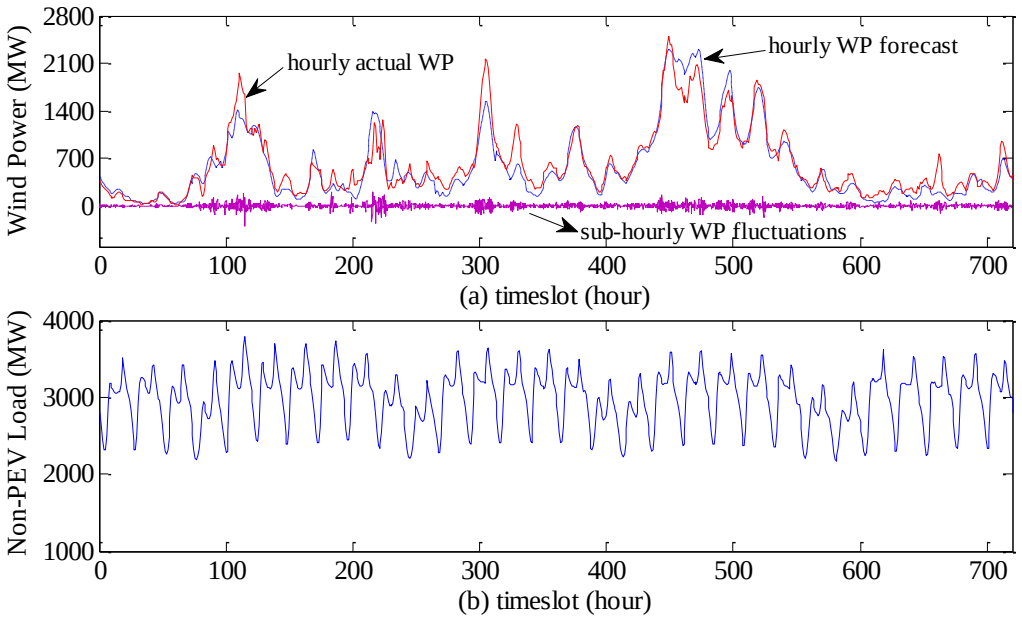

Fig. 5.2 (a) WP profiles; (b) Non-PEV load profile.

5.3.3 PEV Load Data

A total number of 60,000 PEVs is considered in the simulation. Each PEV has one of the following battery capacities: 16.5 kWh, 24 kWh, and 60 kWh. The three capacities account for 30%, 40% and 30% of the total PEVs and correspond to 4.8 kW, 6.6 kW and 7.2 kW chargers, respectively. The charger efficiency is set to 90%.

PEV plug-in and plug-out times are sampled from the distribution models which characterize the daily start time of the first trip and the end time of the last trip of USA household vehicles, as presented in [101]. The initial SOC is uniformly distributed between 15% and 80%, and the desired SOC is assumed to be 90%.

The V2G cost includes the battery degradation cost and the V2G energy cost. The battery degradation cost (C_{BD}) is calculated by (4.58). C_{BC} is set to 500 \$/kWh and L_C is set to 6500 cycles at 50% DOD. Thus, $C_{\mathrm{BD}} = 154$ \$/MWh. The V2G energy cost is set to 121 \$/MWh, which is the US average retail price of electricity to residential ultimate customers in 2013 [115]. Thus, the V2G cost $C_{\mathrm{V2G}} = 275$ \$/MWh.

5.4 Simulation Results and Discussions

5.4.1 Scenarios Investigated

The WPUC with controlled or uncontrolled PEV charging is evaluated by simulating the six scenarios summarized in Table 5.3, where DAUC, IDUC, and IHD represent the top-level day-ahead unit commitment, the middle-level intra-day unit commitment, and the bottom-level intra-hour dispatch, respectively.

Table 5.3 Scenarios investigated

Scenario	PEV power	Hourly WP forecasts	Sub-hourly WP fluctuations	Models involved
U1	Uncontrolled	Perfect	Without	DAUC
U2	Uncontrolled	Imperfect	Without	DAUC, IDUC
U3	Uncontrolled	Imperfect	With	DAUC, IDUC, IHD
C1	Controlled	Perfect	Without	DAUC
C2	Controlled	Imperfect	Without	DAUC, IDUC
C3	Controlled	Imperfect	With	DAUC, IDUC, IHD

Table 5.4 WPUC evaluation

System operating cost comparison	WPUC evaluated
U2 - U1	the cost due to forecast errors on hourly WP, w/o. PEV charging control
U3 - U2	the cost due to sub-hourly WP fluctuations, w/o. PEV charging control
U3 - U1	the overall WPUC, w/o. PEV charging control
C2 - C1	the cost due to forecast errors on hourly WP, with PEV charging control
C3 - C2	the cost due to sub-hourly WP fluctuations, with PEV charging control
C3 - C1	the overall WPUC, with PEV charging control

System operating costs in the ideal WP scenarios (U1 and C1) are compared with those in the non-ideal WP scenarios (U2, U3, C2 and C3) to reveal the amount induced by WPUnV. The WPUnV is decomposed into hourly WP forecast errors and sub-hourly WP fluctuations, and the cost raised by each of the WPUnV component will be evaluated. The evaluation is outlined in Table 5.4.

5.4.2 Results and Findings

The calculated costs in each of the scenarios described in Table 5.3 are shown in Table 5.5 and 5.6. The corresponding WPUCs calculated according to Table 5.4 are displayed in Fig. 5.3.

It can be seen that the generator cycling cost (on/off cycling cost + ramp cycling cost) accounts for a large portion of the WPUC, namely 49.9% and 25.8% in the cases of uncontrolled and controlled PEV charging, respectively. Therefore, it is imperative to model the generator cycling cost for a comprehensive and accurate assessment of the WPUC in high wind penetrated systems.

Table 5.5 Costs in the scenarios with uncontrolled PEV power

	U1	U2	U3
Generator fuel cost (US$)	41,258,217	41,366,975	41,494,904
Start-up fuel cost (US$)	65,938	92,374	98,217
On/off cycling cost (US$)	489,190	607,682	651,882
Ramp cycling cost (US$)	285,709	307,726	391,080
V2G cost (US$)	0	0	0
No. of on/off cycling operations	85	114	126
No. of ramp cycling operations	383	419	649
WP curtailment (MWh)	379.37	320.14	147.28

Table 5.6 Costs in the scenarios with controlled PEV power

	C1	C2	C3
Generator fuel cost (US$)	41,044,156	41,222,232	41,290,559
Start-up fuel cost (US$)	41,494	66,711	65,430
On/off cycling cost (US$)	433,074	492,918	489,498
Ramp cycling cost (US$)	116,468	121,048	153,886
V2G cost (US$)	0	0	0
No. of on/off cycling operations	66	97	91
No. of ramp cycling operations	158	168	265
WP curtailment (MWh)	0	55.3	16.75

With respect to the WPUC induced by forecast errors on hourly WP, the result with controlled PEV charging is only slightly better (i.e. 2.7% less) than that with uncontrolled PEV load. By further looking into each cost item displayed in Fig. 5.3(a), it is found that the controlled PEV power does help reduce the start-up cost, on/off cycling cost and ramp cycling cost induced by the hourly WP forecast errors. These cost savings, however, are largely compromised by the increase in generator fuel cost from Scenario C1 to C2.

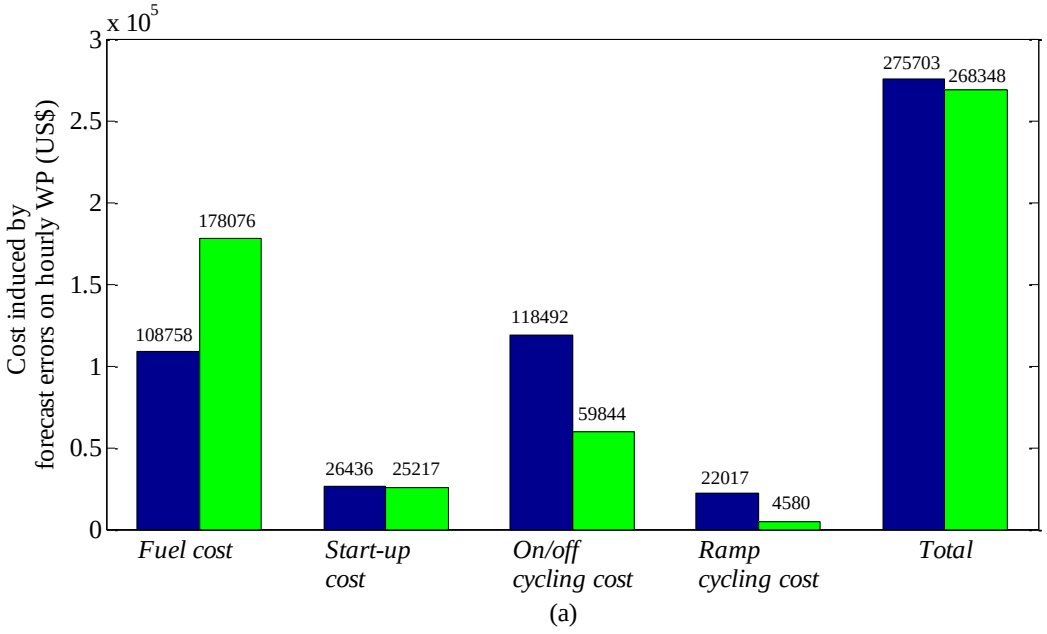

(a)

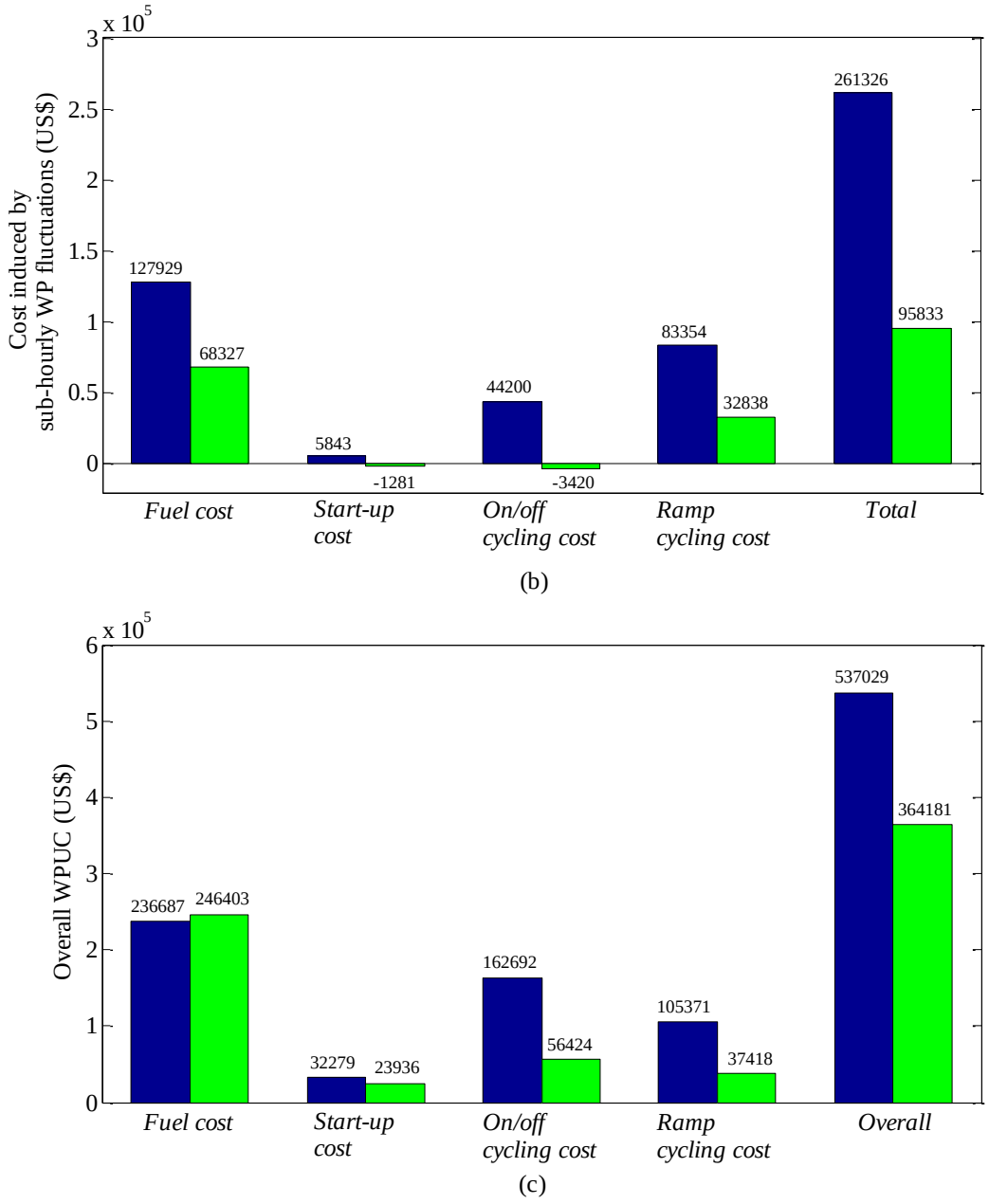

Fig. 5.3 Results of the WPUC. (a) the components of the WPUC induced by forecast errors on hourly WP, corresponding to U2-U1 (blue bar) and C2-C1 (green bar); (b) the components of the WPUC induced by sub-hourly WP fluctuations, corresponding to U3-U2 (blue bar) and C3-C2 (green bar); (c) the components of the overall WPUC, corresponding to U3-U1 (blue bar) and C3-C1 (green bar).

To understand the cause of this fuel cost increase, the fuel cost change in each generator type is investigated, as shown in Table 5.7. It can be observed that

the fuel cost increase of the fast-reacting generators (i.e. the 150 MW and 30 MW gas-fired units) from Scenario C1 to C2 is much greater than that from Scenario U1 to U2. This indicates that the system with the controlled PEV charging even relies more heavily on the fast-reacting generators to compensate the hourly WP forecast errors, which disagrees with the common expectation that PEV demand response would reduce the dependence on expensive fast-reacting generators. On the other hand, it is worth noting that the fuel cost change of the 76 MW coal-fired units from Scenario C1 to C2 is very small. Also, the operating hours of the 76 MW coal-fired units in C1 and C2 are only 7 and 14 hours, respectively, far less than the 136 and 168 hours in U1 and U2. In fact, the more frequent use of the fast-reacting gas-fired units in C2 is a result of the under-utilization of the 76 MW coal-fired units. Specifically, in the day-ahead UC of C2, the controlled PEV power helps to moderate the variance of system net load. This allows the system load to be fully supplied by the 350 MW and 155 MW base-load units without needing the relatively more expensive 76 MW coal-fired units for most of the time. As a result, when the day-ahead scheduled generating capacity is insufficient to compensate the WP forecast errors, the expensive fast-reacting gas-fired units have to be brought online through the intra-day UC, which is the cause of the significant fuel cost increase from Scenario C1 to C2.

The above analysis reflects that integrating controllable PEV power into normal UC program may lead to insufficient commitments of the non-fast-reacting units and consequently, more frequent use of the expensive fast-reacting units is needed to compensate the WP forecast errors. Thus, if the WP uncertainty is not properly considered in UC, the controlled PEV power will only have fairly limited effect on mitigating the WPUC induced by the hourly WP forecast errors.

Table 5.7 Changes in the fuel cost of each generator type

Unit type	From U1 to U2 (US$)	From C1 to C2 (US$)
350 MW Coal-fired	− 467742	− 430292
155 MW Coal-fired	+424782	+386541
76 MW Coal-fired	+30190	+8027
150 MW Gas-fired	+81652	+164096
30 MW Gas-fired	+39876	+49704
Total	+108758	+178076

The cost induced by sub-hourly WP fluctuations is the other important component of the WPUC, accounting for 48.7% and 26.3% of the overall WPUC in the cases of uncontrolled and controlled PEV charging, respectively. With regard to the generator cycling costs, the increase in on/off cycling cost from U1 to U2 amounts to $118,492, which is much more significant than the $44,200 from U2 to U3; conversely, the increase in ramp cycling cost from U1 to U2 is $22,017, much smaller than the $83,354 from U2 to U3. These comparisons indicate that hourly WP forecast errors mainly contribute to the on/off cycling cost, while sub-hourly WP fluctuations mainly affect the ramp cycling cost.

With PEV charging control, the WPUC due to hourly WP forecast errors is only slightly reduced from $275,703 to $268,348, while the WPUC due to sub-hourly WP fluctuations is reduced from $261,326 to $95,833. Therefore, the controlled PEV power is comparatively much more effective in avoiding the WPUC induced by the sub-hourly WP fluctuations. This is because with the variance of the system net load moderated by the PEV power coordination, the load following onus on the online generators can be alleviated. Hence, the online generators can maintain more ramping reserve, which indicates greater flexibility for handling the sub-hourly WP fluctuations. The upward/downward ramping

reserve of unit *i* in timeslot *t* is the maximum amount of power that can be added to or subtracted from the scheduled power output of unit *i* in timeslot *t* without incurring an additional ramp-up/-down cycling operation or violating the generator ramp rate limits. In Fig. 5.4, the results from Scenario C3 show that the less varying system net load produced by the controlled PEV power allows the online generators to carry sufficient ramping reserve to avoid the URC operations completely. On the other hand, the results from Scenario U3 show that with uncontrolled PEV charging, less amount of ramping reserve is maintained in the online generators. Consequently, the ramping reserve is exhausted several times, leading to some URC operations.

In summary, the controlled PEV charging can effectively help reduce the WPUC for systems with high wind penetration level. However, it has been found that integrating controllable PEV power into normal UC program may lead to insufficient commitments of the non-fast-reacting units, which further leads to more frequent use of the expensive fast-reacting units to compensate the WP forecast errors. Thus, if the WP uncertainty is not properly considered in the UC, the controlled PEV power may not as helpful as expected in mitigating the WPUC induced by the hourly WP forecast errors. On the other hand, the controlled PEV power is effective in lowering the cost raised by the sub-hourly WP fluctuations, because the controlled PEV power moderates the variance of the system net load such that more ramping reserve can be maintained in the online generators to better compensate the sub-hourly WP fluctuations.

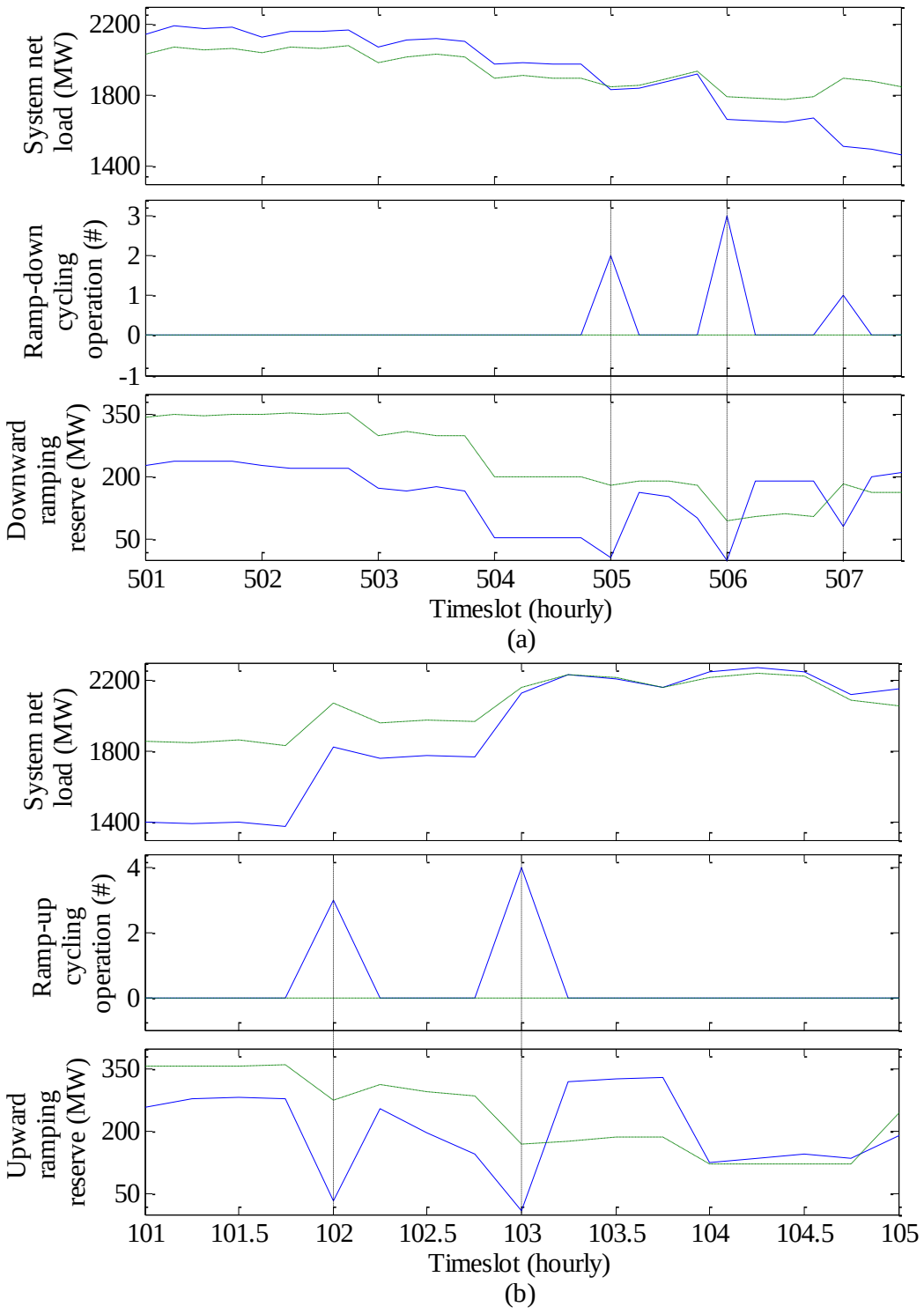

Fig. 5.4 System net load, URC operations, and ramping reserve in online generator in selected timeslots in Scenario U3 and C3. The green dashed lines represent the results of Scenario C3 and the blue solid lines represent those of Scenario U3

5.5 Summary

This chapter investigates the effect of controlled PEV charging on the WPUC. Compared with the existing literature, this study takes the evaluation of WPUC a step further. A more comprehensive WPUC model is proposed, in which the generator cycling costs are included. Also, by adopting the decentralized charging control scheme proposed in Chapter III, a realistic response of the PEV load to the system dispatch instruction can be modeled to facilitate more accurate evaluation of the effect of controlled PEV charging on the WPUC.

The overall WPUnV is decomposed into two components: the hourly WP forecast errors and the sub-hourly WP fluctuations. The WPUC induced by each WPUnV component is evaluated by simulating the six scenarios listed in Table 5.3 and comparing the resultant costs as in Table 5.4. The results show that generator cycling costs are non-negligible parts of the WPUC and the controlled PEV power has a favorable effect on reducing the WPUC. Nevertheless, we found that integrating controllable PEV power into normal UC program may lead to insufficient commitments of the non-fast-reacting units, which further leads to more frequent use of the expensive fast-reacting units to compensate the WP forecast errors. Therefore, without properly taking the WP uncertainty into account in the UC, the controlled PEV power may not be as helpful as expected to mitigate the WPUC induced by the hourly WP forecast errors. On the other hand, the cost raised by sub-hourly WP fluctuations can be largely reduced with the aid of the controlled PEV power because of increased ramping reserve maintained in the online generators.

Chapter VI

Conclusions and Future Work

6.1 Conclusions

With PEVs emerging in many countries, a rapid increase of PEV charging load can be expected in the years to come. PEV load presents both challenges and opportunities to the power system. On one hand, uncontrolled PEV charging may severely stress the grid, which weakens the system reliability and lowers its efficiency. On the other hand, controlled PEV charging enables large-scale DR to participate in system regulations. DR is identified as a very effective tool to help realize smooth WP integration. This research devises an implementable decentralized PEV power control scheme and explores several applications of controlling PEV power for WP integration enhancement. Specifically, the primary conclusions and contributions of this research are summarized as follows:

i) A simple but effective real-time scheduling scheme for PEV charging in low-voltage residential distribution feeder is proposed

This scheme schedules PEV charging either to minimize system losses or prevent over-low voltage, depending on whether the PEV penetration level is high enough to make the voltage drop become the binding constraint. Involving no computationally intensive optimization algorithms, the proposed scheduling scheme is fast and suitable for real-time applications to handle frequent PEV arrivals and departures. Besides, the proposed scheduling scheme can be flexibly adjusted from being loss-minimization-oriented to voltage-safety-oriented, or vice versa. Specifically, when voltage drop is not a blinding constraint, the

scheduled charging power profile can give a circuit loss close to the optimal value, whereas when excessive voltage drops are foreseen, the scheduled charging power profile will enlarge the voltage safety margin at a proper compromise of system loss optimality.

ii) A decentralized PEV charging control scheme is devised to enable the PEV power to participate in system regulations

A responsive PEV in the proposed charging control scheme will autonomously adjust its power according to the received DS, SS and its own ULC. The DS and SS are system level signals used to guide PEV power, and they are continuously updated at an information hub and broadcasted to all PEVs. Without relying on a central control entity, the proposed decentralized charging control scheme is scalable to a large population of dispersedly located PEVs. The charging power distribution among PEVs is consistent with their ULCs, which facilitates satisfying the heterogeneous PEV charging requirements. The automatic PEV charging state transition ensures the required charging energy to be fulfilled in time. Moreover, two potential performance degradations of the proposed charging control scheme are thoroughly analyzed, namely the divergent PEV power adjustment triggered by excessively large DS and the interruption to individual PEV power. Based on the analysis effective remedies are proposed and proved accordingly.

iii) A hierarchical scheme is proposed to schedule, dispatch and control the PEV power to hedge against the URC operations in a system with considerable WP

To the best of the author's knowledge, this research is the pioneering work that proposes a general-form representation of the URC operation. The proposed hierarchical scheme captures WP forecast uncertainty by considering WP uncertainty intervals. The top-level scheduling model reshapes the NLVR to minimize the number of URC operations that can be caused by the possible net

load realizations in the NLVR. The reshaped NLVR is then passed down to the middle-level dispatch model and serves as boundaries for the actually dispatched net load to ensure effective URC operation mitigation. Based on the latest update of WP forecasts, the middle-level dispatch model will exempt the over-scheduled anti-URC regulation onus to promote PEV charging. The bottom-level model is the decentralized control scheme proposed in Chapter III. Compared with its deterministic version and a benchmark scheme, the proposed scheme is more effective in mitigating URC operations while it is able to preserve most of the desired PEV charging energy and satisfy the charging requirements for the majority of PEVs. Moreover, the proposed scheme is more robust to severe WP fluctuations, which indicates its greater capability to withstand WP forecast errors.

iv) The effect of controlled PEV charging on reducing the WPUC is investigated by using a comprehensive WPUC model in which generator cycling costs are included

The decentralized charging control scheme proposed in Chapter III is adopted to obtain a realistic response of the PEV load to the system dispatch instruction. System operating costs in ideal and non-ideal WP situations are computed and then compared to reveal the WPUC. From the simulation results, the following conclusions can be reached: i) Generator cycling costs are non-negligible parts of the WPUC. ii) Controlled PEV power has a favorable effect on reducing the WPUC. iii) Integrating dispatchable PEV power into normal UC program may lead to insufficient commitments of the non-fast-reacting units, which further leads to more frequent use of the expensive fast-reacting units to compensate the WP forecast errors. Therefore, without proper consideration of the WP uncertainty in UC, the controlled PEV power may not be as helpful as expected to mitigate the WPUC induced by the hourly WP forecast errors. v) The cost

raised by sub-hourly WP fluctuations can be largely reduced with the controlled PEV power because of increased ramping reserve in online generators.

6.2 Future Work

This thesis has proposed a decentralized PEV charging control scheme and showed the benefits of controlled PEV power to the safe and economic operations of future smart grid with high penetration of intermittent WP. However, the current work could be further consolidated with the incorporation of the following research topics in the future:

(1) The effectiveness of the system regulation services provided by PEVs is highly dependent on the PEV power and energy capacities available for DR. The current work obtained PEV charging load by sampling the probability distributions characterizing the mobility behaviors of private cars. The uncertainties involved in PEV charging have not been fully considered yet. Therefore, one of the on-going researches is to identify the uncertainties of PEV charging load and investigate how these uncertainties would affect the scheduling and dispatch of PEV power.

(2) Controlling PEV charging load for system regulation purposes should not create intolerable discomfort for PEV users. The current work modeled the discomfort level of PEV users simply as unsatisfied battery SOC. In reality, the driving habits and needs of PEV users are complex and may change over time. Hence, an adaptive measurement on the discomfort level of PEV user is desired to incorporate the user feedback into the PEV charging planning. Machine learning algorithms, such as reinforcement learning, could be applicable to determine a customized index of discomfort level for each individual PEV user, and entertain PEV users' heterogeneous driving concerns and needs.

(3) The effectiveness of controlling PEV power for compensating WPUnV is affected by power network constraints, and the distribution of PEV load depends on the location of charging station and the real-time traffic condition. Therefore, the scheduling and dispatch of PEV power for system regulation purposes should consider not only the operation of power grid but also the impact on transportation system. How to improve the efficiency of both the power system and transportation system is a complex issue and will be a promising research direction in the future. The results shall facilitate the planning of PEV charging infrastructure and the development of a smart navigation system for PEVs.

(4) In the real world application of PEV load control, business models would define the interaction between PEV owners and PEV aggregators. Thus, new constraints may be imposed on the proposed PEV scheduling, dispatch and control schemes. Also, a study of PEV owners' behavior is important to PEV load modeling. Thus, how business models and PEV user behavior models would affect the control of PEV load shall be carefully studied in the future.

(5) Communication network is the basis of the proposed decentralized PEV charging control scheme. The communication requirements of the charging control scheme need to be clarified. Furthermore, what types of communication technology are technically and economically suitable for implementing the proposed charging control scheme and what constraints the communication technology would impose on the charging control scheme are also worth further examination.

(6) A comprehensive PEV control scheme should consider not only the system-level power dispatches but also local network conditions. Here, a hierarchical structure and the bi-level programming method are proposed to be used to incorporate local control with system-level dispatch. The general principle is that the upper-level controller will determine the system-level

dispatches without considering detailed local network constraints. The upper-level controller communicates with lower-level regional controllers. Taking into account local network constraints, the lower-level controllers will determine to what extend the target dispatch from the upper-level controller can be implemented and then give feedback to the upper-level controller. The upper-level controller will adjust the dispatch instruction accordingly. The process goes on until equilibrium is reached. More detailed study on this issue is planned in the future work.

Appendices

A. Data of Low-Voltage Residential Distribution Feeder

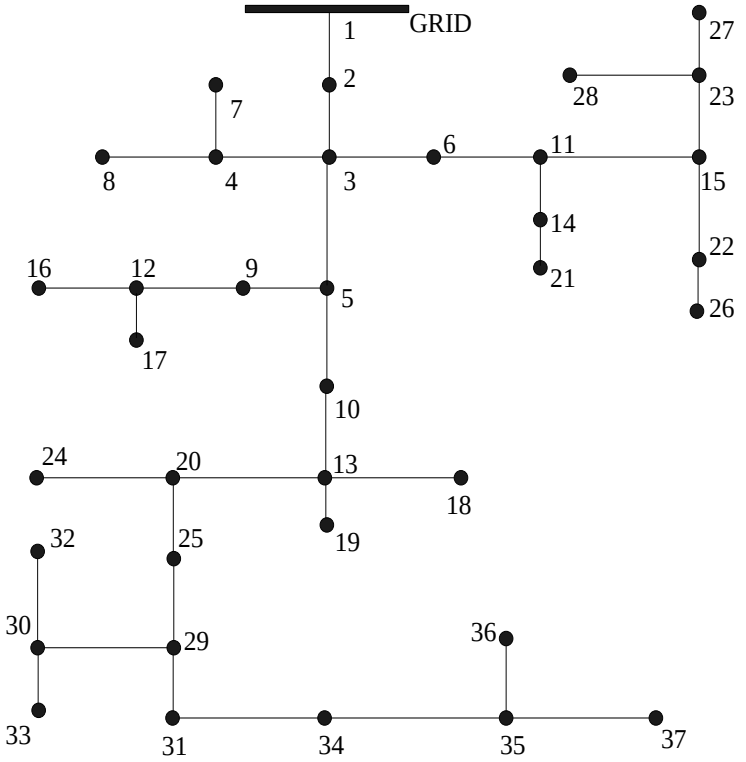

Fig. A.1 The low-voltage residential distribution feeder

Table A.1 Impedances of the low-voltage residential distribution feeder (all line segments assumed to be 100 meters)

From node	To node	Z_{self} ($10^{-2}\Omega$)	Z_{mutual} ($10^{-2}\Omega$)		
			Phase A-B	Phase B-C	Phase A-C
1	2	0.60+0.17j	0.15+0.06j	0.15+0.06j	0.14+0.05j
2	3	0.60+0.17j	0.15+0.06j	0.15+0.06j	0.14+0.05j
3	4	6.07+1.74j	1.52+0.64j	1.52+0.64j	1.41+0.50j
3	5	0.60+0.17j	0.15+0.06j	0.15+0.06j	0.14+0.05j

3	6	0.60+0.17j	0.15+0.06j	0.15+0.06j	0.14+0.05j
4	7	6.07+1.74j	1.52+0.64j	1.52+0.64j	1.41+0.50j
4	8	6.07+1.74j	1.52+0.64j	1.52+0.64j	1.41+0.50j
5	9	2.15+0.62j	0.54+0.23j	0.54+0.23j	0.50+0.18j
5	10	0.60+0.17j	0.15+0.06j	0.15+0.06j	0.14+0.05j
6	11	2.15+0.62j	0.54+0.23j	0.54+0.23j	0.50+0.18j
9	12	3.73+1.07j	0.93+0.39j	0.93+0.39j	0.87+0.30j
10	13	0.60+0.17j	0.15+0.06j	0.15+0.06j	0.14+0.05j
11	14	3.73+1.07j	0.93+0.39j	0.93+0.39j	0.87+0.30j
11	15	2.15+0.62j	0.54+0.23j	0.54+0.23j	0.50+0.18j
12	16	6.07+1.74j	1.52+0.64j	1.52+0.64j	1.41+0.50j
12	17	6.07+1.74j	1.52+0.64j	1.52+0.64j	1.41+0.50j
13	18	6.07+1.74j	1.52+0.64j	1.52+0.64j	1.41+0.50j
13	19	6.07+1.74j	1.52+0.64j	1.52+0.64j	1.41+0.50j
13	20	0.60+0.17j	0.15+0.06j	0.15+0.06j	0.14+0.05j
14	21	6.07+1.74j	1.52+0.64j	1.52+0.64j	1.41+0.50j
15	22	3.73+1.07j	0.93+0.39j	0.93+0.39j	0.87+0.30j
15	23	3.73+1.07j	0.93+0.39j	0.93+0.39j	0.87+0.30j
20	24	6.07+1.74j	1.52+0.64j	1.52+0.64j	1.41+0.50j
20	25	0.60+0.17j	0.15+0.06j	0.15+0.06j	0.14+0.05j
22	26	6.07+1.74j	1.52+0.64j	1.52+0.64j	1.41+0.50j
23	27	6.07+1.74j	1.52+0.64j	1.52+0.64j	1.41+0.50j
23	28	6.07+1.74j	1.52+0.64j	1.52+0.64j	1.41+0.50j
25	29	0.60+0.17j	0.15+0.06j	0.15+0.06j	0.14+0.05j
29	30	3.73+1.07j	0.93+0.39j	0.93+0.39j	0.87+0.30j
29	31	2.15+0.62j	0.54+0.23j	0.54+0.23j	0.50+0.18j
30	32	6.07+1.74j	1.52+0.64j	1.52+0.64j	1.41+0.50j
30	33	6.07+1.74j	1.52+0.64j	1.52+0.64j	1.41+0.50j
31	34	2.15+0.62j	0.54+0.23j	0.54+0.23j	0.50+0.18j
34	35	3.73+1.07j	0.93+0.39j	0.93+0.39j	0.87+0.30j
35	36	4.86+1.39j	1.21+0.51j	1.21+0.51j	1.13+0.40j
35	37	4.86+1.39j	1.21+0.51j	1.21+0.51j	1.13+0.40j

B. Models of Wind Speed and Wind Turbine Power Output

The wind speed model consists of four components, including the base wind component (V_{wb}), the ramp component (v_{wr}), the gust component (v_{wg}), and the turbulence (v_{wt}) [90, 91]:

$$v_w = V_{wb} + v_{wr} + v_{wg} + v_{wt} \tag{B.1}$$

The base wind component varies slowly at hourly scale. The ramp component can be modeled as follows:

$$v_{wr}(t) = \begin{cases} 0, & t < T_{r1} \text{ or } t > T_{r2} \\ V_{wr}(t - T_{r1}) / (T_{r2} - T_{r1}), & T_{r1} < t < T_{r2} \end{cases} \tag{B.2}$$

where V_{wr} is the magnitude of the ramp component; T_{r1} and T_{r2} are the start time and end time of the ramp component, respectively. The gust component can be represented as follows:

$$v_{wg}(t) = \begin{cases} 0, & t < T_{g1} \text{ or } t > T_{g2} \\ \dfrac{V_{wg}}{2} - \dfrac{V_{wg}}{2}\cos(2\pi(t - T_{g1}) / (T_{g2} - T_{g1})), & T_{g1} < t < T_{g2} \end{cases} \tag{B.3}$$

where V_{wg} is the magnitude of the gust component; T_{g1} and T_{g2} are the start time and end time of the gust component, respectively. The turbulence captures the random wind speed changes and is modeled by a normal distribution.

The model for wind turbine power output is given as follows [90, 116]:

$$\tau_w v'_{ws} = -v_{ws} + v_w \tag{B.4}$$

$$p_{wt} = \begin{cases} 0, & v_{ws} \le V_{cut\text{-}in} \text{ or } v_{ws} \ge V_{cut\text{-}off} \\ 0.5\rho\pi R_{wt}^2 C_p(\beta, \lambda) v_{ws}^3, & V_{cut\text{-}in} < v_{ws} \le V_{rated} \\ P_{wt}^{rated}, & V_{rated} < v_{ws} < V_{cut\text{-}off} \end{cases} \tag{B.5}$$

where the first-order low pass filter in (B.4) represents the smoothing effect of the wind turbine on high frequency components of the wind speed; τ_w is a time constant determined by the turbine size; v_{ws} is the smoothed wind speed; p_{wt} is the wind turbine power output; ρ is the air density; R_{wt} is the radius of the rotor;

C_p is the performance coefficient; β is the blade pitch angle; λ is the tip-speed ratio (v_{tip} / v_{ws}), the ratio between blade tip speed, v_{tip} (m/s), and the smoothed wind speed; $V_{cut\text{-}in}$ and $V_{cut\text{-}off}$ are the cut-in and cut-off wind speeds of the wind turbine, respectively; and V_{rated} is the wind speed at which the wind turbine generates its rated power. The parameters of the wind turbine power output model are summarized in Table B.1.

Table B.1 Parameters of the wind turbine power output model

Parameters	Values
τ_w	30 s
ρ	1.225 kg/ m^3
R_{wt}	40 m
C_p	0.214
$V_{cut\text{-}in}$	3.5 m/s
$V_{cut\text{-}off}$	25 m/s
V_{rated}	14.5 m/s
P_{wt}^{rated}	2 MW

C. Power-Frequency Droop Controller of PEVs

In Section 3.4.2, the load frequency control performance when the PEVs are equipped with the power-frequency droop controller proposed in [60] is compared with that when the PEV power is guided by the proposed decentralized control scheme to compensate undesired WP fluctuations. This droop controller is designed for distributed PEV loads to respond to the system frequency deviation. Along with regulating system frequency, this controller also takes the PEV charging requirement into consideration. Its formulation is briefly introduced as follows.

A PEV's duration for semi-rated charging is calculated as:

$$T_{\mathrm{SR}} = 2E / P_{\max} \tag{C.1}$$

where E is the battery capacity to be filled for the desired SOC; and $P_{\max}$ is the rated charging power.

If T_{SR} is longer than the plug-in period, the PEV power range will be fully used against the frequency deviation. The PEV power is determined as follows:

$$P = \begin{cases} K \cdot \Delta f & (|K \cdot \Delta f| \le P_{\max}) \\ P_{\max} & (P_{\max} < |K \cdot \Delta f| \text{ and } \Delta f > 0) \\ -P_{\max} & (P_{\max} < |K \cdot \Delta f| \text{ and } \Delta f < 0) \end{cases} \tag{C.2}$$

where K is the power-frequency droop; and Δf is the frequency deviation. The value of K depends on the PEV SOC. When $\Delta f > 0$:

$$K_{\mathrm{G2V}} = \begin{cases} K_{\max}\left[1-\left(\dfrac{SOC - SOC_{\mathrm{low}}}{SOC_{\max} - SOC_{\mathrm{low}}}\right)^{n}\right], & SOC_{\mathrm{low}} \le SOC \le SOC_{\max} \\ K_{\max}, & SOC < SOC_{\mathrm{low}} \\ 0, & SOC > SOC_{\max} \end{cases} \tag{C.3}$$

and when $\Delta f < 0$:

$$K_{\mathrm{V2G}} = \begin{cases} K_{\max}\left[1-\left(\dfrac{SOC - SOC_{\mathrm{high}}}{SOC_{\min} - SOC_{\mathrm{high}}}\right)^{n}\right], & SOC_{\min} \le SOC \le SOC_{\mathrm{high}} \\ 0, & SOC < SOC_{\min} \\ K_{\max}, & SOC > SOC_{\mathrm{high}} \end{cases} \quad \text{(C.4)}$$

The determination of K for $\Delta f > 0$ indicates that the higher the battery SOC is, the less responsive to the G2V power request the PEV will be; and the determination of K for $\Delta f < 0$ indicates that the lower the battery SOC is, the less responsive to the V2G power request the PEV will be. If the following condition is met:

$$\begin{cases} SOC_{\min} + SOC_{\max} = 100\% \\ SOC_{\mathrm{low}} + SOC_{\mathrm{high}} = 100\% \end{cases} \quad \text{(C.5)}$$

then $K_{\mathrm{G2V}} = K_{\mathrm{V2G}}$ when SOC = 50%; $K_{\mathrm{G2V}} > K_{\mathrm{V2G}}$ when SOC < 50%; and $K_{\mathrm{G2V}} < K_{\mathrm{V2G}}$ when SOC > 50%. Thus, the PEV SOC will be automatically held around 50%.

When the plug-in period becomes shorter than T_{SR}, the PEV will take net charging power and only perform load frequency control in its G2V power range. The PEV power is now determined as follows:

$$P = \begin{cases} (K_{\max}/2)\Delta f + P_{\max}/2 & (|K_{\max}\cdot\Delta f| \le P_{\max}) \\ P_{\max} & (P_{\max} < K_{\max}\Delta f) \\ 0 & (K_{\max}\Delta f < -P_{\max}) \\ -P_{\max} & (\Delta f < \Delta f_{\min}) \end{cases} \quad \text{(C.6)}$$

By taking the semi-rated power for T_{SR}, the PEV could approximately satisfy its charging requirement. Here, the underlying assumption is that the mean value of the frequency deviation is approximately zero. The parameter setting for this power-frequency droop controller used in Section 3.4.2 is presented in Table C.1.

This droop controller enables fully distributed load frequency control from PEVs. Yet, it has several major drawbacks identified. First, installing frequency

measurement devices for plenty of PEVs can be very costly. Second, the

Table C.1 Parameters of the PEV power-frequency droop controller

Parameters	Values
P_{max} (kW)	5.06
K_{max} (kW/Hz)	50
n	2
SOC_{max} , SOC_{low}	90%, 20%
SOC_{high} , SOC_{min}	80%, 10%
Δf_{min} (Hz)	-0.12

accuracy of the measured Δf can be readily affected by noises and errors [62], and the effectiveness of the PEV-aided frequency regulation would be degraded as a result. This is proved by the load frequency control performances in Section 3.4.2. Third, fast frequency fluctuations would stimulate substantial fluctuations in the PEV power controlled by the power-frequency droop, as shown in Fig. C.1, which can aggravate the PEV battery degradation [117].

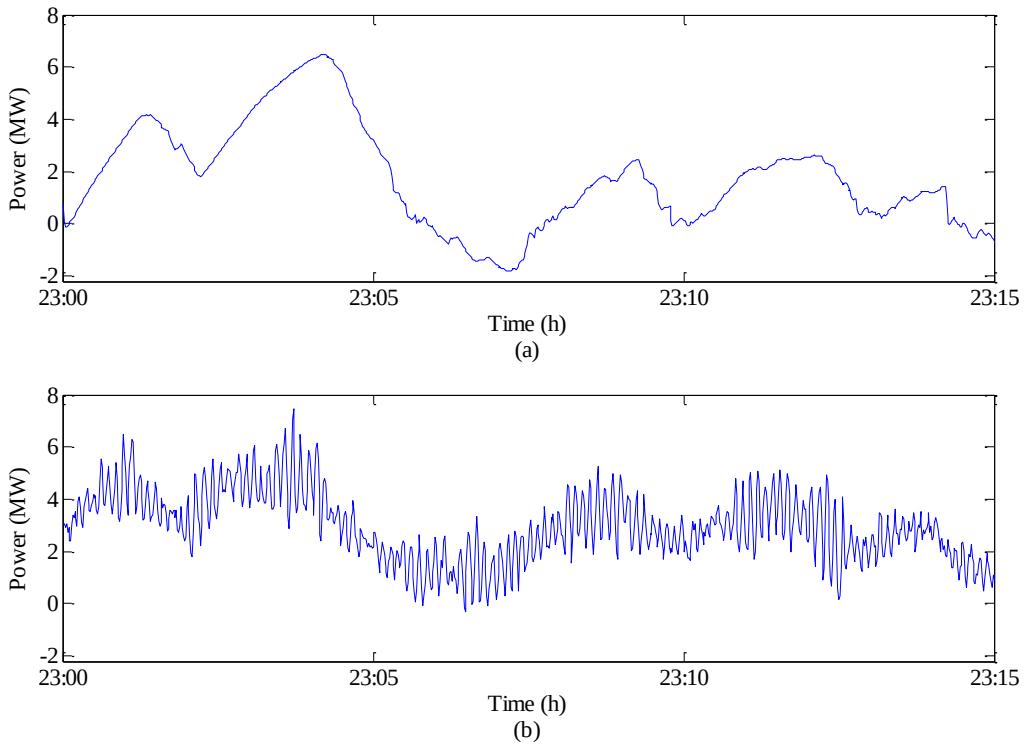

Fig. C.1 PEV power in the simulation in Section 3.4.2: (a) under the proposed decentralized charging control; (b) with the power-frequency droop controller

Reference

[1] F. Lew, T. Peter, K. Tom, W. Jake, C. Pierpaolo, C. Francois, *et al.*, "Technology Roadmap-Electric and plug-in hybrid electric vehicles," International Energy Agency, France, June 2011.

[2] U.S. Department of Transportation. (2014, 10 September). *Transportation and Greenhouse Gas Emissions*. Available: http://climate.dot.gov/about/transportations-role/overview.html

[3] M. Shomik, "The China New Energy Vehicles Program: Challenges and Opportunites," World Bank, Beijing, 2011.

[4] The Internal Revenue Service, U.S.. (2013, 2 April). *New Qualified Plug-in Electric Drive Motor Vehicle Credit*. Available: https://www.irs.gov/irb/2009-48_IRB/ar09.html

[5] Office for Low Emission Vehicles, UK Government. (2015, 4 July). *Plug-in car grant eligibility guidance.* Available: https://www.gov.uk/government/publications/plug-in-car-grant/plug-in-car-grant-eligibility-guidance

[6] U. S. Department of Energy. (2015, 10 May). *Availability of Hybrid and Plug-In Electric Vehicles*. Available: http://www.afdc.energy.gov/vehicles/electric_availability.html

[7] T. Tali and P. Telleen, "Global EV Outlook: Understanding the Electric Vehicle Landscape to 2020," International Energy Agency, April 2013.

[8] Wikipedia. (2016, 27 January). *Electric car use by country*. Available: https://en.wikipedia.org/wiki/Electric_car_use_by_country

[9] A. Elgowainy, J. Han, L. Poch, M. Wang, A. Vyas, M. Mahalik, *et al.*, "Well-to-Wheels Analysis of Energy Use and Greenhouse Gas Emissions of Plug-in Hybrid Electric Vehicles," Argonne National Laboratory, June 2010.

[10] GoElectricDrive. (2015, 12 July). *Environmental Benefits*. Available: http://www.goelectricdrive.org/drive-electric/environmental-benefits

[11] M. Duvall, E. Knipping, and M. Alexander, "Environmental Assessment of Plug-in Hybrid Electric Vehicles," Electric Power Research Institute, U.S., July 2007.

[12] P. Grahn, J. Munkhammar, J. Widen, K. Alvehag, and L. Soder, "PHEV Home-Charging Model Based on Residential Activity Patterns," *Power Systems, IEEE Transactions on*, vol. 28, pp. 2507-2515, 2013.

[13] S. Shafiee, M. Fotuhi-Firuzabad, and M. Rastegar, "Investigating the Impacts of Plug-in Hybrid Electric Vehicles on Power Distribution Systems," *Smart Grid, IEEE Transactions on*, vol. 4, pp. 1351-1360, 2013.

[14] J. A. Peas Lopes, F. J. Soares, and P. M. R. Almeida, "Identifying management procedures to deal with connection of Electric Vehicles in the grid," in *PowerTech, 2009 IEEE Bucharest*, 2009, pp. 1-8.

[15] M. D. Galus, R. A. Waraich, F. Noembrini, K. Steurs, G. Georges, K. Boulouchos, *et al.*, "Integrating Power Systems, Transport Systems and Vehicle Technology for Electric Mobility Impact Assessment and Efficient Control," *Smart Grid, IEEE Transactions on*, vol. 3, pp. 934-949, 2012.

[16] J. M. Sexauer, K. D. McBee, and K. A. Bloch, "Applications of probability model to analyze the effects of electric vehicle chargers on distribution transformers," *Power Systems, IEEE Transactions on,* vol. 28, pp. 847-854, 2013.

[17] M. Tan and O. A. Mohammed, "Optimal Charging of Plug-in Electric Vehicles for a Car-Park Infrastructure," *Industry Applications, IEEE Transactions on,* vol. 50, pp. 2323-2330, 2014.

[18] J. Van Roy, N. Leemput, F. Geth, R. Salenbien, J. Buscher, and J. Driesen, "Apartment Building Electricity System Impact of Operational Electric Vehicle Charging Strategies," *Sustainable Energy, IEEE Transactions on,* vol. 5, pp. 264-272, 2014.

[19] G. Qinglai, X. Shujun, S. Hongbin, L. Zhengshuo, and Z. Boming, "Rapid-Charging Navigation of Electric Vehicles Based on Real-Time Power Systems and Traffic Data," *Smart Grid, IEEE Transactions on,* vol. 5, pp. 1969-1979, 2014.

[20] L. Cong, W. Jianhui, A. Botterud, Z. Yan, and A. Vyas, "Assessment of Impacts of PHEV Charging Patterns on Wind-Thermal Scheduling by Stochastic Unit Commitment," *Smart Grid, IEEE Transactions on,* vol. 3, pp. 675-683, 2012.

[21] H. Lunci, W. Jia, and Z. Chi, "Adaptive Electric Vehicle Charging Coordination on Distribution Network," *Smart Grid, IEEE Transactions on,* vol. 5, pp. 2666-2675, 2014.

[22] W. Di, D. C. Aliprantis, and Y. Lei, "Load Scheduling and Dispatch for Aggregators of Plug-In Electric Vehicles," *Smart Grid, IEEE Transactions on,* vol. 3, pp. 368-376, 2012.

[23] A. Mohamed, V. Salehi, M. Tan, and O. Mohammed, "Real-Time Energy Management Algorithm for Plug-In Hybrid Electric Vehicle Charging Parks Involving Sustainable Energy," *Sustainable Energy, IEEE Transactions on,* vol. 5, pp. 577-586, 2014.

[24] A. S. Masoum, S. Deilami, P. S. Moses, M. A. S. Masoum, and A. Abu-Siada, "Smart load management of plug-in electric vehicles in distribution and residential networks with charging stations for peak shaving and loss minimisation considering voltage regulation," *Generation, Transmission & Distribution, IET,* vol. 5, pp. 877-888, 2011.

[25] J. Tomić and W. Kempton, "Using fleets of electric-drive vehicles for grid support," *Journal of Power Sources,* vol. 168, pp. 459-468, 6/1/ 2007.

[26] M. Rahmani-andebili, "Spinning reserve supply with presence of electric vehicles aggregator considering compromise between cost and reliability," *Generation, Transmission & Distribution, IET,* vol. 7, pp. 1442-1452, 2013.

[27] M. R. Sarker, Y. Dvorkin, and M. A. Ortega-Vazquez, "Optimal Participation of an Electric Vehicle Aggregator in Day-Ahead Energy and Reserve Markets," *Power Systems, IEEE Transactions on,* vol. PP, pp. 1-10, 2015.

[28] D. Dallinger, D. Krampe, and M. Wietschel, "Vehicle-to-Grid Regulation Reserves Based on a Dynamic Simulation of Mobility Behavior," *Smart Grid, IEEE Transactions on,* vol. 2, pp. 302-313, 2011.

[29] J. Chenrui, S. Xiang, and P. Ghosh, "Optimized Electric Vehicle Charging With Intermittent Renewable Energy Sources," *Selected Topics in Signal Processing, IEEE Journal of,* vol. 8, pp. 1063-1072, 2014.

[30] L. Chiao-Ting, A. Changsun, P. Huei, and S. Jing, "Synergistic control of plug-in vehicle charging and wind power scheduling," *Power Systems, IEEE Transactions on*, vol. 28, pp. 1113-1121, 2013.

[31] W. Guibin, Z. Junhua, W. Fushuan, X. Yusheng, and G. Ledwich, "Dispatch Strategy of PHEVs to Mitigate Selected Patterns of Seasonally Varying Outputs From Renewable Generation," *Smart Grid, IEEE Transactions on*, vol. 6, pp. 627-639, 2015.

[32] C. Lin, C. Yao, L. Jin, and C. Singh, "Power System Reliability Assessment With Electric Vehicle Integration Using Battery Exchange Mode," *Sustainable Energy, IEEE Transactions on*, vol. 4, pp. 1034-1042, 2013.

[33] H. Farzin, M. Moeini-Aghtaie, and M. Fotuhi-Firuzabad, "Reliability Studies of Distribution Systems Integrated With Electric Vehicles Under Battery-Exchange Mode," *Power Delivery, IEEE Transactions on*, vol. PP, pp. 1-1, 2015.

[34] N. Z. Xu and C. Y. Chung, "Reliability Evaluation of Distribution Systems Including Vehicle-to-Home and Vehicle-to-Grid," *Power Systems, IEEE Transactions on*, vol. 31, pp. 759-768, 2016.

[35] N. Z. Xu and C. Y. Chung, "Well-Being Analysis of Generating Systems Considering Electric Vehicle Charging," *Power Systems, IEEE Transactions on*, vol. 29, pp. 2311-2320, 2014.

[36] N. Taheri, R. Entriken, and Y. Yinyu, "A Dynamic Algorithm for Facilitated Charging of Plug-In Electric Vehicles," *Smart Grid, IEEE Transactions on*, vol. 4, pp. 1772-1779, 2013.

[37] B. Zhang and M. Kezunovic, "Impact on Power System Flexibility by Electric Vehicle Participation in Ramp Market," *Smart Grid, IEEE Transactions on,* vol. PP, pp. 1-1, 2015.

[38] M. Gonzalez Vaya and G. Andersson, "Optimal Bidding Strategy of a Plug-In Electric Vehicle Aggregator in Day-Ahead Electricity Markets Under Uncertainty," *Power Systems, IEEE Transactions on,* vol. 30, pp. 2375-2385, 2015.

[39] D. Bohme, W. Durrschmidt, and M. v. Mark, "Renewable energy sources in figures: national and international development," German Federal Ministry for the Environment, Nature Conservation and Nuclear Safety, Berlin, June 2009.

[40] F. B. Alhasawi and J. V. Milanovic, "Techno-Economic Contribution of FACTS Devices to the Operation of Power Systems With High Level of Wind Power Integration," *Power Systems, IEEE Transactions on,* vol. 27, pp. 1414-1421, 2012.

[41] K. Chongqing, C. Xinyu, X. Qianyao, R. Dongming, H. Yuehui, X. Qing, *et al.*, "Balance of Power: Toward a More Environmentally Friendly, Efficient, and Effective Integration of Energy Systems in China," *Power and Energy Magazine, IEEE,* vol. 11, pp. 56-64, 2013.

[42] L. Tsung-Ying, "Optimal Spinning Reserve for a Wind-Thermal Power System Using EIPSO," *Power Systems, IEEE Transactions on,* vol. 22, pp. 1612-1621, 2007.

[43] S. Kamalinia, M. Shahidehpour, and A. Khodaei, "Security-constrained expansion planning of fast-response units for wind integration," *Electric Power Systems Research,* vol. 81, pp. 107-116, 2011.

[44] M. Ghofrani, A. Arabali, M. Etezadi-Amoli, and M. S. Fadali, "Smart Scheduling and Cost-Benefit Analysis of Grid-Enabled Electric Vehicles for Wind Power Integration," *Smart Grid, IEEE Transactions on,* vol. 5, pp. 2306-2313, 2014.

[45] P. B. Eriksen, T. Ackermann, H. Abildgaard, P. Smith, W. Winter, and J. M. Rodriguez Garcia, "System operation with high wind penetration," *Power and Energy Magazine, IEEE,* vol. 3, pp. 65-74, 2005.

[46] S. N. Salih, C. Peiyuan, and O. Carlson, "The Effect of Wind Power Integration on the Frequency of Tap Changes of a Substation Transformer," *Power Systems, IEEE Transactions on,* vol. 28, pp. 4320-4327, 2013.

[47] X. Le, J. Jhi-Young, and M. D. Ilic, "Integration of intermittent resources with price-responsive loads," in *North American Power Symposium (NAPS), 2009*, 2009, pp. 1-6.

[48] A. S. Kowli and S. P. Meyn, "Supporting wind generation deployment with demand response," in *Power and Energy Society General Meeting, 2011 IEEE,* 2011, pp. 1-8.

[49] K. Dietrich, J. M. Latorre, L. Olmos, and A. Ramos, "Demand Response in an Isolated System With High Wind Integration," *Power Systems, IEEE Transactions on,* vol. 27, pp. 20-29, 2012.

[50] A. Moshari, A. Ebrahimi, and M. Fotuhi-Firuzabad, "Short-Term Impacts of DR Programs on Reliability of Wind Integrated Power Systems Considering Demand-Side Uncertainties," *Power Systems, IEEE Transactions on,* vol. PP, pp. 1-10, 2015.

[51] H. Weihao, S. Chi, C. Zhe, and B. Bak-Jensen, "Optimal Operation of Plug-In Electric Vehicles in Power Systems With High Wind Power Penetrations," *Sustainable Energy, IEEE Transactions on*, vol. 4, pp. 577-585, 2013.

[52] M. Vasirani, R. Kota, R. L. G. Cavalcante, S. Ossowski, and N. R. Jennings, "An Agent-Based Approach to Virtual Power Plants of Wind Power Generators and Electric Vehicles," *Smart Grid, IEEE Transactions on*, vol. 4, pp. 1314-1322, 2013.

[53] L. Kelly, A. Rowe, and P. Wild, "Analyzing the impacts of plug-in electric vehicles on distribution networks in British Columbia," in *Electrical Power & Energy Conference (EPEC), 2009 IEEE*, 2009, pp. 1-6.

[54] S. Shengnan, M. Pipattanasomporn, and S. Rahman, "Challenges of PHEV penetration to the residential distribution network," in *Power & Energy Society General Meeting, 2009. PES '09. IEEE*, 2009, pp. 1-8.

[55] G. A. Putrus, P. Suwanapingkarl, D. Johnston, E. C. Bentley, and M. Narayana, "Impact of electric vehicles on power distribution networks," in *Vehicle Power and Propulsion Conference, 2009. VPPC '09. IEEE*, 2009, pp. 827-831.

[56] K. J. Dyke, N. Schofield, and M. Barnes, "The Impact of Transport Electrification on Electrical Networks," *Industrial Electronics, IEEE Transactions on*, vol. 57, pp. 3917-3926, 2010.

[57] J. R. Pillai and B. Bak-Jensen, "Integration of Vehicle-to-Grid in the Western Danish Power System," *Sustainable Energy, IEEE Transactions on*, vol. 2, pp. 12-19, 2011.

[58] M. Yunfei, W. Jianzhong, J. Ekanayake, N. Jenkins, and J. Hongjie, "Primary Frequency Response From Electric Vehicles in the Great Britain Power System," *Smart Grid, IEEE Transactions on,* vol. 4, pp. 1142-1150, 2013.

[59] T. Masuta and A. Yokoyama, "Supplementary Load Frequency Control by Use of a Number of Both Electric Vehicles and Heat Pump Water Heaters," *Smart Grid, IEEE Transactions on,* vol. 3, pp. 1253-1262, 2012.

[60] Y. Ota, H. Taniguchi, T. Nakajima, K. M. Liyanage, J. Baba, and A. Yokoyama, "Autonomous Distributed V2G (Vehicle-to-Grid) Satisfying Scheduled Charging," *Smart Grid, IEEE Transactions on,* vol. 3, pp. 559-564, 2012.

[61] C. Ahn, C.-T. Li, and H. Peng, "Optimal decentralized charging control algorithm for electrified vehicles connected to smart grid," *Journal of Power Sources,* vol. 196, pp. 10369-10379, 12/1/ 2011.

[62] Y. Hongming, C. Y. Chung, and Z. Junhua, "Application of plug-in electric vehicles to frequency regulation based on distributed signal acquisition via limited communication," *Power Systems, IEEE Transactions on,* vol. 28, pp. 1017-1026, 2013.

[63] N. Troy, D. Flynn, M. Milligan, and M. O'Malley, "Unit Commitment With Dynamic Cycling Costs," *Power Systems, IEEE Transactions on,* vol. 27, pp. 2196-2205, 2012.

[64] L. Xiangjun, H. Dong, and L. Xiaokang, "Battery Energy Storage Station (BESS)-Based Smoothing Control of Photovoltaic (PV) and Wind Power Generation Fluctuations," *Sustainable Energy, IEEE Transactions on,* vol. 4, pp. 464-473, 2013.

[65] J. Quanyuan, G. Yuzhong, and W. Haijiao, "A Battery Energy Storage System Dual-Layer Control Strategy for Mitigating Wind Farm Fluctuations," *Power Systems, IEEE Transactions on,* vol. 28, pp. 3263-3273, 2013.

[66] K. W. Wee, S. S. Choi, and D. M. Vilathgamuwa, "Design of a Least-Cost Battery-Supercapacitor Energy Storage System for Realizing Dispatchable Wind Power," *Sustainable Energy, IEEE Transactions on,* vol. 4, pp. 786-796, 2013.

[67] H. Daneshi and A. K. Srivastava, "Security-constrained unit commitment with wind generation and compressed air energy storage," *Generation, Transmission & Distribution, IET,* vol. 6, pp. 167-175, 2012.

[68] F. Islam, A. Al-Durra, and S. M. Muyeen, "Smoothing of Wind Farm Output by Prediction and Supervisory-Control-Unit-Based FESS," *Sustainable Energy, IEEE Transactions on,* vol. 4, pp. 925-933, 2013.

[69] J. Quanyuan and W. Haijiao, "Two-Time-Scale Coordination Control for a Battery Energy Storage System to Mitigate Wind Power Fluctuations," *Energy Conversion, IEEE Transactions on,* vol. 28, pp. 52-61, 2013.

[70] F. Zhou, G. Joos, C. Abbey, L. Jiao, and B. T. Ooi, "Use of large capacity SMES to improve the power quality and stability of wind farms," in *Power Engineering Society General Meeting, 2004. IEEE,* 2004, pp. 2025-2030 Vol.2.

[71] L. Yun, X. Huanhai, W. Zhen, and G. Deqiang, "Control of virtual power plant in microgrids: a coordinated approach based on photovoltaic systems and controllable loads," *Generation, Transmission & Distribution, IET,* vol. 9, pp. 921-928, 2015.

[72] L. Jin, S. Yuanzhang, S. Yonghua, G. Wenzhong, and P. Sorensen, "Wind Power Fluctuation Smoothing Controller Based on Risk Assessment of Grid Frequency Deviation in an Isolated System," *Sustainable Energy, IEEE Transactions on*, vol. 4, pp. 379-392, 2013.

[73] R. Sioshansi and W. Short, "Evaluating the Impacts of Real-Time Pricing on the Usage of Wind Generation," *Power Systems, IEEE Transactions on*, vol. 24, pp. 516-524, 2009.

[74] R. Sioshansi, "Evaluating the Impacts of Real-Time Pricing on the Cost and Value of Wind Generation," *Power Systems, IEEE Transactions on*, vol. 25, pp. 741-748, 2010.

[75] C. De Jonghe, B. F. Hobbs, and R. Belmans, "Value of Price Responsive Load for Wind Integration in Unit Commitment," *Power Systems, IEEE Transactions on*, vol. 29, pp. 675-685, 2014.

[76] J. Kondoh, "Direct load control for wind power integration," in *Power and Energy Society General Meeting, 2011 IEEE*, 2011, pp. 1-8.

[77] K. Clement, E. Haesen, and J. Driesen, "Coordinated charging of multiple plug-in hybrid electric vehicles in residential distribution grids," in *Power Systems Conference and Exposition, 2009. PSCE '09. IEEE/PES*, 2009, pp. 1-7.

[78] K. Clement-Nyns, E. Haesen, and J. Driesen, "The Impact of Charging Plug-In Hybrid Electric Vehicles on a Residential Distribution Grid," *Power Systems, IEEE Transactions on*, vol. 25, pp. 371-380, 2010.

[79] E. Sortomme, M. M. Hindi, S. D. J. MacPherson, and S. S. Venkata, "Coordinated Charging of Plug-In Hybrid Electric Vehicles to Minimize

Distribution System Losses," *Smart Grid, IEEE Transactions on,* vol. 2, pp. 198-205, 2011.

[80] P. Richardson, D. Flynn, and A. Keane, "Optimal Charging of Electric Vehicles in Low-Voltage Distribution Systems," *Power Systems, IEEE Transactions on,* vol. 27, pp. 268-279, 2012.

[81] P. Richardson, D. Flynn, and A. Keane, "Local Versus Centralized Charging Strategies for Electric Vehicles in Low Voltage Distribution Systems," *Smart Grid, IEEE Transactions on,* vol. 3, pp. 1020-1028, 2012.

[82] S. A. Pourmousavi and M. H. Nehrir, "Real-Time Central Demand Response for Primary Frequency Regulation in Microgrids," *Smart Grid, IEEE Transactions on,* vol. 3, pp. 1988-1996, 2012.

[83] D. Thukaram, H. M. Wijekoon Banda, and J. Jerome, "A robust three phase power flow algorithm for radial distribution systems," *Electric Power Systems Research,* vol. 50, pp. 227-236, 6/1/ 1999.

[84] W. H. Kersting, "Radial distribution test feeders," in *Power Engineering Society Winter Meeting, 2001. IEEE,* 2001, pp. 908-912 vol.2.

[85] F. Shahnia, M. T. Wishart, A. Ghosh, G. Ledwich, and F. Zare, "Smart demand side management of low-voltage distribution networks using multi-objective decision making," *Generation, Transmission & Distribution, IET,* vol. 6, pp. 968-1000, 2012.

[86] W. M. Lin and T. C. Ou, "Unbalanced distribution network fault analysis with hybrid compensation," *Generation, Transmission & Distribution, IET,* vol. 5, pp. 92-100, 2011.

[87] F. Kelly, "Charging and rate control for elastic traffic," *European Transactions on Telecommunications,* vol. 8, pp. 33-37, 1997.

[88] F. Zhong, "A Distributed Demand Response Algorithm and Its Application to PHEV Charging in Smart Grids," *Smart Grid, IEEE Transactions on,* vol. 3, pp. 1280-1290, 2012.

[89] F. P. Kelly, A. K. Maulloo, and D. K. H. Tan, "Rate control for communication networks: shadow prices, proportional fairness and stability," *J Oper Res Soc,* vol. 49, pp. 237-252, 03/14/print 1998.

[90] M. Torres and L. A. C. Lopes, "An optimal virtual inertia controller to support frequency regulation in autonomous diesel power systems with high penetration of renewable," in *International Conference of Renewable Energy & Power Quality*, Spain, 2001.

[91] T. Yu, B. Zhou, and H. Liang, "Smart power generation control for microgrids islanded operation based on R(lambda) learning," *Power System Protection and Control,* vol. 40, pp. 7-13, 2012.

[92] P. Kundur, "Control of active power and reactive power," in *Power System Stability and Control,* ed New York: Mc-Graw-Hill, 1994, pp. 581-626.

[93] S. Roy, O. P. Malik, and G. S. Hope, "A k-step predictive scheme for speed control of diesel driven power plants," *Industry Applications, IEEE Transactions on,* vol. 29, pp. 389-396, 1993.

[94] A. N. Brooks, "Vehicle-to-grid demonstration project: Grid regulation ancillary service with a battery electric vehicle," AC Propulsion, Inc., San Dimas, CA, December 10 2002.

[95] T. S. Sidhu, "Accurate measurement of power system frequency using a digital signal processing technique," *Instrumentation and Measurement, IEEE Transactions on*, vol. 48, pp. 75-81, 1999.

[96] N. Kumar, P. Besuner, S. Lefton, D. Agan, and D. Hilleman, "Power Plant Cycling Costs," Intertek APTECH, Sunnyvale, CA, Technical Report, April 2012.

[97] N. Troy, E. Denny, and M. O'Malley, "Base-Load Cycling on a System With Significant Wind Penetration," *Power Systems, IEEE Transactions on*, vol. 25, pp. 1088-1097, 2010.

[98] Z. Zhao-Sui, S. Yuan-Zhang, D. W. Gao, L. Jin, and C. Lin, "A Versatile Probability Distribution Model for Wind Power Forecast Errors and Its Application in Economic Dispatch," *Power Systems, IEEE Transactions on*, vol. 28, pp. 3114-3125, 2013.

[99] Elia. (2013, 23 Dec.). *Wind power generation data*. Available: http://www.elia.be/en/grid-data/power-generation/wind-power

[100] Carrion, M. and J. M. Arroyo, "A computationally efficient mixed-integer linear formulation for the thermal unit commitment problem," *Power Systems, IEEE Transactions on*, vol. 21, pp. 1371-1378, 2006.

[101] Y. Weifeng, Z. Junhua, W. Fushuan, X. Yusheng, and G. Ledwich, "A Hierarchical Decomposition Approach for Coordinated Dispatch of Plug-in Electric Vehicles," *Power Systems, IEEE Transactions on*, vol. 28, pp. 2768-2778, 2013.

[102] S. H. Madaeni and R. Sioshansi, "Measuring the Benefits of Delayed Price-Responsive Demand in Reducing Wind-Uncertainty Costs," *Power Systems, IEEE Transactions on*, vol. 28, pp. 4118-4126, 2013.

[103] P. Wong, P. Albrecht, R. Allan, R. Billinton, Q. Chen, C. Fong, *et al.*, "The IEEE Reliability Test System-1996. A report prepared by the Reliability Test System Task Force of the Application of Probability Methods Subcommittee," *Power Systems, IEEE Transactions on*, vol. 14, pp. 1010-1020, 1999.

[104] Electrical and Computer Engineering Department of Illinois Institute of Technology. (19 November 2014). *Data sheet: 118bus abreu*. Available: http://motor.ece.iit.edu/Data/

[105] U.S. Energy Information Administration. (26 August, 2014). *Statistics on electric power plants, capacity, generation, fuel consumption, sales, prices and customers*. Available: http://www.eia.gov/electricity/data.cfm#avgcost

[106] The Australian Energy Market Operator (AEMO). (12 February 2015). *Electricity Data: Price and Demand*. Available: http://www.aemo.com.au/Electricity/Data/Price-and-Demand

[107] U.S. Department of Energy. (27 Feb. 2015). *Developing Infrastructure to Charging Plug-in Electric Vehicles*. Available: http://www.afdc.energy.gov/fuels/electricity_infrastructure.html

[108] Gurobi Optimization, Inc., "Gurobi Optimizer Version 5.6.3," ed. Houston, Texas, 2015.

[109] P. Sankey, D. T. Clark, and S. Micheloto, "The end of the oil age 2011 and beyond: a reality check," Deutsche Bank Securities Inc., New York, Dec. 2010.

[110] U.S. Department of Energy, "EV everywhere grand challenge-road to success," Jan. 2014.

[111] B. Nykvist and M. Nilsson, "Rapidly falling costs of battery packs for electric vehicles," *Nature Climate Change,* vol. 5, pp. 329-332, Mar. 2015.

[112] F. Kalhammer, "Batteries for electric drive vehicles - status 2005," Electric Power Research Institute, Palo Alto, CA, Nov. 2005.

[113] Tennet. (26 Aug. 2014). *Actual and forecast wind energy feed-in*. Available: http://www.tennettso.de/site/en/Transparency/publications/network-figures/actual-and-forecast-wind-energy-feed-in

[114] The Australian Energy Market Operator (AEMO). (26 Oct. 2014). *Aggregated price and demand data files, Aggregated Price & Demand: 2011-2015*. Available: http://www.aemo.com.au/Electricity/Data/Price-and-Demand/Aggregated-Price-and-Demand-Data-Files/Aggregated-Price-and-Demand-2011-to-2015

[115] U.S. Energy Information Administration. (20 Nov. 2015). *Table 5.3. Average price of electricity to ultimate customers, total by end-use sector, 2005-Augest 2015*. Available: http://www.eia.gov/electricity/monthly/epm_table_grapher.cfm?t=epmt_5_3

[116] S. Libao, W. Chen, Y. Liangzhong, N. Yixin, and M. Bazargan, "Optimal Power Flow Solution Incorporating Wind Power," *Systems Journal, IEEE,* vol. 6, pp. 233-241, 2012.

[117] H. Yifeng, B. Venkatesh, and G. Ling, "Optimal Scheduling for Charging and Discharging of Electric Vehicles," *Smart Grid, IEEE Transactions on,* vol. 3, pp. 1095-1105, 2012.